RICE UNIVERSITY

Mechanisms of Cooperation in Systems of Multiple Processive Motors

by

Jonathan Driver

A THESIS SUBMITTED
IN PARTIAL FULFILLMENT OF THE
REQUIREMENTS FOR THE DEGREE

Doctor of Philosophy

APPROVED, THESIS COMMITTEE

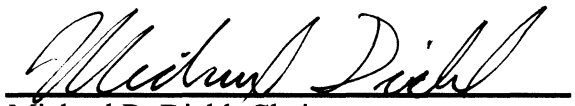

Michael R. Diehl, Chair
Assistant Professor of Bioengineering,
Assistant Professor of Chemistry

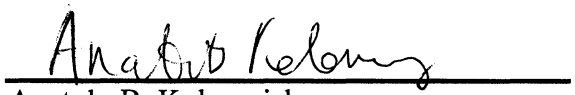

Anatoly B. Kolomeisky
Professor of Chemistry,
Associate Professor of Chemical and
Biomolecular Engineering

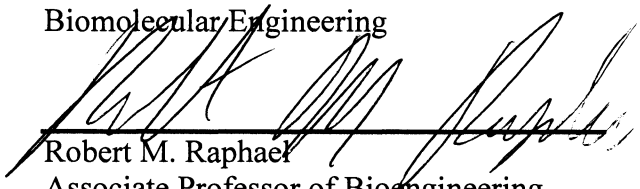

Robert M. Raphael
Associate Professor of Bioengineering

HOUSTON, TEXAS
September 2011

Abstract

Mechanisms of Cooperation in Systems of Multiple Processive Motors

by

Jonathan Driver

The inside of a eukaryotic cell is a highly organized microscale factory that shuttles components that are created or obtained in one place for use or further modification in another. Diffusion cannot accomplish the feat of translocating an object in the cytoplasm to a particular location that is a micron or more away in a timely fashion, so cells rely instead on processive motor proteins. Microtubule motor proteins are enzymes that harness the chemical energy from ATP hydrolysis to produce force and carry vesicles, membrane-bound organelles, and other cargos along paths in the cell's microtubule filament network to their destinations in the cytoplasm. These proteins recognize the polarity of the microtubule, and different classes of motors walk in different directions with respect to this polarity, giving the cell control over the direction in which a cargo is carried. It has been observed experimentally that many cargos are carried by more than one motor simultaneously, and that these multiple-motor systems can consist both of motors of the same type and of varying numbers of motors of different types. Multiple-motor systems present the possibilities of both enhanced transport performance and of tunable behavior, where the number, type, and arrangement of motors on a group of cargos can be modulated by the cell like an analog-style control to induce those

cargos to arrive at a particular distribution of locations in the cytoplasm. In order to resolve the mechanisms by which these things might occur, the combination of experimental and theoretical studies in this thesis focus on the relationship between the basic biophysical properties of the constituent motors in small multiple-motor systems and the degree and nature of the cooperation observed, from the standpoint of several relevant metrics. The results highlight the importance of both the mechanochemistry of the motors and the geometry of the system itself, and offer substantial new insights into why different classes of motors cooperate to different extents, with broad implications.

Acknowledgments

This work would not have been possible without the guidance of my adviser, Dr. Michael Diehl, and the help of Dr. Anatoly Kolomeisky. I would like to thank all of the members of the Diehl lab for their contributions, both scientific and not, to the work presented in this thesis and to me personally. I would also like to thank my mother, father, and the rest of my family for their love and support.

Contents

List of Figures

List of Tables

List of Equations

Chapter 1

Introduction: The Biophysics of Transport by Multiple Molecular Motors

Molecular motor proteins are specialized enzymes created by the cell to solve the problem of fast microscale transport of its nanoscale components. They carry various cargos as they walk along polar filaments that are arranged in a network throughout the cell, consuming a molecule of adenosine triphosphate (ATP) each time they step directionally and produce force. Some motor proteins, called "processive" motor proteins, can take a large number of steps along these filaments before they dissociate and transport ends, while others (non-processive) can take only one or very few.

The notion that processive motors like kinesin-1 and cytoplasmic dynein would have reason to operate collectively when they are apt transporters as

individual molecules is not universally accepted. The contrast between the mechanochemistry of these motors and muscle myosins, which function exclusively within large assemblies, was noted long ago by Liebler and Huse, who delineated the two motor classes and named them "porters" and "rowers", respectively.[1] Muscle myosins generally spend most of their time unbound from the filament on which they work because they detach at the end of their duty cycles in a rowing motion. In the absence of a sufficient number of partners, a filament under load would slip away during the detached phase of the cycle, as has been observed experimentally.[2] Porters, on the other hand, repeat their duty cycles 50-100 times prior to detachment when under small loads of 1 pN or less,[3,4] and can move their cargos for some distance without the aid of others.

Nonetheless, the transport properties of individual kinesins and dyneins are clearly insufficient for some tasks, and evidence for the simultaneous action of multiple microtubule motors on intracellular cargos has existed for over 25 years.[5-7] Run lengths on the order of one micron might facilitate transport in some smaller cell types, but transport along axons that are a hundred microns or more in length would be painfully slow. It is also worth noting that the paths along which these motors pull their cargos are not nearly so immaculate as they are in most *in vitro* assays. Electron microscopy reveals that the cytoplasm is a heterogenous gel with pores much smaller than vesicular cargos,[6] and the microtubules on which the motors walk are decorated extensively with myriad types of MAPs that can obstruct their progress.[8] Individual motors are also unable to produce the rapid bidirectional motions observed from some cargos.[9] Yet, much remains unresolved about the

relationship between the types and numbers of motors on a cargo and its transport behavior. Understanding this relationship is critical to understanding the underlying nature of intracellular transport, which could be switch-like, where movement in one direction or the other is simply turned on and off by exogenous factors, or tunable, where the spatiotemporal distribution of cargos of a particular type is controlled by the properties (*e.g. velocity, run length, force production*) of the motor system addressed to them. Tunable transport lessens the need for regulatory mechanisms that require spatial organization themselves because patterning is achieved through the composition of motor systems that can be controlled homogenously throughout the cell.

Elucidating the transport behaviors of multiple-motor systems has to date been a parallel effort primarily driven by a combination of theoretical analyses and experiments *in vitro*. These studies have demonstrated the power of a first-principles approach by accounting for the influence of such things as system geometry, molecular strain, and mechanochemistry on collective dynamics,[10-16] but in doing so they have also demonstrated just how context-dependent transport behaviors can be. This fact may eventually help to reconcile divergent *in vitro* and *in vivo* observations, but it also places stringent demands on the design of future experiments. The field is not yet ready to infer the composition of a multiple-motor system from generic characterizations of cargo movements.

Many inroads to address this need have already been made. Like most proteins, the cellular expression levels of different molecular motor types can be

manipulated, potentially tuning their copy numbers on individual cargos.[17,18] The cargos to which recombinant and even wild type motors are addressed can be controlled as well.[19,20] Fluorescent tags have been used to identify and track molecular motors, and the high bandwidth back focal plane detection that has been so critical to informing our mechanistic understanding of multiple-motor systems *in vitro* has been adapted, with some limitations, to the *in vivo* setting.[18] There is much to be gained from applying these technologies in combination simultaneously and across a broad range of scenarios.

This review focuses on the role of biophysics in determining the transport properties of systems of motor proteins, with the aim of equipping the experimentalist with a firm grasp of the range of phenomena that arise from collective dynamics and why they must be controlled for. To be sure, regulators of motor activity are integral to some transport processes,[21,22] but those regulators operate on systems that are quite complex and whose transport behaviors ultimately determine the range of regulatory options. Processive microtubule motors do not possess the characteristics for ideal and robust collective function under all circumstances, but this may actually serve to increase their versatility.

1.1. Experimental methods and systems

A diverse array of experimental systems have been developed to study multiple-motor biophysics, from fully synthetic systems to those isolated from living cells to recombinant proteins *in vivo*. The different classes of systems address

different classes of questions: synthetic in vitro systems offer the most control and are used to resolve fundamental biophysical properties of multiple motor systems in the absence of confounding effects from additional proteins and physical obstructions in the cellular environment; systems isolated from living cells naturally have the advantage of reflecting the composition and structure of those *in vivo* while maintaining in vitro levels of precision in measurements; the study of motor proteins *in vivo* is certainly the most challenging endeavor, but it is the ultimate goal and has already yielded insight into fundamental behaviors of multiple-motor systems.

A large number of current in vitro systems are clever extensions and variations on the classical gliding assay, in which motors are deposited on the coverglass surface with their motor domains extending upward so that they contact microtubules or actin filaments and walk along them, causing them to "glide" across the surface. The concentration dependent density of the deposition of motors affords control over the average number of motors interacting with a filament. Using such an assay, the performance of these systems can be characterized in terms of the velocity and directionality of motion of the microtubules, often measured by TIRF microscopy. Bieling et al. were able to show that molecular friction between kinesins, observed as a decrease in gliding velocity, decreases as the length (and therefore the compliance) of the individual motor stalks increases.[23] More recently, the same group discovered a surface density dependent switching in the directionality of the tetrameric kinesin Cin8.[24] The displacement sizes of microtubules can be resolved as well,[25] though this usually requires the use of low

(non-physiological) ATP fuel concentrations. A novel antagonistic system has even been described that joins antiparallel filaments using bivalent anti-tubulin antibodies, allowing standard assumptions about the distribution of loads between the motors and their resultant detachment behaviors to be tested,[26] with the caveat that these tests only evaluate the internal consistency of assumptions about motor force-velocity, binding, and detachment, as none of these parameters are directly measured.

Force production and run length in multiple-motor systems are of great interest as a potential example of a gain-in-function over and above the capabilities of a single motor and for its role in bidirectional transport. Accordingly, a number of groups have assembled multiple-motor systems on polystyrene beads so that their cargo transport performance could be measured.[12,15,27,28] In the simplest case, these multiple-motor systems are assembled at random in much the same fashion as those in the gliding assay: motors are anchored to the bead at random positions, and the average number of motors that engage a filament is controlled by the concentration of motors incubated with the beads. Poisson statistics is combined with measurements of the motile fraction of beads as a function of motor concentration to calibrate the assay. Beeg et al. and Mallik et al. follow this methodology to study transport by multiple kinesins and cytoplasmic dyneins, respectively,[15,28] and report trends of increasing run length and force production in an optical trap with increasing motor number for both motor types, though the absolute number of motors interacting with the microtubule at any given time remains unclear in these assays given the random arrangement of motors on the

bead. Schroeder et al. recover a similar result for a competitive system of dynein and myosin V, finding that the probability of a bead switching from microtubules to actin filaments and vice versa depends on the relative number of dyneins and myosins deposited on it.[27] The challenge of controlling motor number was addressed synthetically by Rogers et al. and Jamison et al. by creating recombinant kinesin constructs that can be targeted to DNA, which serves as a controlled-length linkage between the motors.[10,12] This is highly advantageous because a multiple-motor system that is synthesized in high yield can be studied in the single-molecule limit with the same certainty as a single motor. These studies point strongly to a weaker dependence of run length and force production on motor number in systems of multiple kinesins.

Vesicles and membrane-bound organelles have been isolated from cell extracts and studied in vitro rather than in their normal intracellular settings. Hendricks et al. used this methodology in tandem with analogous experiments in the axons of live neurons to substantiate a biophysical basis for bidirectional motion of neuronal vesicles.[29] The field of multiple-motor biophysics will need to make increasing use of this in order to separate behaviors originating from complex dynamics from those that are the result of regulatory factors in the cytoplasm.

Standard techniques in molecular cell biology have been proven to be quite powerful unto themselves as well as in combination with other biophysical tools. These techniques are most often helpful when used to modulate the number and type of motors associated with cargos. Shubeita et al. used drosophila embryos that

were heterozygous for an inactive, mutant kinesin to show that lipid droplet transport in these cells is insensitive to the expressed amount of wild type kinesin.[18] Ally et al. used RNAi to establish that both kinesin-1 and cytoplasmic dynein are required together for either to function properly in S2 cells, but that if one that is removed is replaced by a different motor of the same directionality, function of the other is recovered.[17] Kapitein et al. developed a new tool for dynamic motor targeting to specific organelles, synthesizing technologies from several other reports into a technique that could allow an experimentalist to observe the transport behavior of cargos prior to and after the association of a motor or motors of a particular type on a much faster timescale than protein expression.[20] To further advance the field of multiple-motor biophysics, it will be equally important to measure motor number as it will be to change it. Hendricks et al. used quantitative photobleaching analysis of GFP-motor fusions in live cells corroborated with quantitative western blotting on purified vesicles to estimate the number of motors of each type present.[29] This type of information makes it possible to test model predictions without the confounding interplay between motor number and binding, detachment, and stepping rates.

1.2. Characterizing properties of multiple-motor systems

Individual molecular motors can be described biophysically by a limited set of fundamental properties: step size, step frequency, and dissociation rate. Step frequency and dissociation rate are robustly load-dependent, though step size can be also for some motor types. These properties have been measured extensively for

the many motor types, generally by tracking the motions of their cargos, either unloaded or under known applied loads in an optical trap. Multiple-motor systems can be probed in a similar manner, but interpreting the results can be much more complicated than in the single-motor case, due largely to the mechanical and geometric properties of the system.

1.2.1. Multiple-motor 'step' sizes

When a single motor steps against either no load or a constant load, the displacement of the motor's "center of mass" and the displacement of any cargo that it carries are the same. Since the motor walks along a lattice, these displacements occur in units of lattice size, e.g., an 8.2 nm step for kinesin corresponds to the size of a tubulin subunit within a protofilament. These full lattice steps are observed both in vitro and *in vivo*,[30] and are often taken as compelling evidence that only one motor is present on the cargo. As discussed below, this is not necessarily the case, nor is it true that an attenuated or fractional step size absolutely means that multiple motors are present if the cargo is under a variable load.

One might expect that a step of one motor in a team of two transporting a cargo would result in a cargo displacement of one half of the motor's step size because a full step size displacement would stretch the motor that did not step without affecting the one that did; the cargo seemingly should average the motions of the motors transporting it. This is, in fact, what was observed by Leduc et al. in their gliding assays when exactly two kinesins, labeled with GFP, transported a microtubule: the microtubule advanced forward in discrete 4 nm steps, as opposed

to the 8 nm steps observed when only one kinesin was bound.[25] This finding was corroborated by Rogers et al. using their synthetic, DNA-coupled two-motor system.[10] Results like these fuel the expectation that cargo displacement sizes can be used as simple metrics for motor number, with a unitary step size indicating one motor, a half step size indicating two, one third indicating three and so on, but this conjecture has severe limitations.

When single molecular motors are interrogated in a static optical trap, the load they experience increases as the motor pulls its cargo. As the load increases, the motor stretches along its stalk, causing the cargo to displace less than the motor's filament bound heads. Attenuated step sizes are thus produced, and the degree of attenuation depends on the compliance of the motor, but in principle, any step size between zero and the unitary step size is possible.[12] Therefore, in settings where variable loads may be present, non-unitary cargo displacements are not an unambiguous signature of multiple motor transport.

Step sizes are a function of both load and system geometry in a multiple-motor system. In the step size experiments mentioned previously, the motor systems being studied were inherently symmetric because they were linear; apart from the motors being separated in physical space, there was nothing to distinguish them or the loads they experienced. This is quite different from the geometry seen when two or more motors pull a cargo *in vivo*. When piconewton-sized or even subpiconewton (e.g. viscous) loads are imposed on a cargo, it trails the motor or motors pulling it.[12,16,32] Depending on the separation between the motors on the

microtubule, the motors may share the load equally, or a motor in front may bear the majority (or all) of the load.[12,16] The step size and compliance of that leading motor would dominate the step sizes observed from the cargo; motors that bear no load do not produce any motion of the cargo, giving them an apparent step size of zero. In this way, the presence of additional motors can be masked by geometry in the distribution of cargo displacement sizes.

1.2.2. Cargo run lengths

A 'run' of a cargo begins when a motor on it binds a filament and begins walking along it, and ends when all of the motors have detached from the filament. Practically speaking, runs are observed as processive, directional motions of cargos between periods of diffusive motion (all of which, of course, must be identifiable). The distribution of run lengths produced by a single molecular motor is a function of two parameters: the motor's velocity and its detachment rate from the filament. Because detachment under a constant load is a stochastic process that occurs with equal probability in any equivalently-sized time window (i.e., the motor has the same probability of detaching in the second 100 ms of its run as it did in the first, if it gets that far), run time distributions of single motors are exponential in character, with a decay constant that is equivalent to the average detachment rate. This decay is a decay in the population of motors that remain bound at longer and longer times, which helps to explain why a run time of zero is most common because, initially, all motors are bound. It is important to remember that "average" and "most common"

are not the same when dealing with run times, and that a run time of zero is not measurable. Run length is equivalent to run time multiplied by average velocity.

Runs of multiple-motor systems are a bit more complex than those of single motors. They begin with the binding of a single motor to the filament, and continue with the possibility of any of the motors binding and detaching so long as at least one remains bound. This means that the average number of filament-bound motors can vary through a run, which means that unlike the case of a single motor, the cargo's average detachment rate is not necessarily uniform in time. Klumpp et al. solved this problem theoretically and found that the run length distribution of an N motor system should be a sum of N exponentials, and that the average run length of the system should increase exponentially with increasing N.[14] The rate of this exponential increase was found to be proportional to the affinity (the ratio of the binding and detachment rates) of the individual motors in the system.

The binding of a multiple-motor system to a filament can be thought of in the same terms as multivalent ligand-receptor binding. The binding of each of the individual motors in the system has an intrinsic affinity, but the observed affinity of their binding is also a product of any energy of interaction that arises when multiple motors are bound simultaneously.[31] The standard literature value for kinesin's microtubule binding rate is taken from a lipid membrane pulling experiment, in which the binding of kinesins on a lipid membrane nanotubule positioned over a microtubule could diffuse along the surface of the membrane and bind to any site along the microtubule.[32] Because the motors could diffuse along the membrane,

there was no mechanical energy cost to their binding to any microtubule binding site. In contrast, if the motor/cargo system must stretch for two motors to reach two respective binding sites, then the binding rate of the system into that pair of sites is reduced exponentially by the strain energy in that configuration.[11] Since detachment rates can be measured in an optical force clamp, the attenuation of motor binding rates can be derived using detailed balance if the energies of the system in the different bound configurations are known. The stiffer the system, the more energy is stored in each bound configuration and the lower the binding rate is, and, in turn, the lower the affinity and run lengths are. The shorter-than-expected run lengths observed in Rogers et al. can be explained by a quantitative model based on this reasoning.[11]

One clear difference between a system of motors on a cargo and a multivalent receptor is that, once bound to the microtubule, the motors step in a manner that is generally believed to be asynchronous.[10,12,32] Asynchronous steps cause the motors' on-filament spacings to change, and the system strain energy along with it. The model mentioned above found that while asynchronous stepping does decrease a system's microtubule binding affinity by increasing its detachment rate, this decrease is small relative to the decrease in affinity that occurs from binding rate attenuation.[11]

1.2.3. Cargo velocities

A cargo propelled by multiple motors moves with a velocity that is equal to the sum of the stepping rates of the attached motors times the cargo 'step' sizes that

the motor steps induce (see the previous step size section). Both motor stepping rates and cargo displacements are dependent on the sharing of any load between the motors. When a load is not shared, the motor bearing that load determines the velocity of the cargo because its steps are the only steps that induce cargo displacement.[11,16] Non-load-bearing motors will certainly step faster than load-bearing ones, but they do not add to cargo velocity. When a load is shared, cargo step sizes are approximately fractional (under a constant applied load) and the motors step at a higher rate than in the case of the single load-bearing motor. A simple, approximate way to compare the two extremes is to say that, in the load sharing case, there are *N* motors that each produce one *N*th of a unitary cargo displacement at the rate those motors step when carrying one *N*th of the load. Since the first two parts of that statement cancel one another out, the cargo velocity is just approximately what it would be if one motor were present under one *N*th the load, which is not really very surprising. However, the myriad possibilities between these two extremes are less trivial and have a substantial effect on the dynamics of the system.

1.3. Multiple-motor load sharing and cooperativity

The capability of a multiple-motor system to share the load on its cargo either unequally or equally between the constituent motors adds a great richness to its transport behavior and a great deal of complexity to the biophysics that must be developed and used to understand it. Load sharing affects every observable transport parameter discussed in the previous sections: motor teams that share

their load generate fractional steps sizes, longer run lengths, and pull their cargos faster than ones that do not. In short, the extent to which a load is shared within a multiple-motor system determines the extent to which the behavior of the system is distinguishable from the behavior of a single motor.

A cargo being transported by multiple motors under load is a dynamic, three-dimensional mechanical system; the internal distribution of loads is determined by the points at which the motors anchor to the cargo and the filament. The further a motor leads its cargo, the more it must elastically stretch to reach both the cargo and the filament, and the greater the force it experiences.[13,16] Therefore, the more one motor leads its partner or partners, the greater the portion of the load it assumes. The filament lattice makes the possibilities for inter-motor separation discrete, such that a leading motor can be one, two, three, or more lattice sites ahead of its nearest partner, and the next motor could lead the third (if it exists) by some integer number of sites, etc. Each set of relative on-filament positions of the motors on a cargo has a unique internal distribution of loads and can be accessed from other relative motor positionings through different combinations of motor binding, detachment, and stepping events. We will refer to these inter-converting on-filament motor configurations as "microstates" because they represent a refinement of the concept of the state of a cargo being defined by the number of motors on its surface. Observed average transport behaviors reflect a weighted average of the behaviors of the microstates accessed by the system. The probability that the system will be found in one microstate or another is therefore of central concern to the field of multiple-motor biophysics.

A multiple-motor system's preference for one class of microstates (i.e., load-sharing vs. non-load-sharing) arises at least in part from the fundamental properties of the motors that make up the system, all of which vary by motor type. The rate of filament binding determines the extent to which the motors in a system engage, but strain energy and detailed balance dictate that binding occurs into non-load-sharing microstates.[13] Once a trailing motor is bound, the distance between it and its leading partner narrows according to the difference in their stepping rates as determined from the loads they bear and their force-velocity relationship(s). Detachment of either motor aborts this process, and detachment is most probable in non-load-sharing configurations. If multiple-motor systems composed of motors of a particular class fail to reach load-sharing configurations, then that class exhibits negative-cooperative behavior with respect to increases in motor number: the force production and run length properties of these systems is less than the sum of the parts. If the same motor systems were to attain load-sharing configurations and exhibit additive properties, the motor class' cooperation could be said to be non-negative (neither negative nor positive). True or "positive" cooperativity in this definition then requires an actual enhancement in the activity of the constituent motors when acting in a group. Evidence for positive cooperativity in multiple-motor systems exists for kinesin motors in vitro, both in the absence and the presence of load.[12,33]

1.4. Spatial and temporal dependence of loads

The loads transmitted to motor teams *in vivo* are not carefully controlled as they are in the optical force clamp *in vitro*. Viscous loads may remain steady for relatively long times, but the influence of a sudden obstacle or a newly-bound opposing motor team is to rapidly change the load imposed, and the response of a multiple-motor system to these changes is more complex than that of a single motor. In the simplest case, the response of a single motor is to instantaneously alter its properties to those measured in the optical force clamp under the same applied load, though as with all single-molecule associations, the possibility of enhanced affinity (decreased microtubule detachment rate) remains as loading rate increases.[34] In contrast, the distribution of microstates assumed by a multiple-motor system can evolve in time as loads on the motors change and the average separation between them narrows or widens as a result. When working against a rapidly increasing load, the system is caught in configurations inherited from lower loads because it did not have time to reach the configurations it would prefer to adopt at higher loads. Depending on the rate of increase in the applied load, these holdover configurations from lower loads can substantially increase the system's detachment rate (lower affinity), in opposition to the trend observed with single molecules.

A spatially-varying applied load adds more complications. When a motor team pulls a cargo against an elastic resistance, like another motor or motors, or the cargo itself when it is obstructed, the load imposed on the motors has a spatial dependence. In such cases, detachment of one of the motors in the system will cause

a relaxation and a decrease in the load, potentially giving the system a chance to recover. Since detachment is faster in non-load-sharing microstates than in load-sharing ones, these events tend to deplete non-load-sharing configurations at high applied loads,[12] yeilding a higher apparent cooperativity. While this is true, it is important to remember that it does not correspond to a net increase in cooperative behavior against the elastic load as a whole because it is achieved through a relative rather than absolute increase in the abundance of load-sharing microstates.

1.5. Response of motor types

The basic dynamics that drive multiple-motor systems to load-sharing microstates and vice-versa provide clues as to how cooperativity might be distinguished between motor types with different stepping mechanics and rates. The convergence of a multiple-motor system to load-sharing is driven by differences in the stepping rates of its load-bearing and non-load-bearing motors; if the force-velocity relationship for a particular motor type dicates that its sensitivity to load is high, it would be predicted to exhibit greater cooperativity than a motor type with a low sensitivity to load. Conventional kinesin and cytoplasmic dynein produce similar velocities in the absence of load, but most optical trapping experiments to date suggest that dynein's velocity falls much more rapidly than kinesin's as load increases,[35] a fact which has been interpreted to mean that the presence of multiple kinesins on a cargo would make it virtually impossible for it to display retrograde transport behavior. However, several theoretical, *in vitro*, and *in vivo* studies demonstrate kinesin's tendancy for highly negative cooperativity[10-13,16,18], while

dynein's mechanochemistry should dispose it to more non-negative cooperativity, though direct experimental evidence for this is still lacking. The fact that the stoichiometries of these motors on neuronal vesicles that move bidirectionally pit a single kinesin against seven dyneins nevertheless suggests that dynein's strength in groups is additive (non-cooperative).[29] It seems plausible that an anti-correlation between motor strength and cooperativity would increase the relevance of weaker motors and would make their number on cargos the more sensitive parameter for the cell to tune.

1.6. Future challenges and opportunities

The future of multiple-motor biophysics lies in accurately and fully characterizing systems *in vivo* so that their behaviors can be compared to those observed *in vitro* with the same or similar systems. These characterizations must center around independent, quantitative measurements of motor number that do not rely on assumptions about the very behaviors in question. This problem is a synthetic problem; high-yield, unitary labeling techniques are in order, and it seems that fluorescent protein fusions may be in a position to deliver, though the imaging performance of these probes leaves room for improvement. The ability to modulate motor number to study its effects within the same setting will also add valuable information and provide a much more complete picture.

Ultimately, understanding these behaviors means being able to reconstitute them in a model. The reason microscopic treatments of geometry and strain energy

are important is that not only do they affect multiple-motor behaviors, they are inconsistent from system-to-system and could be mistaken for non-physical phenomena. It is difficult to extract information about the mechanical properties of a system from the quality of data that can be currently obtained *in vivo*, so it is probably best done with mimetic *in vitro* systems at present. Developing the ability to predict motor affinities and binding rates in different *in vivo* settings should be a primary goal for the biophysical community moving forward as it essentially determines the extent of all other effects.

It will be very interesting to see how the cell leverages the parameters that it has at its disposal to tune the effectiveness and behaviors of multiple-motor systems. Accomplishing this feat will be meticulous and challenging, but a framework and tools now exist to begin to address the last layer of questions.

Chapter 2

Coupling between Motor Proteins Determines Dynamic Behaviors of Motor Protein Assemblies

Transport of intracellular cargos by multiple microtubule motor proteins is believed to be a common and significant phenomenon *in vivo*, yet signatures of the microscopic dynamics of multiple motor systems are only now beginning to be resolved. Understanding these mechanisms largely depends on determining how grouping motors affects their association with microtubules and stepping rates, and hence, cargo run lengths and velocities. We examined this problem using a discrete state transition rate model of collective transport. This model accounts for the structural and mechanical properties in binding / unbinding and stepping transitions between distinct microtubule-bound configurations of a multiple motor system. In agreement with previous experiments that examine the dynamics of two coupled kinesin-1 motors, the energetic costs associated with deformations of

mechanical linkages within a multiple motor assembly are found to reduce the system's overall microtubule affinity, producing attenuated mean cargo run lengths compared to cases where motors are assumed to function independently. With our present treatment, this attenuation largely stems from reductions in the microtubule binding rate and occurs even when mechanical coupling between motors is weak. Thus, our model suggests that, at least for a variety of kinesin-dependent transport processes, the net 'gains' obtained by grouping motors together may be smaller than previously expected.

2.1. Chapter summary

This chapter describes a model that I developed to explain experimental data collected by my colleague, Arthur R. Rogers. This data and the model are published separately in the *Journal of Physical Chemistry and Chemical Physics*. Dr. Anatoly B. Kolomeisky and his student, Rahul K. Das, provided the model's conceptual framework. My work in extending the model was informed by numerous conversations with Dr. Kolomeisky. Dr. Michael R. Diehl (my thesis adviser) and I developed the published manuscript collaboratively.

Kinesin-1 is a motor protein that walks in a hand-over-hand fashion along polar filaments called microtubules, hydrolyzing one ATP per step. Kinesins attach to and detach from microtubules stochastically. The process of a kinesin binding a microtubule, walking a distance, and then detaching is called a "run ", the distance traveled a "run length", and the time of attachment a "run time". Because its

detachment is a stochastic process, kinesin does not have a unitary run length or run time, but instead (over many runs) produces a statistical distribution of run lengths. This distribution decays exponentially, with the most common run length being zero. The exponential rate constant describing the decay of the run time distribution is the average rate of the motor's detachment. This quantity is of central importance when trying to understand the transport behavior of individual motor proteins.

The dynamics of systems of multiple, mechanically-coupled motor proteins is more complicated. So long as one motor remains bound to the microtubule, the entire system is held in proximity and progresses forward, continuing the run. Motors can bind to and detach from the microtubule any number of times until they all happen to be detached simultaneously, whereupon the run ends. Depending on what the average rates of attachment and detachment are, the system could produce substantially longer runs than individual motors of the same type.

To study these behaviors, we designed and synthesized a system of two recombinant kinesins that were mechanically coupled through an assembly of artificial protein and DNA. The system was labeled with a quantum dot and tracked as it walked along microtubules via total internal reflection fluorescence microscopy (TIRF-M). The run lengths produced by the system and by individual motors were extracted from the TIRF-M data and analyzed.

Surprisingly, the two-kinesin complexes showed only a modest enhancement in their run lengths above the run lengths produced by single kinesins. Initially, we

attempted to explain this as the result of internal forces within the assembly that increased the detachment rates of the motors drastically when both were bound. These forces arise because the motors step asynchronously, meaning that the distance separating them fluctuates. Because the motors were mechanically coupled, fluctuations in separation distance would lead to forces within the system that would tend to restore it to its preferred, unstrained separation distance. The difficulty we faced was that the magnitude of the average internal force needed to explain our run length data, given the published estimate of kinesin's binding rate, seemed implausible. Such forces (approximately half of kinesin's stalling force) would surely affect the complex's velocity, yet the average velocity measured in assays was nearly identical to that of single motors.

The mechanistic description above fails because it is incomplete. While internal forces can certainly increase the detachment rates of assembly motors, the work that an unbound motor is required to do against these forces when binding the microtubule reduces its binding rate. The reduction with increasing system stiffness is precipitous and is sufficient to explain the run lengths observed in our experiments when incorporated into a transition rate model that treats the various bound configurations of the system explicitly. This model is described in detail in this chapter.

2.2. Introduction

The transport of organelles and other sub-cellular cargos along polymeric cytoskeletal filaments is critical to mechanisms that regulate the internal organization of eukaryotic cells. These processes are largely driven by molecular motor proteins, active enzymes that consume ATP as fuel in order to produce the mechanical work necessary to propel sub-cellular commodities within the viscous and highly crowded environments of cells. In recent years, significant attention has been devoted to studying biophysical and biochemical properties of single motor proteins such as kinesins, dyneins and myosins.[36] Yet, there are numerous examples where intracellular transport processes are driven by collections of multiple motor molecules. [18,32,37-39] It is often assumed that grouping motors should yield significant gains in motor functionality (*i.e., increased travel lengths, higher force production capabilities, and greater velocities under load*). However, critical issues surrounding multiple motor mechanics have not been resolved, and the precise dependence of most transport parameters on the number of motors responsible for cargo motion remains unclear.

Recent assays and analyses of multiple motor behaviors have become increasingly sophisticated, and have further highlighted the role collective motor mechanics plays in intracellular transport.[8,25,32,36,37,40,41] Nevertheless, transport parameters are often found to depend differently on the number of motors bound to cargos, and in particular, there are significant distinctions between reported *in vivo* and *in vitro* collective behaviors of motor proteins.[15,18,38] Optical trapping

experiments have shown that beads coated with multiple kinesins can produce higher forces than those outfitted with single motor molecules.[38] In the same study, cargo run lengths are also found to increase substantially when multiple motors are present. Yet, much less pronounced run length enhancements are observed in other *in vitro* experiments possessing a similar assay format,[15] which leaves questions about the extent to which motors 'benefit' from functioning together. Furthermore, *in vivo* assays of lipid droplet transport that incorporate methods to carefully manipulate and examine the net levels of motors bound to cargo surfaces have shown that neither cargo velocity nor the run length distributions change appreciably with motor copy number.[18] Instead, droplet particles carried by multiple motors were found to move with slightly lower velocities and somewhat smaller run lengths than when single kinesins were responsible for transport. To date, these distinct results have not been reconciled. It may be that the different behaviors observed *in vivo* and *in vitro* stem from unknown regulatory or environmental factors that reduce the enhancements gained by the collective function of motors. However, there are still critical questions regarding the fundamental principles governing the action of multiple motors that must be addressed in order to justify this explanation.

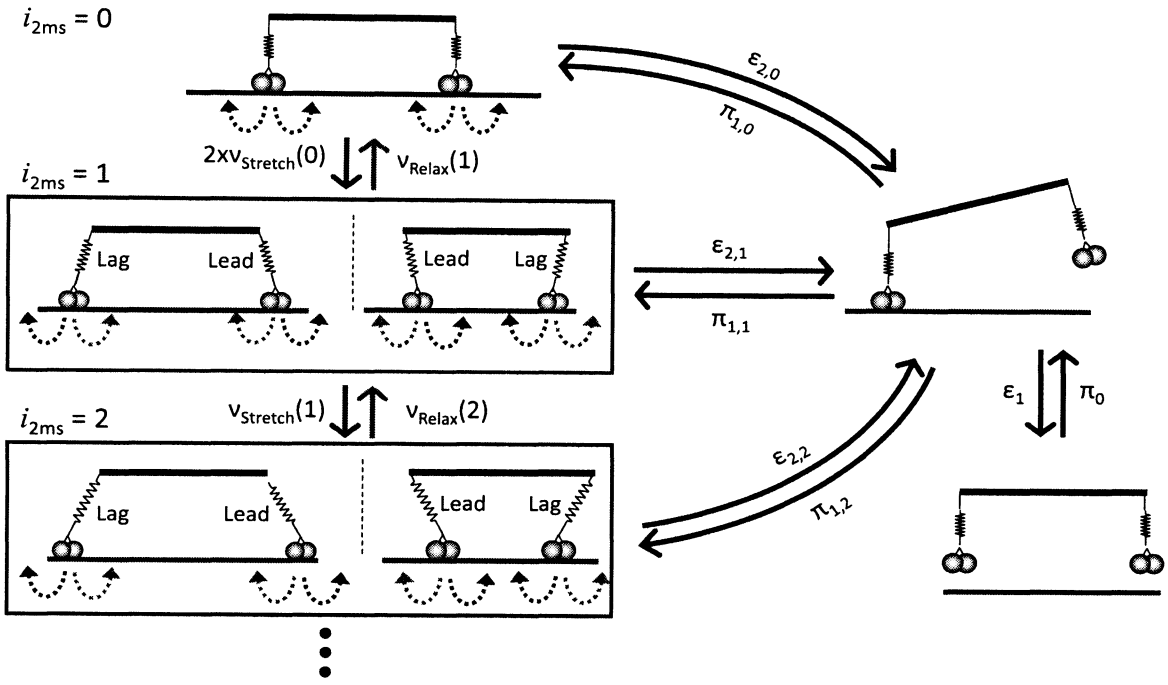

Figure 2.1 - Schematic representation of the discrete state transition rate model.
Degenerate two-motor-bound microstates, enumerated by the index i_{2ms}, are boxed. In each microstate, the leading and lagging motors feel opposing and assisting loads, respectively. A forward step of the leading motor or a backward step of the trailing motor leads to the microstate i_{2ms}+1, while a forward step of the lagging motor or a backward step of the leading motor leads to the microstate i_{2ms}-1. Microstate transitions involving motor stepping are indicated by the solid arrows. The stepping of individual motors is denoted by the dashed arrows. The color coding indicates relationships between the individual motor stepping events and their respective assembly microstate transitions. When i_{2ms} = 0, all steps lead to i_{2ms} = 1, and $v_{Stretch}$ = v_{Relax}. The motors unbind out of each i_{2ms} microstate into the single-motor-bound state with a rate $\varepsilon_{2,i}$ and rebind with a rate $\pi_{1,i}$. The single-motor-bound state transitions to the fully unbound state with a rate ε_1, which rebinds with a rate π_0.

Current understandings of multiple motor function have been advanced by recent theoretical efforts.[14,42,43] Specifically, a theoretical framework for understanding mechanisms of cooperation between motor proteins has been developed by Lipowsky and coworkers.[14] In their approach, a cellular cargo is

driven by a system of motor proteins that can independently bind to or unbind from their microtubule track, and do not interact in any fashion. The system therefore remains associated with the microtubule for longer periods of time, yielding run length enhancements. While this is almost undoubtedly qualitatively correct, it seems that the model's quantitative predictions do not explain the diversity of responses reported. Notably, the effects of the structural and mechanical properties of cargos and the linkages that connect motors together are not taken into account, which could influence the lifetime over which a cargo remains attached to a microtubule. Such factors are widely recognized as being important to a host of non-motile, multi-valent biochemical systems, and have been incorporated into more recent computer simulations of multiple motor dynamics.[43] In addition, new data from our laboratory provides more conclusive evidence that interactions between assembly motors alter collective behaviors.[10] Thus, a more comprehensive description of the mechanics and dynamics of multiple motor systems might provide an explanation for experimental observations.

In this paper, we present a new theoretical treatment of multiple motor dynamics that explicitly takes into account mechanical coupling between motors. Using a model experimental system of two coupled kinesin-1 motors as a test case,[10] a solvable discrete state transition rate model of multiple motor dynamics is described that incorporates the relationships between the structural / mechanical properties of multiple motor systems and the rates at which those systems transition between different microtubule-bound configurations (microstates). In agreement with our prior report, we show that the density of microstates where

multiple motors drive cargo motion simultaneously can be substantially reduced by interactions between kinesins. These interactions are parameterized as distance-dependent strain energies that arise when two motor must stretch in order to reach their respective microtubule binding sites. The presence of strain energy reduces average cargo run lengths since it results in enhanced motor detachment rates, but also, attenuated motor binding rates. Considering that motors will be coupled together elastically on many biological cargos, our work indicates that fundamental features of multiple kinesin dynamics dictate that cargo transport by multiple kinesins will often be insensitive to kinesin copy number.

2.3. Discrete state transition rate model

2.3.1. Model definitions and assumptions

A successful model of multiple motor dynamics must be capable of correctly predicting the relative probabilities of the different configurations in which a system of motors can be bound to its filament track. The microstates available to a system of motors can be generically classified by the number of microtubule-bound molecules (i.*e., 0, 1 or 2 bound motors in a two-kinesin assembly*). As in the previous work,[10] we assume that assemblies will transition between these microstates via the binding and unbinding of a single motor within the multi-unit system (Fig. 2.1). When modeling a system of motors that do not interact, transition rates involving motor detachment can be expressed as $n \bullet \varepsilon_1$, where n is the number of bound motors prior to detachment, and ε_1 is the single motor detachment rate. Similarly, motors

attach to the microtubule at the single motor binding rate π_0. We consider a transition rate model that relies exclusively on these assumptions to be a '*base-case*' or foundational model that serves as a benchmark to assess the effects of inter-motor communication. To be consistent with the treatments of multi-unit (valent) biochemical systems (*e.g., multivalent ligand-receptor complexes*),[31] we now refer to model predictions derived with these assumptions as collective, but non-cooperative behaviors. The average energy of the bond between a motor and a microtubule in a multi-unit system is identical to that of a single motor, and grouping motors results in neither a net loss, nor a synergistic gain in affinity on a per-motor basis.[44]

The present model is designed to account for basic structural and mechanical properties of assemblies of molecular motors and to allow their relative roles in collective motor function to be assessed. As a test case, we examined the collective dynamics of a structurally-defined motor system composed of two human kinesin-1 motors that we previously developed and studied at the single-assembly level.[10] Motors in this system are organized along a linear molecular scaffold formed from a 50 nm long duplex of DNA. The DNA scaffold in these systems is presently treated as a rigid rod (the persistence length of DNA is 50 nm), while the motors are modeled as linear springs with a specified elastic spring constant (κ_{motor}). The motor linkages can therefore stretch and relax, allowing the assemblies to adopt an array of different microtubule-bound configurations that are differentiated by the spacing between the sites at which each motor is bound to its filament track (Fig. 2.1). Each configuration of the assembly is enumerated by our model, and is assigned an

integer (i_{2ms}) that describes the number of 8 nm distance units that the system is away from an assembly microstate where the net force on each motor is zero (*i.e., the base-case microstate where* i_{2ms}=0, *and the strain energy is zero*). When both assembly motors are microtubule-bound, we assume the motor system can transition between these microstates via asynchronous motor stepping, although collective behaviors assuming synchronous stepping were also examined for comparison. Importantly, asynchronous steps change the distance between binding sites of the motors, whereas synchronous steps do not (i_{2ms} *is determined by the binding / unbinding of motors exclusively*). The present treatment also assumes the DNA linkage is always at the same vertical distance from the microtubule, and that all configurations are symmetric with respect to the axis perpendicular to the link and contains its center point (see Fig. 2.1). This assumption seems reasonable, as kinesins have been shown to maintain their cargo at a specific height above a microtubule during transport (~ 17 nm).[45]

Elastic deformations of motor assemblies will cause the free energy of the system to change in time. In the present model, the energies associated with these deformations depend on: (1) the composite elastic compliance of the motor assembly ($\kappa_{assembly} = 2\kappa_{motor}$, assuming a net serial spring behavior), and (2) the distance that their linkages are stretched from their equilibrium position (x_i). Each assembly motor can experience either an assisting or opposing force depending on their positions relative to the relaxed, base-case configuration of the assembly (*i.e., they can lead the motion of the assembly or lag behind*). Configurations possessing identical energies are considered to be degenerate; in the absence of an applied

load, the "stretched" and "compressed" configurations possessing the same i_{2ms} are treated as identical with respect to strain energy (*these groups of microstates are boxed together in Fig. 2.1*). In general, states where i_{2ms} is large are considered to be high-strain configurations that introduce energetic costs to the system.

The influence of strain energy on kinetic transitions involving motor-microtubule binding and unbinding were treated by specifying a distinct transition rate into and out of each i_{2ms} microstate configuration according to the following equations:

$$\varepsilon_{2,i} = 2\,\varepsilon_1 \exp(\mathrm{F}(i)/\mathrm{F_d})$$

Equation 2.1 - Motor detachment rate dependence on internal force.

$$\pi_{1,i} = \pi_0 \exp\left(-\frac{\mathrm{E_2(i)} - \mathrm{E_1}}{k_\mathrm{b}\mathrm{T}} + \mathrm{F}(i)/\mathrm{F_d}\right)$$

Equation 2.2 - Strain dependence of motor binding rate.

In these expressions, π_0 and ε_1 are binding and unbinding rates for a single (*non-interacting*) kinesin motor. The parameter *F(i)* is the effective horizontal internal force imposed on each motor due to the stretching of the assembly, and F_d is the detachment force,[14] which can be written as $F_d=k_BT/d$. Here, the parameter d can be viewed as the distance between the motor and the microtubule above which the motor is considered to be detached.[46,47] The ratio of forces, $F(i)/F_d$ specifies how strongly the free energy difference between single-bound and double-bound motor

states enhances the unbinding transition.[47] For simplicity, this dependence is assumed to not depend on the vectorial direction of the applied load. The term $E_2(i)$ in Eqn. 2.2 is the strain energy of the two-motor system when both motors are bound: $E_2(i) = \kappa_{assembly} \bullet [(8nm) \bullet i_{2ms}]^2$. Note, that transition rates involving motor binding are governed by the difference in the energies of the assembly when they adopt a microstate where one motor is unbound and its linkages are relaxed ($E_1 = 0$), and those where the assembly must stretch to reach between two specific microtubule sites; we consider the motor bound when the assembly is stretched a distance ($8 \bullet i_{2ms} - d$). Importantly, these transitions are driven exclusively by thermal energy, and therefore, transition rates into microstate configurations possessing high strain energies will be lower than transition rates into microstates where the motor linkages are not stretched far from their relaxed positions. Furthermore, while allowing a more microscopic description of the dynamics of motor protein assemblies to be developed, our treatment of energetic costs associated with the binding and unbinding of assembly motors and transitions between microstates satisfies detailed balance.

Individual motor stepping rates are determined using an analytical solution to a two-state kinetic model of kinesin dynamics.[46,47] This model was chosen over other empirical treatments since it not only captures kinesin's non-linear *F-V* dependence, but it should also provide a framework for future assessments of perturbations to a motor's mechanochemical properties that may arise due to specific forms of inter-motor coupling. Herein, we use this model to specify microstate-dependent forward and reverse stepping rates for the motors ($v_{i,+}$ and $v_{i,-}$

). Although the ATP-stimulated motion of motor proteins along the microtubule is a complex multi-step process, for simplicity, we model motor stepping with only two effective rates, $v_{o,+}$ and $v_{o,-}$. The velocity of an assembly when only one motor is microtubule-bound is calculated using: $V_1 = (8\text{ nm})\bullet(v_{o,+} - v_{o,-})$. Strain energy due to inter-motor coupling when both motors are bound is assumed to influence motor stepping according to:

$$v_{i,+} = v_{o,+}\, e^{\frac{-\theta(E(i+1)-E(i))}{k_B T}}$$

Equation 2.3 - Strain dependence of motor forward stepping rate.

$$v_{i+1,-} = v_{o,-}\, e^{\frac{(1-\theta)(E(i+1)-E(i))}{k_B T}}$$

Equation 2.4 - Strain dependence of motor reverse stepping rate.

where the coefficient θ describes the splitting of the effect of free energy difference on transition rates between microstates. To simplify calculations, we assumed that θ=0.10. Such treatment captures both kinesin's non-linear *F-V* dependence and low probability for backward stepping when the forces imposed on a motor due to inter-motor strain are small ($F_{strain} < F_{stall}$).[48]

The instantaneous velocity of each motor in the system is determined by the difference between their forward and backward stepping rates, defined in Eqn. 2.3 and Eqn. 2.4. However, in order to construct the master equations, we need

expressions for the rates of transition between microstates, which are defined by their energy. In each microstate, either a forward step of the leading motor or a backward step of the trailing motor leads to the i_{2ms}+1 microstate. Conversely, a backward step of the leading motor or a forward step of the lagging motor will lead to the i_{2ms}-1 microstate. We therefore define the transition rates between different microstates as: $v_{stretch}(i) = [(v_{i,+})_{lead}+(v_{i,-})_{lag}]$ and $v_{relax}(i) = [(v_{i,-})_{lead}+(v_{i,+})_{lag}]$.

2.3.2. Estimations of collective transport parameters

Before calculating collective transport parameters of interest, the assumptions described above are first used to determine the relative densities of each relevant microstate configuration of the two-motor system by solving the following master equations:

$$\partial_t \psi_0 = \varepsilon_1 \psi_1 - \pi_0 \psi_0$$

$$\partial_t \psi_1 = \pi_0 \psi_0 + \sum_{i=0}^{N} \varepsilon_{2,i} \psi_{2,i} - (\varepsilon_1 + \sum_{i=0}^{N} \pi_{1,i}) \psi_1$$

$$\partial_t \psi_{2,i} = \pi_{1,i} \psi_1 + v_{stretch}(i-1)\psi_{2,i-1} + v_{relax}(i+1)\psi_{2,i+1} - [\varepsilon_{2,i} + v_{stretch}(i)+v_{relax}(i)]\psi_{2,i}$$

Equation 2.5 - Model master equations.

Here, ψ_n denotes the probability that an assembly adopts a configuration possessing n filament-bound motors. When n = 2, ψ_n gains an additional index (i) which specifies the binding-site distance between the two assembly motors as

described above. In Eqn. 2.5, the density of individual assembly configurations are modulated via motor binding, detachment and stepping.

With predicted microstate densities, the 'effective' rates describing how rapidly an assembly transitions between the general classes of assembly microstates can be calculated via:

$$\pi_{1,eff} = \sum \pi_{1,i}$$

Equation 2.6 - Effective motor binding rate.

$$\varepsilon_{2,eff} = \frac{\sum \varepsilon_{2,i}\psi_{2,i}}{\sum \psi_{2,i}}$$

Equation 2.7 - Effective motor detachment rate.

Here, the 'effective' rate of assembly transitions from single into all possible two motor-bound configurations (i_{2ms} microstates) is simply the sum of all individual enumerated binding rates. The 'effective' dissociation rate of a motor from microstates where both motors are bound ($\varepsilon_{2,eff}$) is taken as the population-weighted average of the dissociation rates out of these microstates, and accounts for the relative probabilities of each unique configuration explicitly. These weightings also influence the average force imposed on each motor ($F_{2,av}$), the average system velocity (V_{av}), and the total effective dissociation rate of a two-motor system (ε_{system})[14] as specified by:

$$F_{2,av} = \frac{\sum F_{2,i}\,\psi_{2,i}}{\sum \psi_{2,i}}$$

Equation 2.8 - Average internal force.

$$V_{av} = \frac{\sum V_{2,i}\,\psi_{2,i} + V_1\psi_1}{\sum \psi_{2,i} + \psi_1}$$

Equation 2.9 - Average velocity.

$$\varepsilon_{system} = \frac{\varepsilon_1}{\left(1 + \left[\pi_{1,\mathrm{eff}}/\varepsilon_{2,\mathrm{eff}}\right]\right)}$$

Equation 2.10 - Average detachment rate.

In Eqn. 2.8, the microstate velocity $V_{2,i}$ is calculated using: $V_{2,i}$ = (4 nm)•{[$(v_{i,+})_{\mathrm{lead}}$ - $(v_{i,-})_{\mathrm{lead}}$] + [$(v_{i,+})_{\mathrm{lag}}$ - $(v_{i,-})_{\mathrm{lag}}$]}. Here, we assume that the motors step asynchronously and use a fractional motor displacement size to account for the stretching of the assembly linkages. Potential enhancements or net-losses in collective motor function relative to the non-cooperative model behaviors can be evaluated by examining the ratios $\pi_{1,eff}/\pi_{1,0}$, $\varepsilon_{2,eff}/\varepsilon_{2,0}$, and V_{av}/V_o, where $\varepsilon_{1,0}$, $\varepsilon_{2,0}$, and V_o correspond to the binding / unbinding rates and cargo velocities expected when motors function non-cooperatively. Similarly, whether the structural / mechanical properties of multiple motor systems lead to deviations from idealized (*non-interacting*) behaviors can be assessed by examining RL/RL_o, where average predicted run lengths in each case are calculated via $RL = V/\varepsilon_{system}$.

Finally, the relative influence of motor stepping and binding / unbinding kinetics on multiple motor dynamics was examined by comparing two-motor microstate distributions and transition rates produced when the motors are assumed to advance either synchronously or asynchronously; synchronous stepping was treated by eliminating stepping transitions between microstates from Eqn. 2.5. In each case, the master equations for the two motor system are defined using measured single-kinesin and collective transport parameters obtained from our previous analyses of two-kinesin run length distributions (Table 2.1).[10]

Measured Constants (Single Motor)		Measured and Predicted Constants (Two Motor)			Mean Field	Discrete Microstate Model
ε_1	0.61 s^{-1}†	$\kappa_{assembly}$	0.025 pN/nm	$\varepsilon_{2,eff}$	~ 4 s^{-1}	1.47 s^{-1}
π_0	4.7 s^{-1}§	$RL_{o(pred.)}$	3.9 μm§	$\pi_{1,eff}$	~ 2.5 s^{-1}	0.67 s^{-1}
κ_{mot}	0.05 pN/nm*	$RL_{(meas.)}$	1.4 μm†	$\pi_{1,eff}/\varepsilon_{2,eff}$	0.625	0.46
$RL_{(meas.)}$	0.83 μm†	-----	-----	F_c or $F_{2,av}$	3.6 pN	0.52 pN
-----	-----	-----	-----	$RL_{(pred.)}$	-----	1.17 μm

† Results from fits reported in reference 10.
‡ Values are calculated assuming motors advance via asynchronous stepping.
§ Non-cooperative run lengths RL_o were determined using equation 2.10, assuming measured two-motor velocities and single-motor detachment rate for ε_1.[14] The 'partial' two-motor detachment rate was calculated assuming $\varepsilon_2 = 2\varepsilon_1$. The intrinsic binding rate π_o is adopted from previous reports.[14,32]
* Determined from optical trapping experiments performed in-house. The elasticity of our polymer linked kinesins actually increases non-linearly with force due to strain-induced stiffening (e.g., κ_{mot} increases from 0.05 pN/nm to approximately 0.2 pN/nm sharply around an applied load of 2.5 pN).

Table 2.1 – Transport parameters

2.4. Results and discussion

Predicted stationary-state distributions of i_{2ms} microstates for a two-kinesin assembly calculated over a large range of assembly (motor) elasticities are shown in Fig. 2.2.

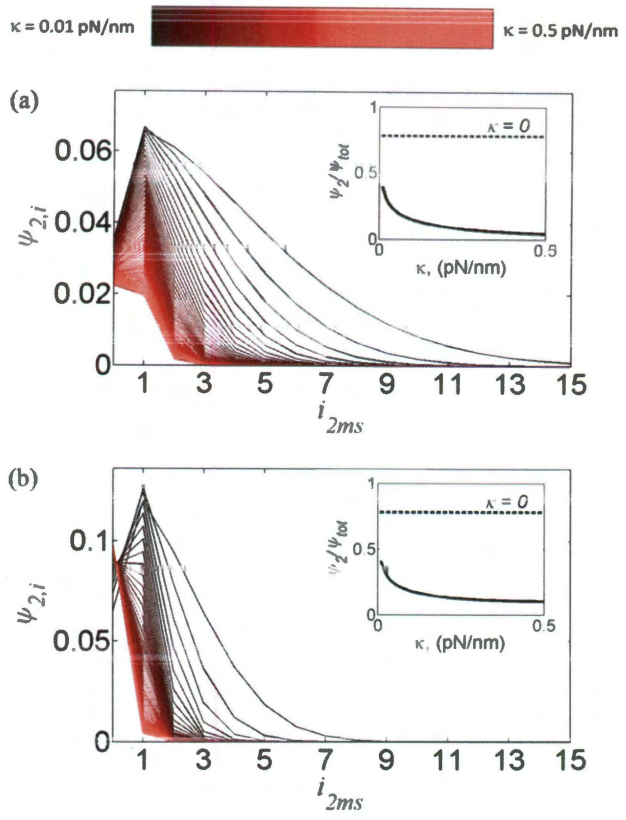

Figure 2.2 - Population distributions of two-motor-bound microstates.
The probabilities that the assembly will adopt the microstates i_{2ms} when motors motors step (a) asynchronously or (b) synchronously for various values of assembly stiffness. The sum of the two-motor-bound microstate populations versus stiffness is shown in the inset.

Two general collective behaviors are revealed by these analyses, both of which appear to be largely independent of the mechanism by which the motors are

assumed to advance forward. First, it is shown that assembly microstates where two motors are filament-bound are much less prevalent than the single-motor-bound configuration ($\psi_1 > \sum \psi_{2,i}$). Furthermore, the total probability that a motor assembly will adopt two-motor-bound microstates ($\psi_2 = \Sigma \psi_{2,i}$) is substantially lower than model predictions where motors behave non-cooperatively, even when the assembly elasticity is small (Fig. 2.2, *inset*). Secondly, as expected, when the assembly is mechanically compliant (*i.e., when* κ_{motor} *is small*), higher probability densities $\psi_{2,i}$ are found for assembly configurations where the i_{2ms} separation distance is large. Yet, for all values of κ_{motor} examined, there is a general tendency for the two motor system to occupy microstate configurations close to the $i_{2ms} = 0$ microstate of the system; note the 'offset' peak as $i_{2ms} = 1$ stems from the fact that there are two degenerate configurations where the motors can be separated by 8 nm from the relaxed state, and that there is only one where the motors do not experience forces due to strain ($i_{2ms} = 0$).

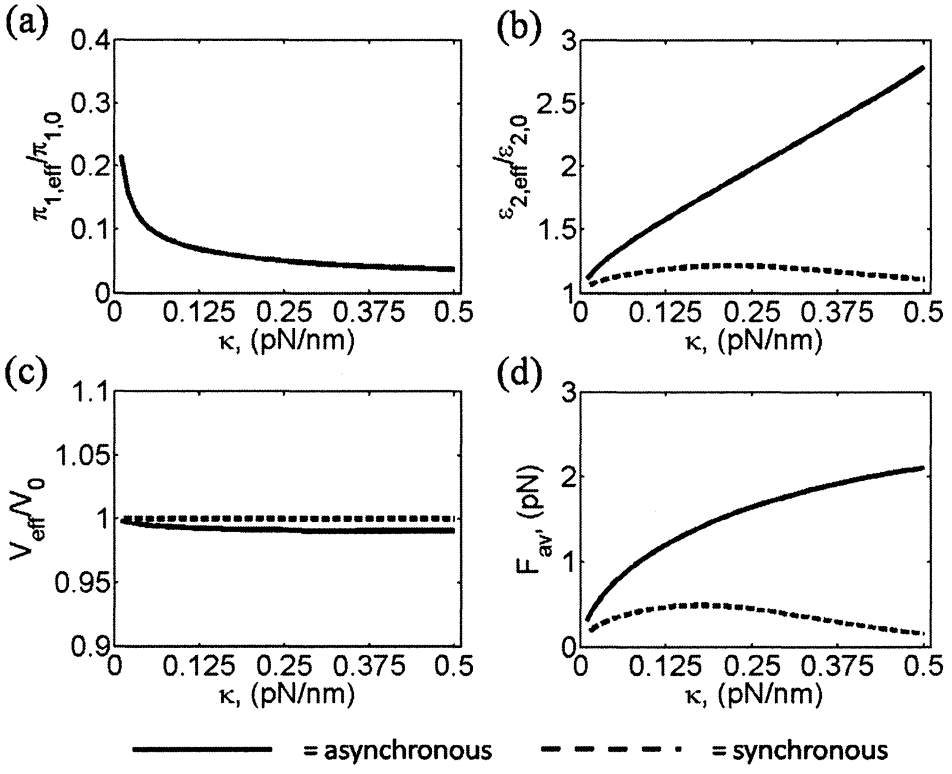

Figure 2.3 - Transport parameters of interest as a function of assembly stiffness.
(a) Normalized effective binding rate, (b) normalized effective dissociation rate, (c) normalized average velocity, (d) average internal force in the two-motor-bound microstates. The solid line in each plot represents the values derived from the model including asynchronous stepping, while the dashed line represents the synchronous case. The dashed line denoting synchronous stepping is not visible in the binding rate plot since it is superimposed on the solid, asynchronous line.

The low probability of assembly configurations where both motors are filament-bound is reflected in the effective binding and unbinding transition rates $\pi_{1,eff}$ and $\varepsilon_{2,eff}$ (Fig. 2.3); $\pi_{1,eff}$ decreases rapidly with increasing κ_{motor}. Such behavior is expected, as a stiffening of motor-motor linkages should reduce the number of sites to which a motor can bind when its partner is already filament-bound. Thus,

the effective concentration of lattice sites available to an unbound assembly motor will be lower in circumstances where they are incorporated into multi-unit assemblies that are rigid compared to those that are more mechanically compliant. While this behavior should not depend on how motors advance once they are filament bound, motor stepping mechanisms are found to play a role in determining the effective detachment rate $\varepsilon_{2,eff}$. When the motors step asynchronously, $\varepsilon_{2,eff}$ is found to increase with increasing κ, and is consistently larger than the values predicted from assumptions of non-cooperative behavior ($\varepsilon_2 = 2\varepsilon_1$). Importantly, this behavior is accompanied by an increase in the average effective force ($F_{2,av}$) experienced by each microtubule-bound motor in the system. Thus, $F_{2,av}$ does not increase indefinitely with increasing κ since i_{2ms} microstates possessing high strain energy become increasingly improbable.

Despite the fact that motors can impose relatively high forces (pN-sized) on one another, the development of these forces appears to have little impact on average two-motor velocities. This result is also explained by the low densities of microstates where two motors are bound, which occurs due to the low binding rates and high detachment rates of the motors within the system, especially for configurations where the i_{2ms} distance is large. Nevertheless, microstate distributions are not governed by motor attachment / detachment kinetics alone. Asynchronous motor stepping behavior is found to increase the probability that the system will adopt configurations with large i_{2ms} separation distances compared to those predicted for a set of synchronized motors. Here, since the motors do not

advance at the same time, there is a finite probability that the motor separation distance that is produced upon motor binding will increase due to the advancement of a leading motor. Thus, stochastic fluctuations in motor stepping can lead to a broadening of the binding site separation distances, and in turn, much higher strain energies. While such behavior appears to be general, the influence of motor stepping on microstate distributions was found to depend on the chosen value of θ assumed in our model for kinesin *F-V* dependence (Eqn. 2.3 and Eqn. 2.4), and was most influential when θ is assumed to be small (*i.e. when low-force, backward stepping rates are nearly negligible*).

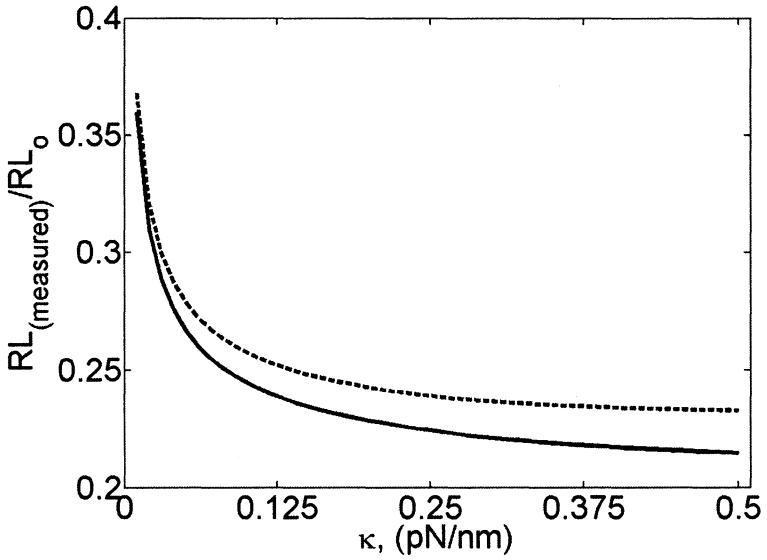

Figure 2.4 - Normalized average run length versus system stiffness.
The average run length of the system as a function of stiffness, normalized by its average run length at zero stiffness, assuming (solid line) asynchronous and (dashed line) synchronous motor stepping. The non-cooperative, base case behavior corresponds to $\kappa = 0$, where $RL_{measured}/RL_o = 1$.

Perhaps most importantly, while the average run lengths are generally expected to increase with increasing motor number, our model suggests that run length enhancements stemming from grouping motors can be attenuated significantly when strain energy influences motor-microtubule binding and detachment. This suggestion is bolstered by the fact that the model predicts the average run length of our experimental system much more accurately than a non-interacting model (Table 2.1). Furthermore, reductions in run lengths compared to non-cooperative behaviors, as indicated by the calculated ratio RL/RL_o (Fig. 2.4), are found to occur despite the assumed mechanism of motor stepping. Such behavior is consistent with the present predictions that the single-motor-bound configuration of the two-motor assembly constitutes the dominant microstate of the system. Thus, unless cargo-motor linkages are exceptionally compliant, the run length enhancements predicted by 'base-case', non-cooperative models of multiple motor mechanics will likely not be realized (RL/RL_o = 0.5 when $\kappa_{motor} \sim 0.005$ pN/nm). Our experimental system in Rogers et. al. consisted of recombinant kinesin motors coupled to a dsDNA spacer through highly compliant elastin domains,[10] and thus likely represents a low stiffness system relative to those found *in vivo*. Furthermore, cargos that are this compliant will still likely exhibit strain-induced stiffening, and therefore, once motors are separated by relatively large i_{2ms} distances, strain energy of multiple motor bound microstates should become significant.

The general agreement between calculated average run lengths when motors advance via either asynchronous or synchronous stepping suggests that transitions involving motor binding can impact collective behaviors more significantly than

motor detachment. This behavior is explained by the tendency for the two-motor system to move with only a single filament-bound motor; the rate for assembly transition out of the 'single-motor' configuration is slow. Accordingly, increases in the 'effective' transition rate $\varepsilon_{2,eff}$ are much less influential since such effects occur in the minority microstates of the system. Thus, even though the average internal force $F_{2,av}$ is much higher in the two-motor system when motors are assumed to step asynchronously, the presence of these forces only results in a slight drop in the average run length and velocity of the system over predictions where the motors advance via synchronous stepping.

Consistent with the model's predictions, we have previously shown that grouping two kinesin-1 motors together does not lead to the run length enhancements expected from non-cooperative model predictions (Table 2.1). Analyses of these experimental results have shown that models assuming non-cooperative behaviors ($\varepsilon_2 = 2\varepsilon_1$) yield inadequate fits to two-motor run length data unless the value for the single-motor binding rate (π_o) is used as an adjustable parameter; agreement is only achieved if the binding rate is much lower than the values that are typically assumed in most reports: $\pi_o \sim 1\ s^{-1}$ instead of $\pi_o = 4.7\ s^{-1}$. Although the lowering of the binding rate appears to be consistent with our present picture of multiple kinesin dynamics, we consider this treatment to be physically unrealistic since some form of inter-motor interactions would likely be necessary to explain such an effect (*i.e. motors should be able to bind rapidly unless there are explicit reasons for the attenuation of their attachment rates; we note that earlier estimates of π_o came from experiments where motors could freely diffuse on their*

cargo (lipid tubules)[32] and although there may be subtle differences in the system geometry that still need to be considered, π_0 is likely approximated reasonably). In our prior report, we attempted to reconcile this issue by assuming that the assembly motors experience a mean-field force due to the stretching of motor linkages when both motors are filament-bound. Here, the forces due to strain, or 'counter-forces' (F_c), were incorporated into the effective detachment rate $\varepsilon_{2,eff}$, and should be considered as a mean-field force developed within the motor system since configuration-dependent forces are not modeled explicitly. It seemed counterintuitive to assume strain energy affects motor binding, and such effects were not included in our analyses. With this treatment, run length data can be fit while using intrinsic single-motor binding rates that appear to be more reasonable ($\pi_0 \sim 2.5\ s^{-1}$). However, such agreement required counter forces that were larger than those generally expected for the experimental system (F_c = 3.6 pN).

2.5. Conclusions

We have developed a discrete state transition rate model of multiple motor dynamics that allows more detailed assessments of how a motor assembly's structural and mechanical properties influence its collective transport. In the present form of this model, such properties are incorporated by specifying strain-dependent motor-microtubule attachment and detachment rates. Compared to treatments where non-cooperative behaviors are assumed, or where a mean-field force is considered to only affect motor detachment, the explicit treatment of strain-

energy in expressions describing the rates at which motors within assemblies bind into and detach from specific microtubule-bound configurations provides more physically realistic predictions of effective rates that assemblies will transition between general classes of microstates (*possessing different numbers of filament-bound motors*). Overall, these analyses show that the enhancements obtained by grouping multiple motors are much less significant than those expected from 'base-case', non-cooperative models. Such behavior is consistent with run length measurements of structurally-defined systems of multiple kinesin-1 molecules, and may also provide an explanation for why kinesin copy number does not seem to influence *in vivo* cargo run lengths appreciably. In both cases, we predict that small systems of kinesins will most commonly transport their cargo primarily via a single microtubule-bound motor.

Although a group of motors working against small loads is generally expected to advance via asynchronous stepping, our comparison of different stepping mechanisms revealed the importance of characterizing inter-relationships between mechanical properties of motor assemblies and effective motor-microtubule binding rates. Such behavior may have implications for cargo transport in cells. For example, the non-motile microtubule associated protein tau has been shown to reduce the rate that kinesin motors bind to microtubules, but does not to influence kinesin's stepping or detachment rates. Consequently, tau is believed to reduce the run lengths of cargos that are transported by multiple kinesins, but not single kinesin molecules.[49] Yet, if a multiple motor system already possesses an intrinsic tendency to transport its cargo while only using a small fraction of the total

number of its surface-bound motors, tau's effect on cargo motion would be diminished. Thus, the organization of motors on cargos and their intrinsic mechanical properties may not only influence mechanisms of multiple motor transport, but also, potential responses to non-motile factors that regulate cargo motility. While validating such ideas ultimately requires further development of experimental methods and refinement of existing theoretical models, recent advances from our group and others are now making such detailed analyses increasingly possible.

Chapter 3

Two Kinesins Transport Cargo Primarily via the Action of One Motor: Implications for Intracellular Transport

The number of microtubule motors attached to vesicles, organelles and other sub-cellular commodities is widely believed to influence their motile properties. There is also evidence that cells regulate intracellular transport by tuning the number and/or the ratio of motor types on cargos. Yet, the number of motors responsible for cargo motion is not easily characterized, and the extent to which motor copy number affects intracellular transport remains controversial. Here, we examined the load-dependent properties of structurally-defined motor assemblies composed of two kinesin-1 molecules. We found that a group of kinesins can produce forces and move with velocities beyond the abilities of single kinesin molecules. However, such capabilities are not typically harnessed by the system.

Instead, two-kinesin assemblies adopt a range of microtubule-bound configurations while transporting cargos against an applied load. The binding arrangement of motors on their filament dictates how loads are distributed within the two-motor system, which in turn influences motor-microtubule affinities. Most configurations promote microtubule detachment and prevent both kinesins from contributing to force production. These results therefore imply that cargos will tend to be carried by only a fraction of the total number of kinesins that are available for transport at any given time, and provide an alternative explanation for observations that intracellular transport depends weakly on kinesin number *in vivo*.

3.1. Chapter summary

This chapter centers on an analysis of trapping data from the same system of two kinesins studied theoretically in Chapter 2. The assays and data workup were done by my colleague, D. Kenneth Jamison. I created the mechanical model of the two-kinesin system mentioned in later sections to interpret these data. The content of this chapter is published in the *Biophysical Journal*.

In our static optical trapping assays, loads imposed on polystyrene beads increased as the attached motor or motors pulled the beads away from the trap center. The performance of both single kinesins and the two-kinesin complexes (see Fig. 3.1 for an illustration) were assessed through velocity (as a function of load) and detachment force (highest force reached prior to a detachment event) analyses. While the two-kinesin complexes were capable of producing forces that were far

greater than those produced by single kinesins, the average force at which the two-kinesin beads detached was statistically indistinguishable from that of the single kinesin beads. The average velocities of the two-kinesin beads were essentially identical to single-kinesin velocities at forces below the single-kinesin stall force; at higher loads, two-kinesin beads moved with velocities that not only exceeded single-kinesin velocities, but also exceeded the velocities predicted by an equal-load-sharing approximation for two kinesins.

When analyzing velocities from individual traces, we noticed that two-kinesin beads tended to accelerate or decelerate rapidly, a behavior that we attribute to transitions between non-load-sharing and load-sharing microtubule-bound configurations. Using mechanical modeling, we show that the sharing of load between two kinesins is dictated by the distance separating them at the microtubule. Generally, the larger the separation distance, the more load the forward or 'leading' motor assumes relative to its 'trailing' partner. Changes in separation distance of just one lattice site can cause a 15-20% shift in relative loads; the range of separation distances over which loads are shared roughly equally is thus quite small compared the range over which they are not. Furthermore, from thermodynamic considerations, we predict that an unbound kinesin should initially bind the microtubule in a non-load-sharing configuration. We also notice that the rate of transition from high velocity states to low velocity states is quite high. Taken together, these observations and analyses help to explain the behavior observed in the assay: trailing kinesins, which bind into non-load-sharing configurations, are

generally unable to close the distance between them and their leading partners (through stepping) before one or the other detaches.

We believe that this work has significant implications for intracellular transport by teams of kinesins. Principally, our results suggest that force production in teams of multiple kinesins depends only weakly on the number of kinesins present. This helps to explain other groups' experimental observations in living cells. It also leads to an intriguing hypothesis regarding bidirectional transport by opposing teams of kinesin-1 and cytoplasmic dynein: force production in teams of kinesin-1 motors may be less-than-additive to allow a team of weaker dynein motors to compete against it. This requires, of course, that dynein motors cooperate more effectively in groups, a topic that is examined in the next chapter.

3.2. Introduction

Microtubule motors are mechano-chemical enzymes that transport organelles and other important cargos in the cytoplasm of eukaryotic cells.[50] Many motors in the kinesin and dynein families are capable of generating piconewton-sized forces and move processively along their filament tracks.[51-53] Although such capabilities imply kinesins and dynein can transport cargos efficiently as single unassisted molecules, cryoelectron microscopy and several *in vivo* studies have demonstrated that cargo motion is often driven by teams of these motors.[5-6,7,39] The combined action of motors may be critical during specific transport challenges that require high-force production or long-distance travel. There is also evidence that

cargo motion can be regulated by tuning the number of motors participating in transport.[37] The motions of neurofilaments, mitochondria, melanosomes, and certain vesicles are all known to be driven by both kinesin and dynein. Since these motors move in opposite directions along microtubules, regulating their stoichiometry should allow net directional transport to be achieved. However, despite efforts to examine multiple motor behaviors, the sensitivity of most cargo transport parameters to motor copy number has been difficult to characterize and, overall, the precise impact of motor number on intracellular transport processes remains unclear.

A significant limitation of current studies of multiple motor dynamics is that the number of motors responsible for cargo motion is not rigorously known. Typically, only the average number of motors on cargos can be controlled *in vitro* by binding motors to beads at different motor/bead ratios. Analogously, motor number can be manipulated *in vivo* by either stimulating cells with external cues or controlling motor expression.[18,37] In all of these cases, the precise number of motors responsible for specific transport behaviors must be inferred from analyses of cargo velocities, run lengths, and detachment forces. Yet, the relationships required for such analyses have not been rigorously validated, and interpretations of collective motor behaviors often rely on idealized model assumptions that motors share their applied loads equally and do not interact with one another during cargo transport.

Understanding the effects of multiple motor number, organization and coupling is particularly important considering recent observations that suggest

motor copy number influences cargo transport differently *in vitro* and *in vivo*.[54] Although significantly different average run lengths are often observed, beads coated with multiple motors are generally found to travel longer distances along microtubules than single motor molecules.[8,15] Such behavior is not necessarily found *in vivo*. Recent *in vivo* studies of lipid droplet motility suggest that cargo velocities and run lengths do not depend on kinesin number.[18] Interestingly, bidirectional motions of melanosomes, and hence whether they aggregate or disperse in the cytoplasm, appear to depend on dynein, but not kinesin number.[37] Given current *in vitro* observations and general notions of multiple motor mechanics, it has been proposed that there are as of yet undefined environmental and/or regulatory factors in living cells that reduce the impact of kinesin copy number on cargo transport. However, since critical aspects of collective motor mechanics remain unresolved, it is also possible that such behavior is derived, at least in part, from inherent biophysical properties of multiple kinesin complexes.

Herein, we used an optical trap to characterize the load-dependent transport properties of structurally-defined motor assemblies containing two elastically-coupled kinesin-1 molecules. These assemblies facilitate more direct comparisons of single-and multiple-motor behaviors, while allowing examination of how a motor assembly's microtubule-bound configuration influences cargo motion. Overall, we show that single and small groups of kinesins can exhibit remarkably similar detachment forces, velocities, and bead displacement sizes *on average*. This behavior occurs since most assembly configurations (i) prevent both kinesins from participating simultaneously in cargo transport, and (ii) create conditions that

promote detachment of the leading (*front*) motor within the assembly. Thus, the net load-dependent transport behavior of the two-motor system resembles the action of a single kinesin to a surprising extent. Furthermore, our work suggests that multiple motor systems possessing varied structural and mechanical properties, and therefore, that a range of intracellular cargos will exhibit this behavior.

3.3. Materials and methods: self-assembly of two-kinesin complexes

Structurally-defined assemblies of two kinesin motors were created using a synthetic procedure that allows multiple proteins to be organized onto DNA-based molecular scaffolds (Fig. 3.1A; Fig. 3.7A).[55] In this method, motor-DNA anchoring is accomplished via DNA-conjugated artificial proteins composed of an engineered leucine zipper (Z_R) and elastin-like polypeptide motifs.[10,33] The artificial proteins were used to link two recombinant human kinesins (hK560EGFP-Z_E) to a 50 nm long DNA duplex that possesses ssDNA attachment sites for motors at each end. The DNA scaffold also incorporates two biotin molecules adjacent to each attachment site for assembly immobilization onto streptavidin-coated beads. Each motor is therefore anchored to beads through its proximal biotin-streptavidin linkage, and hence, the DNA scaffold functions as a template to pattern motors on the bead surface and not as a mechanical element in the assembly.

3.4. Results

3.4.1. Optical trapping of individual two-kinesin assemblies

In our optical trapping assays, a two-kinesin assembly binds to a microtubule and pulls its bead in one direction against the increasing load of the trap until detachment occurs. This process produces traces with clear signatures of multiple motor function (Fig. 3.1; Fig 3.8A). First, two-kinesin beads were observed to detach at forces that cannot be produced without the combined action of two motors (>>7.6 pN, the stalling force of a single kinesin). Additionally, 43% of two-kinesin trajectories contain instantaneous rearward displacements to positions other than the trap center upon microtubule detachment. Such behavior is clearly visible in individual traces (Fig. 3.1B; Fig. 3.8) and is indicative of a two-state unbinding process: the assembly partially detaches from the microtubule via the unbinding of only one assembly motor before detaching completely. The rearward displacement magnitudes produced by this process are distributed about a peak at 47 nm (Fig. 3.1C), indicating that the DNA scaffold confers distinct structural properties to the motor assemblies.

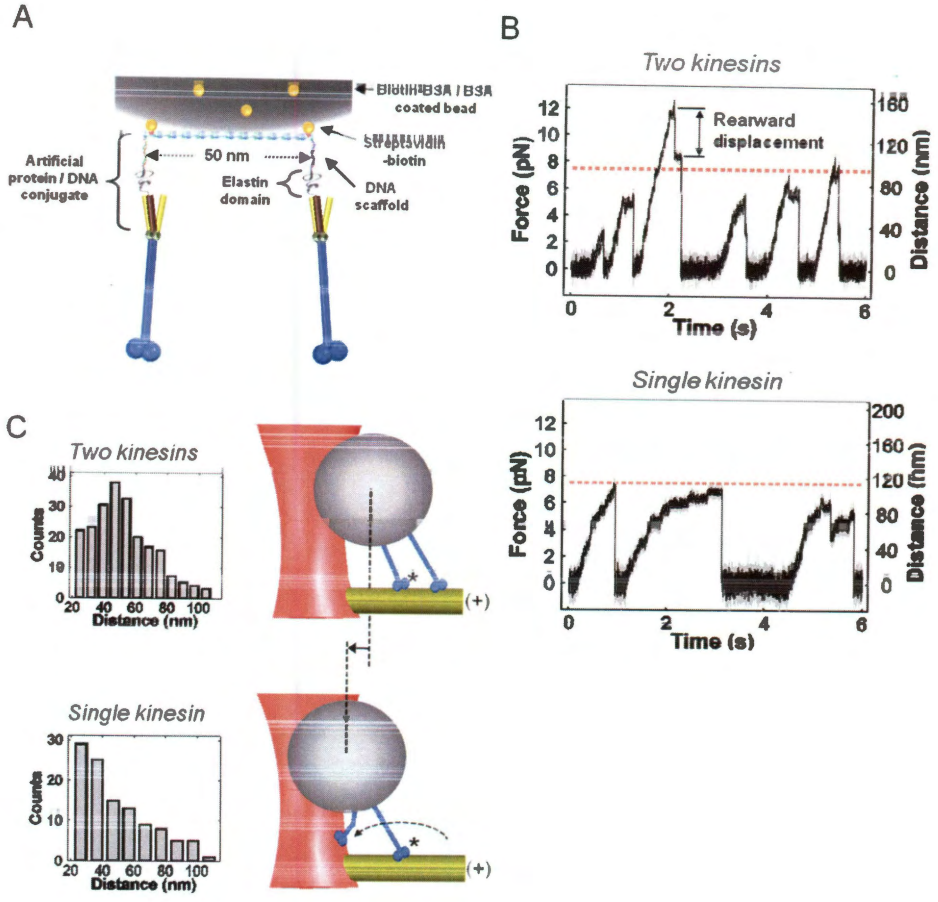

Figure 3.1 - Optical Trapping of Two-Kinesin Assemblies (*data collected by D. K. J.*)

(A) Illustration of a DNA-templated two-kinesin assembly anchored to a streptavidin-coated bead. Assembly components are drawn approximately to scale. **(B)** Optical trapping traces from two-kinesin assays. A representative large rearward displacement that occurred prior to complete bead detachment is indicated. Single-kinesin data is provided in the Supporting Information. The red line indicates the measured 7.6 pN single-kinesin stall force. **(C)** Histograms of rearward-displacement magnitudes that occurred during bead detachment. An illustration of the two-state unbinding process is shown on the right. **(D)** Histogram of the peak forces observed prior to bead detachment in (*top*) single-kinesin assays (n_{beads} = 10; n_{traces} = 405) and (bottom) two-kinesin assays (n_{beads} = 16; n_{traces} = 640). Detachment forces for all traces are reported.

3.4.2. Detachment force distributions of individual two-kinesin assemblies

The ability to trap individual two-kinesin assemblies allowed comparison of bead-microtubule detachment forces in single- and two-kinesin assays (Fig. 3.1D). For these comparisons, we evaluated distributions of the peak force beads reached in the trap prior to detachment regardless of dwell times; all recorded traces are included in our analyses. Single-kinesin detachment forces are found to be asymmetrically distributed about a peak at 7.3 pN; events > 9 pN are rare. In contrast, two-kinesin bead detachments are more broadly distributed and contain events where microtubule unbinding occurred at forces up to 17 pN. Surprisingly, we found that the histogram of two-kinesin detachments contains a peak at 5.6 pN. This peak persists even when our analysis is limited to trajectories that include 40-60 nm rearward displacements (Fig. 3.1D, inset). Further, trapping data collected from individual two-kinesin beads also reflect this behavior; low-force detachments occur more often than high-force detachments. Since our assay conditions dictate that a large majority of two-kinesin beads possess a single surface-bound assembly (Fig. 3.7B), the detachment events recorded from a single bead can be reliably attributed to the same assembly. Therefore, we are confident that the distributions plotted in Fig. 3.1D represent the detachment behavior of a two-kinesin assembly in an optical trap. Finally, we note that detachment force histograms of kinesin-driven lipid droplets display a similar low-force peak.

Overall, analyses of bead detachments show that two kinesins are capable of producing much higher forces than a single kinesin. However, the average

detachment forces measured in our single- and two-kinesin assays are surprisingly similar (6.0 ± 2.0 pN and 5.9 ± 2.6 pN respectively, mean ± s.d.). One might expect that a group of two kinesins would detach at higher forces than single motors since they could remain associated with a microtubule for longer periods of time. Yet, our observations suggest that kinesin within assemblies influence one another's dynamics, yielding enhanced cargo detachment rates.

3.4.3. Two-kinesin assemblies transition between microstates with different numbers of load-bearing motors

We next constructed and compared single- and two-kinesin force-velocity (*F-V*) relationships. First, instantaneous bead velocities were calculated by applying a 200 ms sliding linear regression window to position vs. time traces (Fig. 3.2A).[56] This data was then used to construct load-dependent velocity distribution histograms (Fig. 3.2B,C). Between loads of 4-8 pN, two-kinesin velocity histograms contain two distinct peaks, regardless of whether they are constructed using trajectories where bead detachment occurred above 10 pN (Fig. 3.2B), at lower forces (4.5-6.5 pN), or using all recorded traces (Fig. 3.2C). This result is expected since a two-kinesin assembly can transport beads via different configurations (*microstates*) where either one or both motors are microtubule-bound. Cargo velocities under load should be higher when two motors work together as a team. Yet, the two-motor system can also adopt various two-motor-bound configurations where the system is oriented differently with respect to the microtubule axis and where the motor-microtubule binding-site distances between the motors are

different. Since these factors may also influence cargo velocities, our next challenge is to resolve which assembly configurations produce the different velocity sub-populations.

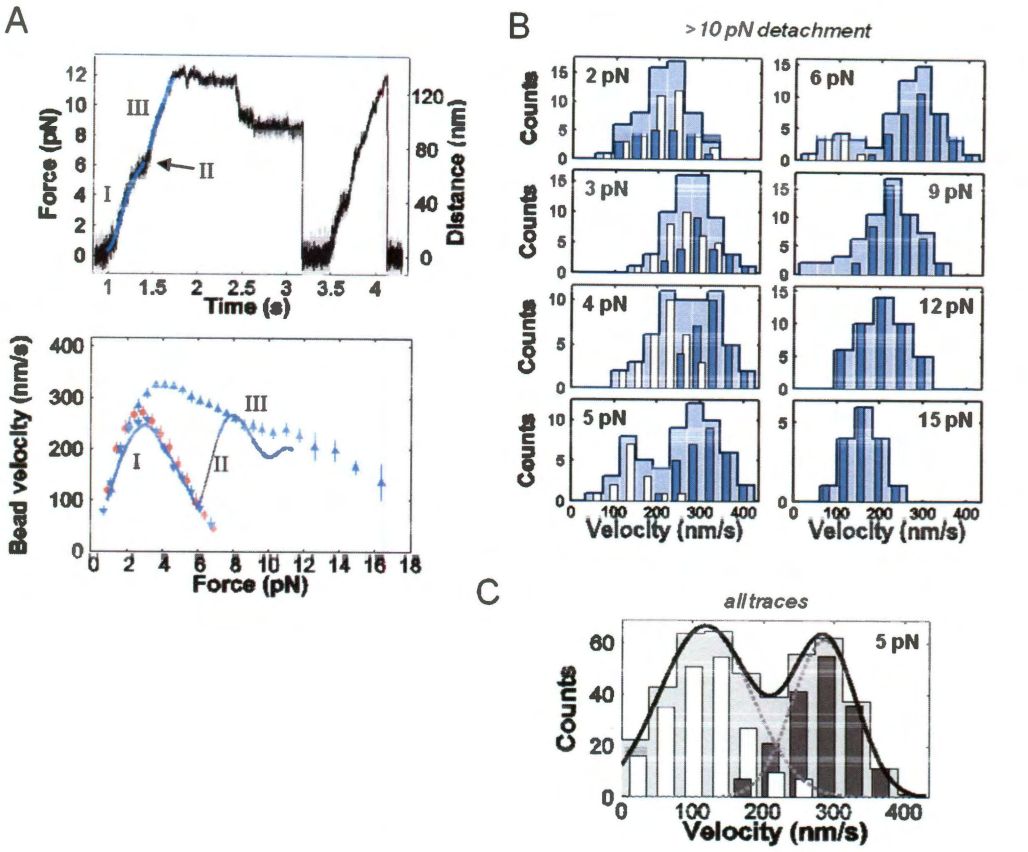

Figure 3.2 - Detection of Transitions Between Distinct Assembly Microstates
(*data collected by D. K. J.*)
(A) A two-kinesin bead trajectory showing a transition between assembly microstates with 'low' (*single load-bearing motor*) and 'high' (*two load-bearing motors*) velocities. Trajectory components are indicated by Roman numerals. The lower *F-V* plot displays the average velocities measured from trajectories where bead detachment occurred above 10 pN (*blue triangles*; $n_{traces} = 58$). The downward- and upward-pointing triangles indicate the average segment velocities for the 'low-velocity' (*single load-bearing motor*) and 'high-velocity' (*two load-bearing-kinesins*) configurations of the assembly respectively. The red circles denote our measured single-kinesin *F-V* relationship. Velocities are displayed as mean ± s.e.m. **(B)** Histograms of two-kinesin bead velocities analyzed in traces where bead detachment occurred at high forces (>10 pN). The white and blue bars correspond to 'low" (*single load-bearing motor*) and 'high' (*two load-bearing-kinesins*) velocity sub-populations respectively. The light blue background indicates the velocity distributions for all measured events before microstate identification. **(C)** Velocity distributions of two-kinesin beads at 5 pN using all measured two-kinesin trajectories.

While calculating two-kinesin *F-V* relationships, we observed clear transitions within most trajectories where beads accelerated or decelerated between distinct non-zero bead velocities (Fig. 3.2A). We next tested whether these transitions could be used to identify portions of trajectories where bead motion is driven by one or two motors. To do so, a threshold acceleration rate ($|dV/dF| > 125$ $nm \cdot s^{-1} \cdot pN^{-1}$) was used to determine the forces at which velocity transitions occurred, and then separate traces into 'low' and 'high' velocity segments depending on whether beads decelerated or accelerated into a segment, respectively. The resulting trace components were then pooled into 'low' or 'high' velocity sub-populations and plotted on top of the raw velocity distribution data (Fig. 3.2B,C). The Gaussian-like shape and overlap of each distribution with the peaks found in our raw velocity histograms demonstrates this method correctly assigns trajectory components to their appropriate microstates. Yet, this method does not distinguish between microstate configurations that yield similar velocities (*i.e., beads should move with near-identical velocities when only one assembly kinesin is bound to the microtubule and when both kinesins are bound but only one assumes the applied load of the trap*). Therefore, the velocity histograms in Fig. 3.2 are best described as a distribution of two general classes of assembly microstates where either one or two assembly kinesins bear the applied load of the trap.

To further examine how two kinesins transport beads when they adopt specific microtubule-bound configurations, we averaged the velocities of each microstate sub-population and generated two distinct curves describing the *F-V* dependence for each detected assembly microstate (Fig. 3.2A,C). One curve follows

the *F-V* relationship measured for a single kinesin, while the second curve extends to greater forces and displays higher velocities. In these plots, bead velocities are attenuated since microtubule-bead linkages stretch as the applied load of the trap increases (*this effect is most significant at low forces and gives rise to the concave-downward curvature of each plot*). Indeed, the close agreement of the 'low-velocity' curve with the single-kinesin *F-V* data indicates that the two-kinesin trace segments assigned to the 'low-velocity' population can be reliably attributed to events where only one assembly motor drives bead motion. The second, 'high-velocity' curve therefore stems from microstates where the assembly motors worked together as a team. Hereafter, we refer to assembly configurations that produce these different behaviors as either 'low-velocity' (single load-bearing motor) or 'high-velocity' (two load-bearing motor) microstates.

3.4.4. Deviations from non-cooperative (non-interacting) two-kinesin force-velocity relationships

We next used measurements of single-motor and two-kinesin assembly elasticities to construct *F-V* plots that account for the stretching of microtubule-bead linkages (Fig. 3.3, and Appendix to Chapter 3). The resultant single-kinesin curve (*red circles*) was then fit to a previously reported *F-V* relationship,[53] which allowed a theoretical two-kinesin curve to be generated assuming that each motor experiences half of the applied load on the bead and that the two motors do not interact. At low loads, two-kinesin microstate *F-V* relationships generally follow their respective theoretical curves. However, when two-kinesin beads moved with

'low' (single-load-bearing motor) velocities, their average velocity tended to be smaller than those measured in single-kinesin experiments; a Welch's t-test shows there is a significant velocity difference ($p < 0.001$ between the two data sets from 2-5 pN). Given these deviations, our results further indicate that motors within the two-kinesin assembly do interact and that there are circumstances where these interactions lower the average velocities of beads and the forces at which they detach.

We also found deviations from predicted *F-V* behaviors at high applied loads (*i.e., loads where transport requires the action of two motors*). Surprisingly, two-kinesin beads moved with appreciably higher velocities than those in the theoretical curve. Nevertheless, the fact that these transport events occur relatively infrequently, as indicated by Fig. 3.1D, suggests that specific conditions (*e.g., assembly orientations and/or motor microtubule binding configurations*) may be required for a two-kinesin assembly to produce large forces.

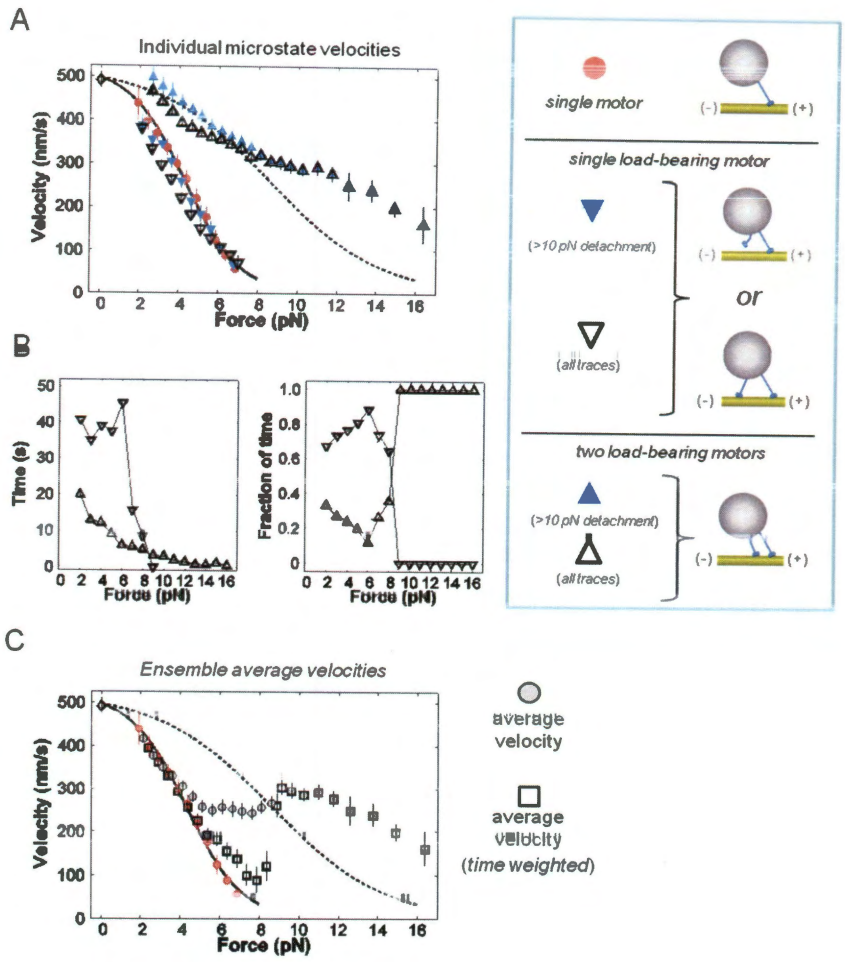

Figure 3.3 - Bead Transport is Most Commonly Driven by a Single Assembly Motor Under Load (*data collected by D. K. J.*)
(A) Force-dependent velocities of two-kinesin beads that account for motor stretching during bead advancement. The solid and dashed lines denote a fit to single-kinesin *F-V* data and predicted two-motor velocities assuming assembly motors share the applied load of the trap equally. Red circles denote single kinesin *F-V* data. Triangles represent the average velocities of traces segments that were assigned to different microstate configurations as indicated by the figure legend. **(B)** Total experimental time (*top*) and proportion of time (*bottom*) two-kinesin beads spend moving with single motor (*downward pointing triangles*) or two load-bearing motor (*upward pointing triangles*) velocities. **(C)** The average trajectory velocity (*grey circles*) and the time-weighted average velocity (*squares*) of two-kinesin beads plotted as a function of the applied load. The zero-load velocities (*diamond*) of single kinesins and two-kinesin assemblies were found to be nearly identical, as previously determined.[10]

3.4.5. Two kinesins tend to transport cargos via a single load-bearing motor

We next evaluated whether two-kinesin assemblies tended to adopt particular microstate configurations during cargo transport by examining the time that beads spent moving with either 'low' (*single load-bearing motor*) or 'high' (*two-load-bearing motor*) velocities as a function of the optical trap's applied load (Fig. 3.3B). In general, single load-bearing motor microstates are much more prevalent at low applied loads; below kinesin's 7 pN single-motor stall force, the assemblies spend >76% of their time moving with single-kinesin velocities. Yet, above kinesin's stall force, these microstates become extremely rare since a single kinesin cannot easily transport beads against such loads without the assistance of a partner.

The prevalence of single load-bearing motor microstates also influences the average velocities of the two-kinesin beads at low applied loads. In this regime, average velocities are affected significantly by the fact that both the number and the duration of two load-bearing motor transport events are smaller than those produced by a single load-bearing kinesin. Overlap between the average single- and two-kinesin *F-V* relationships is found when the velocities of the two-kinesin trajectories are weighed equally (Fig 3.3C. *circles*; Appendix to Chapter 3), indicating the number of single load-bearing motor transport events is greater than those produced by two load-bearing kinesins. This concordance is even stronger when bead velocities are weighted by the time it takes for beads to move through a given force bin (Fig. 3.3C, *plotted squares*). The latter curve denotes the true average

velocity of the two-motor system since it accounts for the fact that beads spend more time within a force bin when only one motor drives transport (*i.e., since bead velocity is lower*). Overall, given these trends, we conclude that two load-bearing kinesin microstates are relatively rare and short-lived, and make minor contributions to cargo velocity at low applied loads.

3.4.6. Composite elastic properties of individual two-kinesin assemblies suggest non-equal load sharing

To gain mechanistic insight into how an assembly's microtubule-bound configuration influences two-kinesin force production and velocity, we characterized the elastic properties of two-kinesin assemblies when both motors were microtubule-bound and engaged in transport by analyzing positional fluctuations of beads over a range of applied optical loads (Appendix to Chapter 3). Single kinesin and assembly elasticities were calculated using identical methods, except that assembly stiffnesses were measured exclusively from trace components where both motors were responsible for bead motion (Fig. 3.4A).

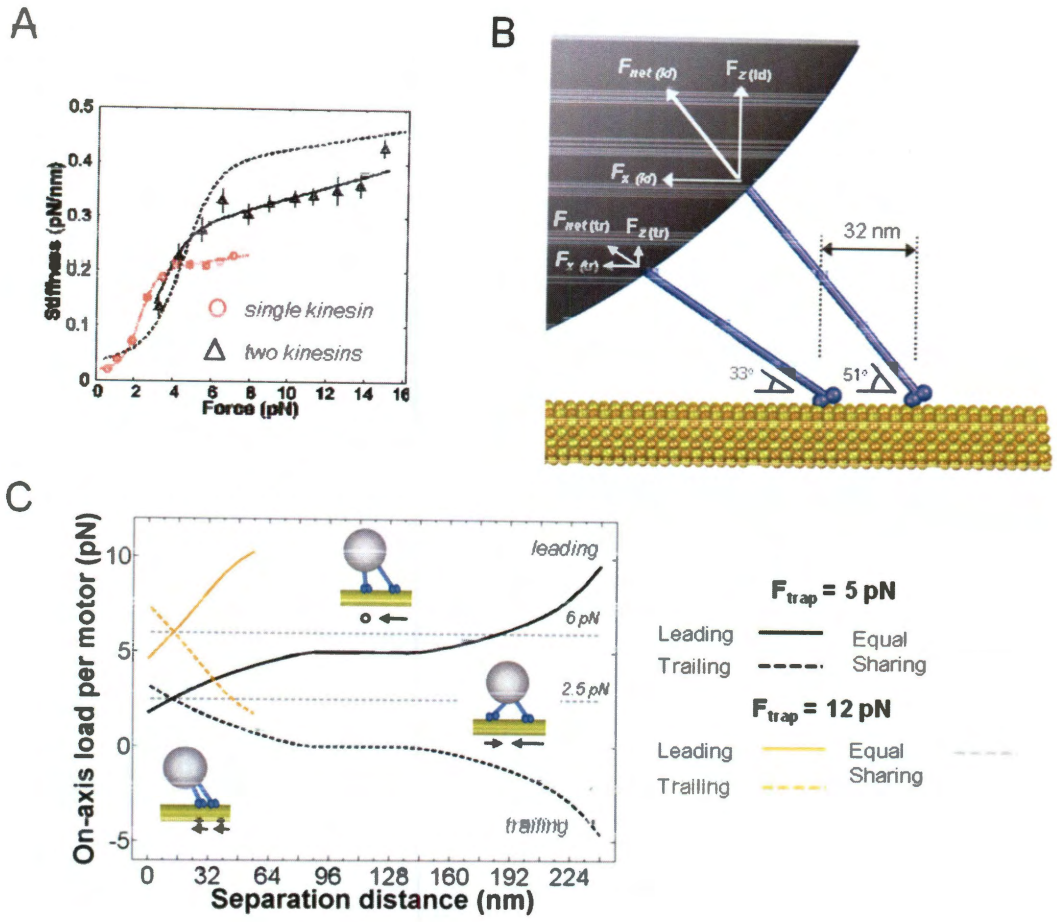

Figure 3.4 - Analyses of Two-Kinesin Assembly Elasticities and Load Distribution. (*data collected by D. K. J.*)

(A) Measured elasticities (*stiffnesses*) of single kinesins (κ_{mot}) and two-kinesin assemblies ($\kappa_{assembly}$). **(B)** Illustration of an assembly's configuration at mechanical equilibrium under 5 pN load and with a specified binding site separation distance of 32 nm. The leading motor experiences substantially larger axial and perpendicular forces than the trailing motor: $F_{x(ld)}$ = 3.4 pN, $F_{z(ld)}$ = 4.2 pN; $F_{x(tr)}$ = 1.6 pN, $F_{z(tr)}$ = 1.0 pN. Configuration-dependent elasticities predicted by the model are presented in the Appendix to Chapter 3 (Fig. 3.9B). **(C)** Predictions of the rearward force imposed on the leading and trailing assembly motors plotted as a function of microtubule binding-site separation distances plotted for applied loads of 5 pN (*black*) and 12 pN (*tan*).

As with previous studies, single motor stiffness (κ_{mot}) is found to increase non-linearly with increasing force.[57] However, the composite stiffness of our hK560EGFP-Z_E/ Z_R-ELS_6-DNA construct is smaller than that of wild-type kinesin motors since the artificial protein linkers employed here include a compliant poly(VPGVG) domain.[33] The dependence of κ_{mot} on the applied load could be fit by a sigmoid function (Appendix to Chapter 3), and then used to approximate the composite stiffness of a two-kinesin assembly ($\kappa_{assembly}$), assuming parallel-springs and equal-load-sharing behaviors: $\kappa_{assembly}(F_{trap}) = 2 \bullet \kappa_{mot}(F_{trap}/2)$, where κ denotes stiffness. Overall, we observed significant deviations from parallel-springs behavior. There is a general shift of the assembly stiffnesses from the predicted curve towards the trend measured for a single-kinesin; the values lie in between the predicted two-motor and single-kinesin curves. This result indicates that the kinesins within the assembly will most likely not be able to share the applied load of the trap equally, and will be stretched to different extents when both motors are filament-bound.

We next examined how the assembly-microtubule binding configurations influence the load distribution between two microtubule-bound kinesins. If the elastic linkages within a two-kinesin assembly are assumed to reach their mechanical equilibrium states in between motor stepping events,[25] distributions of loads between motors can be evaluated via a mechanical modeling procedure that calculates the equilibrium position of the bead given a specified load, the force dependence of κ_{mot}, and the separation distance between the two microtubule binding sites (Fig. 3.4B,C, and Appendix to Chapter 3). To capture generic elastic

properties of the two-kinesin assemblies, load distributions were calculated for assemblies bound in an 'in-line' configuration (*i.e., both motors are bound to the same proto-filament, one in front of the other*). The predominance of such configurations is implied by our stiffness analysis and evidenced more directly by our evaluations of rearward displacements during partial assembly detachment events (Fig. 3.1C).

An illustration of a representative two-kinesin assembly configuration at mechanical equilibrium is depicted in Fig. 3.4B (F_{trap} = 5 pN, binding-site separation distance = 32 nm). Here, the two motor system clearly exhibit deviations from equal-load-sharing behavior. The 'leading' motor is stretched a larger distance than the 'trailing' motor and assumes a significantly higher portion of the load imposed on the bead than its 'trailing' partner ($F_{x(ld)}$ = 3.4 pN and $F_{x(tr)}$ = 1.6 pN, when F_{Trap} = 5 pN).

Overall, we identified two general trends that describe how applied loads are distributed between assembly kinesins. First, when both motors are bound to a microtubule and bear load, the presence of the 'trailing motor' causes the angle between the 'leading motor' stalk and the microtubule axis to increase relative to that of a single kinesin experiencing the same applied load, which should affect motor velocity.[58] Concomitantly, the leading motor experiences a larger upward force (*perpendicular to the microtubule axis:* $F_{Z(ld)}$) which will influence motor-microtubule detachment rates.[59] Second, the difference between the axial (*rearward*) loads assumed by each motor is very sensitive to the distance between

the microtubule-binding sites of the two motors (Fig. 3.4C). An 'optimal' separation distance is found where the applied load of the trap is distributed near-equally between the two motors, but deviations from this distance by even one unit of motor step size (8 nm) can lead to pN-sized differences in the loads imposed on the motors. Together, these results imply that there are consequences if motors within an assembly deviate from specific microtubule-bound configurations that optimize how forces are distributed within the motor system. Importantly, such constraints appear to be significant over a range of assembly structures (*scaffold lengths, bead sizes, motor length and stiffness*; Fig. 3.9).

3.4.7. Cargo displacement magnitudes depend on microtubule-binding configuration

To further characterize how a motor assembly's microtubule-binding configuration influences cargo motion, we examined two-kinesin stepping behaviors under the applied load of the trap (Fig. 3.5). Single kinesin molecules are known to advance in discrete 8 nm steps (Fig. 3.5A).[60] Unless a group of kinesins synchronize their stepping, cargo displacement magnitudes are expected to be smaller than 8 nm.[10,25] Furthermore, cargo displacement sizes should depend on how multiple motors are bound to their filament track. To examine this behavior, we used our mechanical modeling procedure to calculate the distances beads move when the binding-site separation distance between assembly motors changes by 8 nm; a simulation of asynchronous stepping. These analyses revealed that two-kinesin beads can advance in unitary (8 nm) or attenuated (< 8 nm) increments depending

on: (*i*) the separation distance between the assembly motors' microtubule binding sites, (*ii*) whether the 'leading' or 'trailing' assembly motor steps forward, and (*iii*) the total applied load imposed on the bead (Fig. 3.5B). Despite these complications, three characteristically different stepping behaviors can be identified that largely depend on the microtubule-binding site distances between the assembly motors as described below.

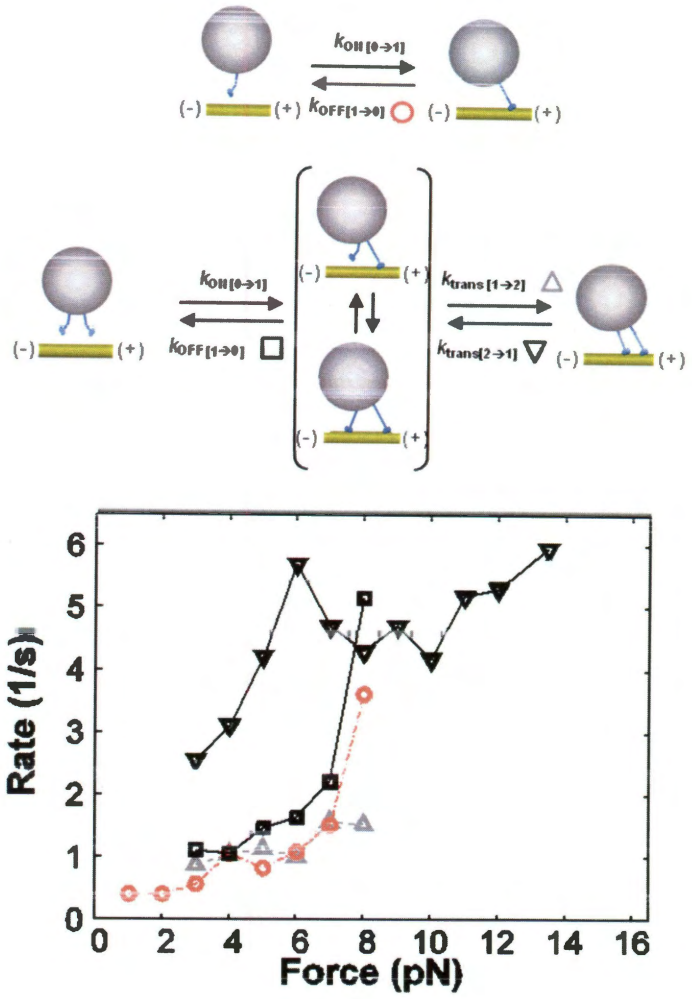

Figure 3.5 - Two-Kinesin Stepping Analyses (*data collected by D. K. J.*)
(A) A pairwise distance distribution histogram for a single kinesin motor and the corresponding spectral analysis. Histogram of displacement sizes found using a step-finding algorithm are provided in the Supporting Information. **(B)** Predicted displacement sizes for two-kinesin beads as a function of microtubule binding-site separation distance for F_{Trap} = 5 pN (*black*) or F_{Trap} = 12 pN (*tan*). **(C)** Step-size distributions for two-kinesin assemblies when they move with 'low' (*single load-bearing motor*) velocities (*black*) from 3-5 pN, and with 'high' (*two load-bearing motors*) velocities above 12 pN (*tan*). Bead displacement histograms, pairwise displacement distributions and the corresponding spectral analyses are shown. The inverse of spatial frequencies corresponding to spectral peaks indicates the dominant periodicities present in the pairwise distributions (*e.g.,* a peak at 0.25 nm^{-1} signifies the presence of 4 nm steps).

When the kinesins are bound in close proximity, bead displacement magnitudes are significantly smaller than 8 nm. Under these conditions, both assembly motors assume a portion of the applied load imposed on the bead. The asynchronous advancement of one assembly motor results in attenuated displacement sizes whose magnitudes are primarily determined by the extent to which the assembly linkages stretch or relax as the binding site separation distance and the load distributions between the two motors change. Yet, at intermediate separation distances, our calculations show that the displacement sizes of single- and two-kinesin beads will be near-identical. In this regime, the 'leading' motor bears nearly the entire applied load on the bead, and advances as a single motor with a partner that largely does not contribute to bead motion. A similar circumstance is found when motor binding site distances are large, except that in this case, the 'trailing' motor 'lags' behind the motion of the bead and imposes a resisting load on the 'leading' motor (Fig. 3.5B). Although one might expect attenuated displacements to be produced in this circumstance, we found that motions associated with bead rotations contribute significantly to displacement sizes in this regime, and that the beads still tend to advance forward in increments near equivalent to kinesin's step size. Attenuated displacement sizes are found when the scaffold center position is used as a reference point (Fig. 3.10D).

Analyses of two-kinesin stepping behaviors largely confirm our calculated predictions. First, pairwise distributions and step-size histograms of two-kinesin bead displacement sizes within trajectory components assigned to 'low-velocity' (single-load-bearing motor) microstates contain a clear periodicity / step-size

corresponding to 6.4 nm (Fig. 3.5C, *top;* Fig. 3.10D). Similar results are found in the single kinesin pairwise distribution and step size histograms, which exhibit a dominant periodicity / step-size of 6.3 nm (Fig. 3.5A, Fig. 3.10A). When single-motor elasticity data is used to adjust displacement sizes for the stretching of microtubule-bead linkages, a displacement magnitude of 6.3 nm equals kinesin's intrinsic 8.2 nm step size (Fig. 3.10). Such agreement is expected, as displacements equivalent to kinesin's unitary step size should be produced when two-kinesin assemblies adopt configurations where only one assembly motor bears the applied load of the trap, regardless of whether one or both motors are microtubule-bound. We note that there is some broadening in both pairwise displacement and step size distribution histograms of the 'low-velocity' two-motor stepping data. This likely reflects variability in two-kinesin bead displacement magnitudes that arises from a percentage of events where assemblies adopted configurations that result in a partial sharing of the applied load.

Significant agreement between measured and calculated two-kinesin bead displacement sizes is also found at high forces (>12 pN), where motors must work together to produce forward motion. The corresponding pairwise distribution histogram possesses a spectrum of small step sizes and a dominant 3.7 nm periodicity (Fig. 3.5C, *bottom*). A histogram of bead displacement magnitudes contains an equivalent peak. A second, smaller peak at 6.8 nm is also observed. However, evaluation of the step finding procedure indicates that a portion of this peak's magnitude (~50%; 15% *of steps in traces*) likely stems from undercounting of small stepping events. While we cannot fully rule out that two kinesins can

coordinate / synchronize their stepping mechanics to some extent, we conclude that a group of two kinesins moving against large applied loads will advance primarily via asynchronous stepping. Importantly, coupled with our analyses of load distributions within motor assemblies, this result highlights why it is so difficult for two-kinesin beads to sustain transport against large loads. Asynchronous stepping will lead to fluctuations in binding-site separation distances, and hence, create transient conditions that promote motor detachment.

3.4.8. Kinetic transition rates between two-kinesin assembly microstates

We also evaluated how rapidly a two-kinesin assembly can transition between microstates with different numbers of load-bearing motors by combining a method to analyze motor-microtubule detachment kinetics with our ability to identify transitions between velocity sub-populations (Fig. 3.6).[56]

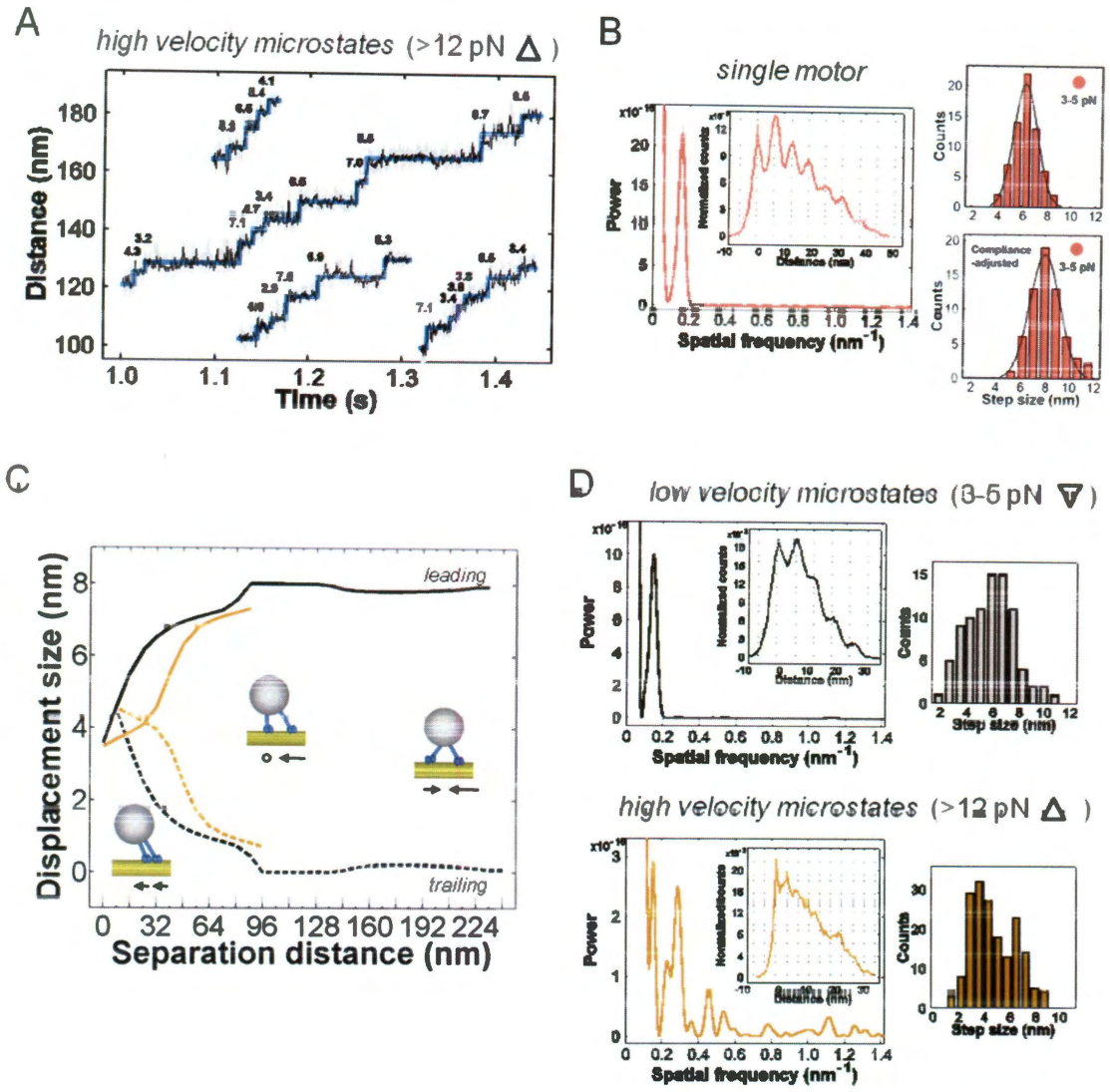

Figure 3.6 - Single and Two-Kinesin Binding / Unbinding Kinetics (*data collected by D. K. J.*)
(A) Schematic of the microstate transitions for a two-kinesin assembly. The subscript indices specify the number of load-bearing motors present before and after the transition. **(B)** Measured transition rates for two-kinesin assemblies.

Again, the above analyses show that 'low' (single load-bearing motor) velocities can be produced regardless of whether one or both motors are attached to the microtubule. When both motors are microtubule-bound, their binding-site

separation distances dictate load distributions, and hence, whether the system will move with 'low' (single load-bearing motor) or 'high' (two load-bearing motor) velocities. Importantly, there are a number of configurations that can produce either behavior. Thus, our measured rates must be considered as average transition rates between different classes of assembly microstate configurations where either one or two motors bear the applied load, and are not purely defined as the rates at which the number of microtubule-bound kinesins change.

As expected, all forms of two-kinesin assembly and single-kinesin detachment rates are found to increase as a function of applied load. Importantly, the transition rates $k_{OFF[1\rightarrow 0]}$ measured for two-kinesin beads are higher than the corresponding single-kinesin detachment rate, indicating inter-motor interactions enhance motor detachment in the two-kinesin system. Furthermore, below kinesin's stall force, the transition rate $k_{trans[2\rightarrow 1]}$ describing how rapidly assemblies switch from 'high-velocity' (*two load-bearing motors*) microstates to 'low-velocity' (*single load-bearing motor*) microstates is found to be significantly larger (> 3x) than the rates of single-kinesin detachment. Moreover, the rate $k_{trans[2\rightarrow 1]}$ is much faster than the rate assemblies transition back into microstates where both motors assume a portion of the applied load ($k_{trans[1\rightarrow 2]}$). Together, these results further confirm that assembly configurations where both motors are engaged in transport are rare and short lived, and support the conclusion that two kinesins primarily transport their cargo through the action of a single load-bearing motor.

We also found that the transition rates describing the addition of a second load-bearing motor, $k_{trans[1\rightarrow 2]}$, are significantly lower than the values commonly used to approximate the rates at which motors bind to microtubules ($k_{on[1\rightarrow 2]}$). This rate is often assumed to be load-independent at ~5 s^{-1}.[14] Yet, when considering the effects of motor-microtubule binding geometry, the attachment of a second assembly kinesin does not necessarily result in load sharing or high cargo velocities since the motors must close any gap between their binding sites that prevents them from both contributing to force production. It is therefore possible that, when defined purely by motor binding, the rate $k_{on[1\rightarrow 2]}$ can be larger than our observed transition rate $k_{trans[1\rightarrow 2]}$.

3.5. Discussion

By studying the load-dependent properties of structurally-defined assemblies of two kinesins, we have resolved new features of collective kinesin dynamics that provide insight into the dependence of cargo transport on kinesin number. Importantly, several lines of evidence confirm the successful examination of *individual* two-kinesin complexes. In particular, we observed that two-kinesin beads: (*i*) regularly reach forces greater than a single kinesin's 'stall' force, (*ii*) detach via a two-state unbinding process that reflects the assembly architecture, and (*iii*) display bi-modal velocity distributions under low loading conditions, among other signatures.

The ability to attribute transport events to a structurally-defined multiple kinesin complex allows the average behaviors of multiple motor systems to be examined with minimal complications originating from variability in the total number of motors and their organization on cargo surfaces. Overall, such analyses show that, despite a capacity to produce large forces and move with high velocities, two kinesin-1 motors will tend to transport their cargo using only one load-bearing motor molecule at a time.

3.5.1. Models for the weak dependence of cargo transport on kinesin copy number

Transition rate models have been developed to describe cargo transport by multiple motors,[44] and, as with models of muscle mechanics,[61] this framework has been extended to evaluate the influence of a motor assembly's structural and mechanical properties, as well as potential inter-motor interactions on collective motor dynamics.[11,30,38,44] However, most predictions have not been unambiguously confirmed by experiments, and analyses of multiple motor behaviors still generally rely on notions that multiple motor velocities and detachment forces depend exclusively on the number of microtubule-bound motors. In contrast, our results show that collective motor dynamics is much more complex since an assembly of motors can adopt ranges of microtubule-bound configurations that confer different mechanical and dynamic properties to the system. Very few of these configurations appear to allow multiple motors to benefit from their combined action, and thus, unexpectedly weak collective behaviors are produced.

As evidenced by our mechanical modeling, two kinesins can only produce large forces and high velocities if the distances between their microtubule-binding sites are maintained within a narrow range (*e.g.*, < 24 nm, at an applied load of 12 pN). Otherwise, the 'leading' motor will assume the majority of the applied load and its detachment rate will increase relative to an idealized case where the motors share the applied load equally. Furthermore, our transition rate analyses, particularly of rate $k_{on[1\rightarrow 2]}$, suggest that when an assembly switches between microstates via the attachment of a second motor, this motor will most likely bind to a site where it cannot contribute significantly to cargo motion. Thus, a newly bound motor faces the challenge of catching its load-bearing partner before either motor releases from the filament track. This challenge is exacerbated by the fact that as the 'trailing' motor moves forward the 'leading' motor will accelerate as its portion of the applied load decreases and experience larger upward forces that lower its microtubule affinity. Thus, while possible, it may be difficult for two kinesins to perform the delicate 'balancing act' required for an assembly to exhibit its full mechanochemical potential.

3.5.2. Implications for transport of endogenous cargos

There are several significant similarities between our results and those from recent *in vivo* studies of cargo transport.[30,37] In particular, behaviors where grouping kinesins does not result in appreciably enhanced motility are consistent with studies of lipid droplet motility in drosophila embryos where motor copy number does not influence cargo transport appreciably.[18] Yet, the role of a biological cargo's

size, shape, and elasticity, as well as how motors are anchored to cargo surfaces, must still be considered to draw comparisons to *in vivo* observations. Our two-kinesin beads possess structural and mechanical properties that are analogous to several natural cargos that are known to be transported by small groups of motors. The stiffness of our present kinesin constructs, which is roughly half of the values reported for a full-length, wild-type kinesin motor,[62] is designed to account for the compliance imparted to motor systems by biological cargos. Our assemblies should approximate the mechanical properties of multiple kinesin systems bound to sub-cellular cargos with an elastic modulus of approximately 10^6 Pa (*the cargo surface elasticity that would impart the same overall assembly stiffness between two wild-type kinesins as measured in our motor constructs*). Elasticities of this magnitude are found in many biological cargos such as: melanosomes,[63] certain vesicular cargos,[64] and potentially ribonucleoprotein particles. Furthermore, our modeling of how configuration-dependent load distributions depend on cargo size, motor spacing and assembly elasticity indicate that the effects of non-equal load sharing will persist even if the structural and mechanical properties of motor assemblies and their cargo deviate from those of our present system (Appendix to Chapter 3).

3.5.3. Implications for intracellular transport regulatory mechanisms

An intrinsic insensitivity of cargo transport to kinesin number would naturally diminish the extent to which cells could control intracellular transport by tuning the total number of active kinesins bound to a cargo. However, such behavior may still be significant to mechanisms that regulate cargo motion. For example, the

average force that a group of kinesins detaches from a microtubule should influence bidirectional cargo motility when multiple kinesins and dyneins participate in transport. There is some evidence that mammalian dyneins stall at significantly lower forces than kinesin-1,[35] implying that extremely large groups of dyneins would be needed to compete with much smaller groups of kinesins (*by some accounts ~14 dyneins if only 2 kinesins are present*). Insensitivity to kinesin number could serve to mitigate this imbalance and allow dynein number to act as a more sensitive control parameter to regulate bidirectional cargo motion. Of course, this prediction assumes that several aspects of multiple-dynein mechanics will differ from those found with multiple kinesins. Indeed, there are unique features of dynein mechanochemistry at the single-motor level[5,65] that could potentially result in different collective behaviors.[40] While understanding these aspects of intracellular transport requires further investigation, the ability to create structurally-defined assemblies of multiple motor molecules and assay their collective function at the single-assembly level should greatly assist these efforts.

Appendix to Chapter 3

3.6. Experimental procedures

3.6.1. Synthesis of two-kinesin systems

The human kinesin-1 motor construct (hK560-EGFP-Z_E) was prepared by inserting genes encoding for an EGFP (Clonetech) and an engineered leucine zipper (Z_E) into the KpnI and XhoI restriction sites of a human K560 motor construct (provided kindly by Ron Vale). Motors were purified using Ni^{2+}-NTA methods followed by a microtubule affinity purification procedure. Motor purity and concentrations were verified against protein standards via SDS-PAGE analysis.

The DNA-conjugated artificial proteins Z_R-$(ELS)_6$-ssDNA and the DNA scaffolds were synthesized as previously described.[55] The DNA scaffolds are composed of two different 170 bp ssDNA oligonucleotides. Once hybridized, these strands form a complex containing a central duplex that is 50 nm long (148 bp, 14 helical turns) and two single-stranded 'overhangs' that extend 22 bp from each end of the scaffold. The 'overhangs' possess complementary sequences to the oligonucleotide-conjugated artificial proteins. Two thiamine bases were placed between the junction of the duplexed portion of the scaffold and the 'overhangs', and remain unhybridized after the full assembly is formed to provide additional flexibility at the motor / scaffold junction. Two internal biotin molecules were also incorporated into the duplexed scaffold and are positioned 3 bp from the overhang junctions (leaving 142 bp, 48 nm, between biotin molecules).

Two-kinesin assemblies were constructed by first preparing 'partial-assemblies' composed of a DNA scaffold coupled to artificial protein polymers by mixing the scaffold and the polymers at a 1:2 stoichiometry and then thermally annealing the complexes (Fig 3.7A). Complete two-kinesin assemblies were prepared immediately before each assay by combining solutions of hK560-EGFP-Z_E motor with the 'partial-assemblies' using a four- to ten-fold excess concentration of motor. Subsequently, the entire assembly was attached to streptavidin-functionalized beads (500 nm diameter), and diluted approximately 50-fold into motility buffer. Single kinesins were anchored to beads via an identical artificial protein linker and a 20-bp duplex that incorporates a biotin.

3.6.2. Two-kinesin trapping assays

The optical trapping instrument is based on previous designs. Trap stiffness was determined using the power spectrum method. Bead assays were performed at room temperature (23 ± 1° C). Data were digitized and stored at 30 kHz after low-pass filtering at 10 kHz. Data analyses were performed using custom software written in MATLAB.

Trapping experiments were performed in motility buffer (20 mM PIPES pH 6.8, 50 mM potassium acetate, 4 mM $MgCl_2$, 1 mM EGTA, 2 mM DTT, 0.5 mg/mL α-casein, 2 mM ATP, and an oxygen scavenging system). Microtubules were purified from bovine brain. Motility buffers were supplemented with 10 μM taxol when microtubules were used. Axonemes were purified from sea urchin sperm. Identical

behaviors were observed in assays with axonemes and microtubules, and hence, we use them interchangeably in the text.

The assay conditions that support optical trapping of *individual* two-kinesin assemblies were determined by incubating beads with motor assemblies over a range of assembly / bead ratios and then measuring the fraction of beads that moved when brought into contact with microtubules. The percentage of motile beads decreased with decreasing assembly concentration in accordance with a Poisson distribution function that describes the probability that the beads are driven by one or more assemblies (Fig. 3.7B). To ensure two-kinesin bead motion was driven by only one assembly, all assays used bead preparations with less than 35% motile fractions. Under these conditions, approximately 93% of beads should possess no more than one surface-bound kinesin assembly. The probability that two assemblies on a bead are positioned close enough such that both can bind a microtubule simultaneously is < 2%.

During our two-kinesin assays, beads were found to bind to microtubules multiple times at random intervals over the time course that beads were interrogated (~ 6 min). Detachment force distributions did not depend on the time individual beads were examined, indicating the trapping of beads did not result in an appreciable loss of motor activity and that the assembly linkages remain intact during trapping assays.

3.7. Data analysis and modeling

3.7.1. Detachment force assays

Detachment forces are reported as the peak force produced in a trace prior to detachment. The majority of two-kinesin detachment events (> 75%) were preceded by only a short (<<200 ms) dwell, generating 'sharp' peaks such as those displayed in Fig. 3.1B and the peak displayed on the right side of Fig. 3.2A. Thus, we characterized all detachment events recorded so that the full distribution of peak forces produced by the two-motor assemblies can be compared more easily to single-kinesin data. Rare events, (e.g., the left side of Fig. 3.2A) possess longer dwells coupled with backward motions that we attribute to a super-stall behavior of one kinesin within a two-kinesin assembly.

The stall force for a single kinesin was determined by evaluating detachment events where beads dwelled for more than 200 ms immediately prior to detachment. Consistent with previous work, this analysis produced a Gaussian distribution of detachment events peaked at 7.6 pN.

3.7.2. Fits to single- and two-kinesin assembly stiffness data

The stiffnesses of single kinesins and two-kinesin assemblies were determined by analyzing load-dependent positional fluctuations of beads.[56] This analysis yields values for the composite stiffness for the motor-bead system in the optical trap (κ_{tot}) at a given applied load. When analyzing single-kinesin data, κ_{tot} is the sum of the motor elasticity and the optical trap's spring constant: $\kappa_{tot}(F_{trap}) =$

$\kappa_{mot}(F_{trap}) + \kappa_{trap}$. In two-kinesin assays, κ_{tot} is the sum of the composite stiffness of the entire two-motor assembly and that of the optical trap $\kappa_{tot}(F_{trap}) = \kappa_{assembly}(F_{trap}) + \kappa_{trap}$. Values for κ_{trap} were measured independently for each bead by the power spectrum method. The data in Fig. 3.4A represents the average stiffness for single-kinesins and fully-bound two-kinesin assemblies calculated using the equations described above. As presented in Fig. 3.4A, $\kappa_{mot/assembly}$ is the effective motor/assembly stiffness measured along the microtubule axis.

Fits to single-kinesin stiffness data in Fig. 3.4A were determined using a mechanical modeling / non-linear regression routine programmed in MATLAB. In this routine, we approximated the axial (along the motor-axis) force-extension properties of our kinesin-1 / polymer construct empirically using a sigmoid function. The unstretched length of the motor is assumed to be ~52 nm (*accounting for the motor, the GFP, and the artificial protein, and the DNA overhang of the scaffold*). With these parameters, our routine models the mechanical state of a trapped bead that is bound to the microtubule via a single kinesin molecule. The equilibrium center position of the bead, the stretched length of the motor, and the angle the motor projects from the microtubule are all determined via a force-balance and/or energy minimization procedure. The component of the single-motor stiffness projected along the microtubule axis (κ_{mot}) can then be calculated directly from the modeled mechanical equilibrium state of the motor by evaluating the change in the force imposed on the bead by the motor when the bead position is modulated. To fit our single-kinesin stiffness data, a regression algorithm was

employed that reiteratively modifies the initial sigmoid function, and repeats the mechanical modeling routine until a function describing the force-dependent single-kinesin stiffness is found.

Calculated single-kinesin stiffness values were also used to make a theoretical prediction of the stiffness that an idealized two-kinesin assembly would exhibit if both assembly motors shared their applied load equally. The true composite stiffness of a two-kinesin assembly, however, should depend on its microtubule-bound configuration, and hence, the experimental two-kinesin stiffness data plotted in Fig. 3.4A represents an average of assembly stiffnesses across a range of assembly configurations. As shown in Fig. 3.9B, fitting this data requires explicit knowledge of the relative probabilities of specific assembly configurations. Thus, for continuity, we generated a trend-line that approximates the average two-kinesin assembly stiffness by fitting the data to the sum of a sigmoid and a line.

3.7.3. Modeling load distributions, two-kinesin elasticities (stiffnesses), and bead displacement sizes

To evaluate the influence of microtubule-binding geometry on the distribution of forces within motor assemblies, we used the force-balance / energy minimization procedure to determine the mechanical equilibrium position of a bead under the applied load of the trap when both assembly motors are attached to the microtubule. Here, the axial stiffness of each motor is assumed to follow the functional dependence found via our single-kinesin fitting routine described above.

The mechanical equilibrium state solution of the model was then used to calculate the forces experienced by each motor (Fig. 3.4C).

Bead displacement magnitudes were predicted using our mechanical model by comparing the equilibrium solution positions of the beads in two different configurations where the spacing between microtubule-binding sites of the assembly was changed by 8 nm (Fig. 3.5D). Displacement sizes produced when scaffold center position was used as a reference point are shown in Fig. 3.10D.

3.7.4. Compliance-dependent adjustments to bead velocities and displacements

Measured stiffness values for a single kinesin (κ_{mot} as defined above; values in Fig. 3.4A) were used to calculate a correction factor $CF_{mot} = (\kappa_{mot} + \kappa_{trap})/\kappa_{mot}$ that adjusts for motor compliance to determine a motor's step size and velocity from measurements of bead displacement ($x_{mot} = x_{bead} \bullet CF_{mot}$) as previously reported.[66] This analysis confirms that the measured single-kinesin bead displacement magnitudes correspond to kinesin's intrinsic 8 nm step size (Fig. 3.10A).

The two-kinesin correction factor $CF_{assembly}$ was calculated using two-kinesin stiffness data as described above by substituting $\kappa_{assembly}$ for κ_{mot} in the CF calculation. These values were used to adjust bead velocities for motor / assembly stretching and to generate the compliance-corrected *F-V* plots in Fig. 3.4A and 3.4C. We note that with increasing force, motor and assembly elasticities increase and the

correction factors correspondingly decreases, and therefore, corrections are small (<25%) in both cases when the applied load is larger than 5 pN (Fig. 3.9C).

The average velocities displayed in Fig. 3.3C were analyzed as follows: The average velocities of bead trajectories were calculated by first determining the average velocity that beads moved within a specified force bin for each trajectory. These values were then averaged to produce an ensemble-average of all two-kinesin trajectory velocities. Time-weighted velocity averages were calculated similarly except that the average velocity of each trajectory component was weighted by the amount of time a bead spent moving within a given force bin. This treatment therefore accounts for the fact that the two-kinesin beads spend different amounts of time within a force bin depending on the number of motors responsible for transport since the number of load-bearing motors in the assembly dictates bead velocity. We present both curves to show that the overlap of the resulting *F-V* relationships with the single-kinesin data is not produced by the time-weighting of velocities alone (*i.e., both the number and duration of single load-bearing motor transport events are larger than those produced by assembly microstates possessing two load-bearing kinesins*). Since the time-averaged velocity curve accounts for the duration of two motor microstate configurations, this curve should be taken as the true average velocity of the two-motor system under load (*given the loading conditions of the static trap*).

3.7.5. Analyses of bead displacement magnitudes in stepping traces

To analyze bead displacement sizes for single-kinesin and two-kinesin assays, pairwise distribution histograms were computed using several position-time traces,[5,6,53] and then summed and normalized to generate distributions representative for each data set in Fig. 3.5. The underlying bead step size(s) were then determined by computing the power spectra of pairwise distributions. To compute each power spectrum, the pairwise distribution magnitudes were multiplied by a modified Bartlett-Hanning window and the discrete Fourier transform was determined using a fast Fourier transform algorithm. The resulting power spectra display peaks at the inverse of the step size(s) present in the bead displacement data (*e.g., 4 nm steps in displacement data would produce a peak at 1/4 nm = 0.25 nm^{-1}*).

Bead displacement magnitudes were also examined using a previously developed step-finding algorithm based on chi-squared minimization.[67] The standard deviation of bead position dwells between identified steps was measured as an indicator of experimental noise. Single-kinesin steps have a measured positional standard deviation of 2.3 nm (Fig. 3.10A). Low- and high-velocity microstate components of two-kinesin traces have a measured s.d. of 2.3 nm and 1.6 nm respectively (Fig. 3.10C). A previous evaluation of step-finding algorithms using simulated data has shown that approximately 90% of full kinesin steps should be correctly identified at this noise level.[68]

To further examine the possibility that full (~ 8nm) displacement sizes are present in two-kinesin traces at high-forces (Fig. 3.5A), the step-finding algorithm was evaluated using simulated data (at the same noise level) and determined that approximately 15% of multiple motor "half-steps" (~ 4 nm) will be misinterpreted as larger full steps. Thus, the dominant peak observed in the step size histogram displayed in Fig. 3.5C represents a lower bound for the probability that a two-kinesin assembly will advance forward by attenuated (<8 nm) steps. The combined evaluation of the step-finding algorithm and integration of the spatial power spectrum for high velocity microstates indicates that > 85% of these two-kinesin assembly steps will be asynchronous.

3.7.6. Calculation of transition rates between different microstate configurations of two-kinesin assemblies

The different rates at which two-kinesin assemblies transition between distinct classes of microtubule-bound configurations (defined by whether beads move with 'low' or 'high' velocities in the optical trap, and hence, whether one or two motors bear the applied load) were determined as follows: The force-dependent rate assemblies switched from microstates with a single load-bearing motor to those where both motors bear the applied load, $k_{trans[1\rightarrow 2]}$, was determined by dividing the number of measured low-to-high velocity transitions by the total amount of time spent in a low-velocity state within any force bin. Correspondingly, the reverse rate, $k_{trans[2\rightarrow 1]}$, was determined by summing the number of high-to-low-velocity transitions with the number of complete microtubule dissociations that

occurred when beads moved at high velocities, and then dividing by the total amount of time spent at high velocity within a force bin. The rate that a single load-bearing kinesin detached, $k_{OFF(1\rightarrow 0)}$, was calculated separately for both single-motor and two-kinesin data. While $k_{OFF(1\rightarrow 0)}$ was determined from all detachment events recorded in single kinesin assays, the two kinesin $k_{OFF(1\rightarrow 0)}$ rate was determined from analyses of complete two-kinesin bead detachments.

3.7.7. Potential effects stemming from the time-dependent loading conditions of static optical traps

It is possible that weak gains in motor function conferred by grouping two kinesins will be more pronounced in static optical trapping experiments when compared to circumstances where applied loads are held constant. Assemblies in a static trap experience increasing loads as they progress along a microtubule filament, which may limit the ability of the trailing motor to catch its partner and affect the distribution of microstate configurations attained by the assembly. Nevertheless, the ability to use the present two-kinesin system to monitor the dynamics of individual multiple-motor complexes should provide unique opportunities to compare the action of multiple motors under time-varying loads and constant loads, and such experiments are currently underway. Furthermore, we expect that groups of motors will experience analogous loading conditions to those presented by a static trap during a number of intracellular transport processes, especially when passing obstructions or during bidirectional transport where loads

will vary in time depending on the number of motor that are pulling on one another and the extent to which their elastic elements are stretched.

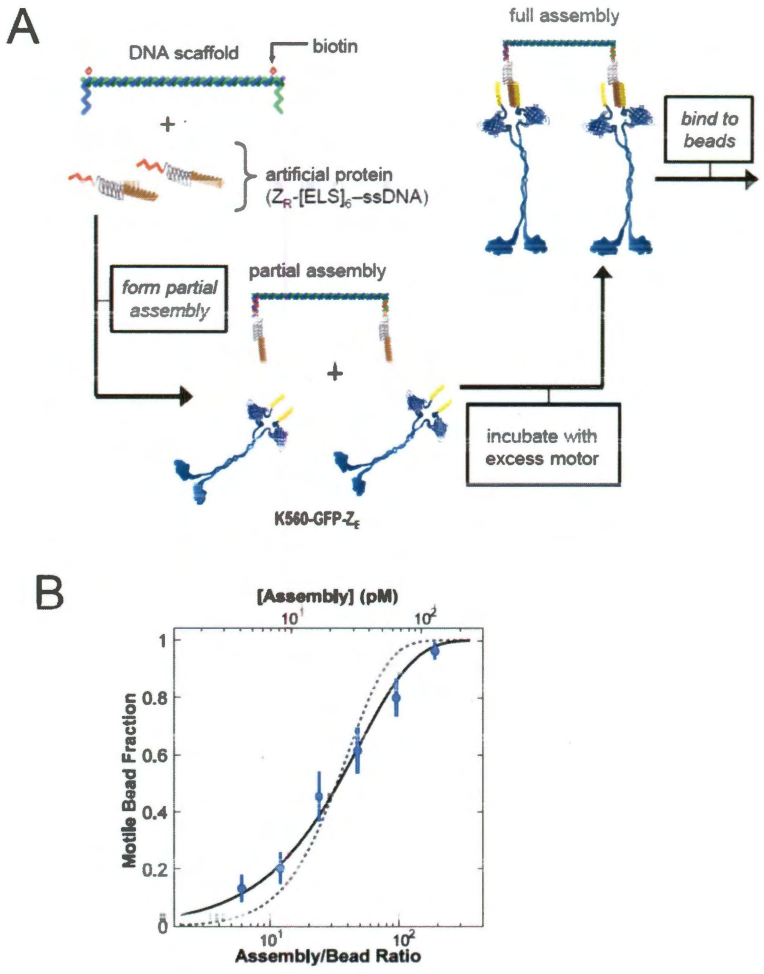

Figure 3.7 - Synthesis and Optical Trapping of Two-Kinesin Assemblies (*data collected by D. K. J.*)

(A) Synthetic scheme depicting the formation of two-kinesin assemblies as outlined in the supporting experimental procedures. **(B)** Plot of the fraction of motile two-kinesin beads measured at various assembly / bead incubation ratios (N_{beads} = 232). Data points are given as $f \pm (f(1- f)/n)^{1/2}$, where 'f' is the fraction of beads that moved along microtubules and the bead number 'n' varied between 26 – 59 from point to point. The Poisson probability that a bead is driven by one or more assemblies of kinesin motors is given by: [$f(C) = 1 - \exp(-\lambda C)$], solid line, $\chi^2 = 0.714$, 5 degrees of freedom, $p = 0.982$). The dashed line indicates a fit to the probability that beads are driven by two or more assemblies: [$f(C) = 1 - \exp(-\lambda C) - \lambda C\exp(-\lambda C)$], $\chi^2 = 16.2$, 5 degrees of freedom, $p = 0.006$). In each case, 'C' is the assembly concentration and λ is a single fitting parameter. The solid line fit is significantly better than the dashed line fit, indicating that one assembly is sufficient for bead motility.

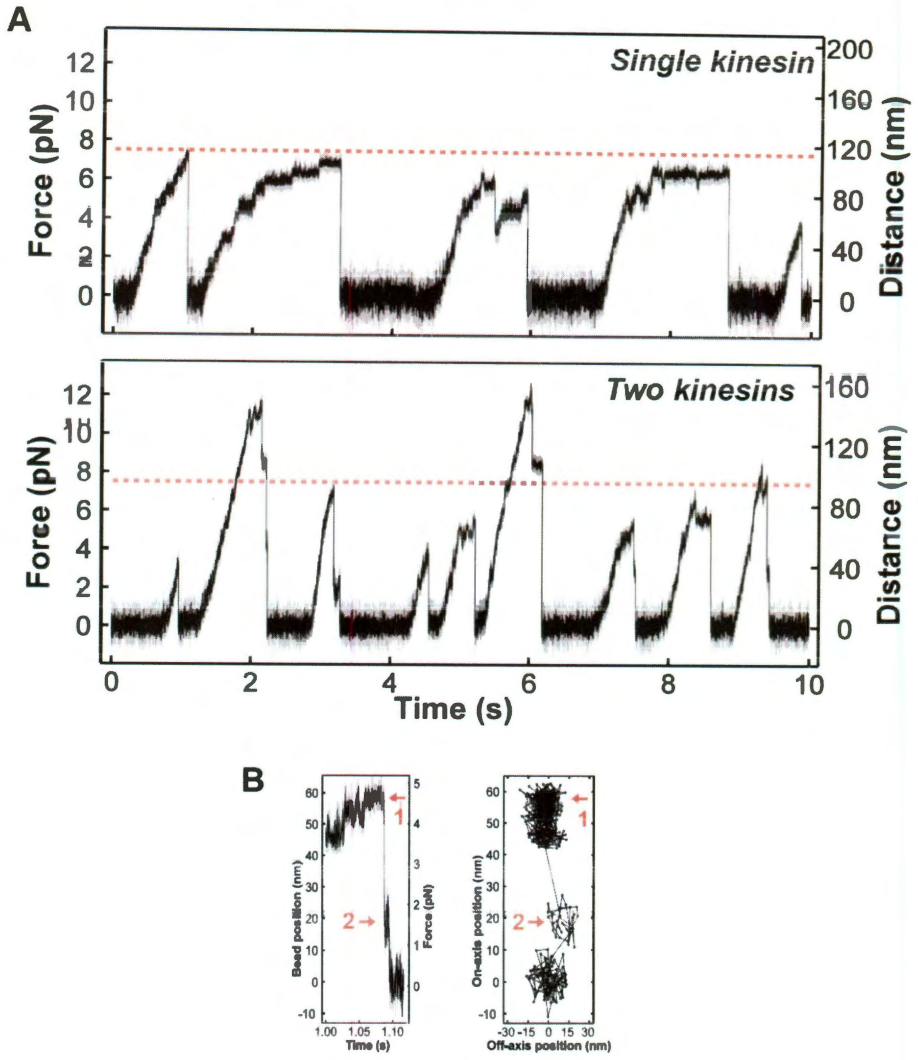

Figure 3.8 - Optical Trapping Traces for a Single and a Two-Kinesin Assembly (*data collected by D. K. J.*)

(A) Force vs. time optical trapping traces for a single hK650EGFP-Z_E (*top*) and a DNA-templated two-kinesin assembly (*bottom*). **(B)** Representative two-kinesin trace showing a large bead rearward displacement to a position other than the trap center upon detachment of the leading assembly motor. The bead positions immediately before and after the rearward displacement event are marked by the arrows and numbers in the position-time (*left panel*) and *x-y* trajectory (*right panel*) plots.

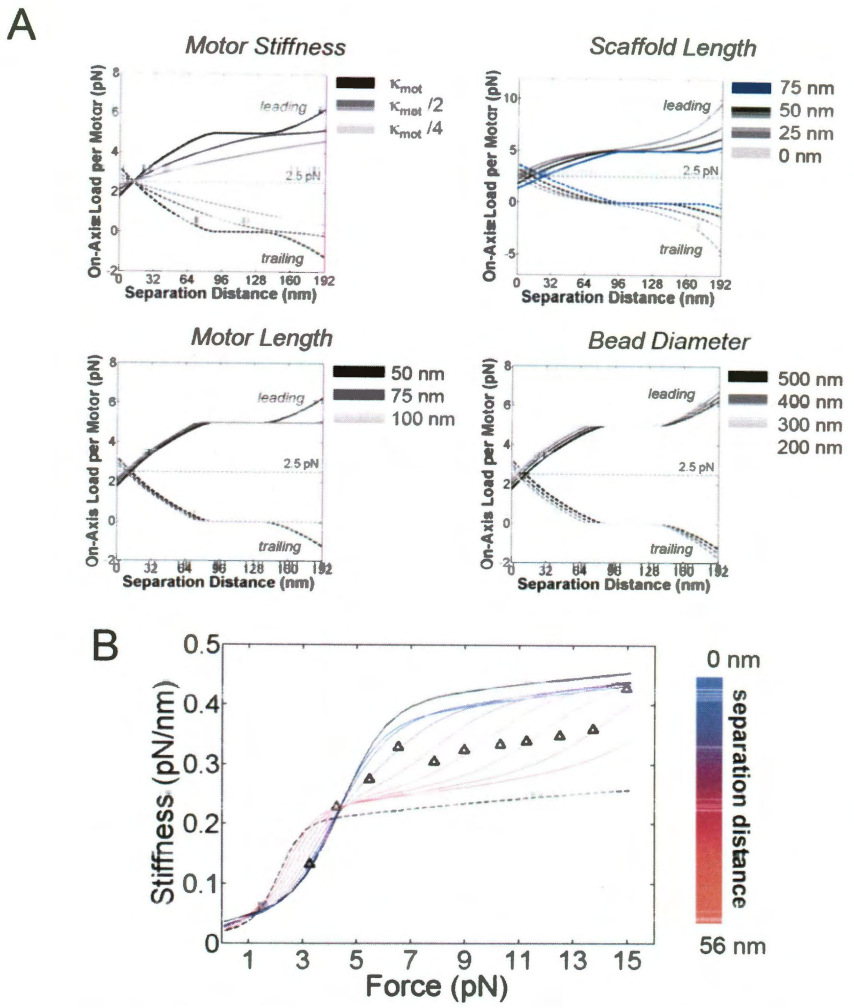

Figure 3.9 - Load-Sharing and Stiffness of Two-Kinesin Assemblies

(A) Calculated components of the applied load imposed on the leading and trailing motors as a function of motor separation distances. Near-identical load distributions are found for a wide range of motor stiffnesses (κ_{mot}), scaffold lengths, motor lengths, and bead diameters. The black line in each plot corresponds to the calculated values presented in Fig. 3.4C. **(B)** Configuration-dependent stiffnesses of two-kinesin assemblies ($\kappa_{assembly}$) plotted as a function of the total applied load. Measured stiffnesses are denoted by the triangles. Fits to the single kinesin data (*black dashed line*) and a predicted two-kinesin curve that assumes equal load sharing by the motors (*black solid line*) are shown. The colored lines denote the calculated stiffnesses of the assemblies using the modeling procedure described in the text and the supporting methods. Values for $\kappa_{assembly}$ are plotted for the range of separation distances indicated in the legend (*separation distances were increased from 0 nm in 8 nm increments*).

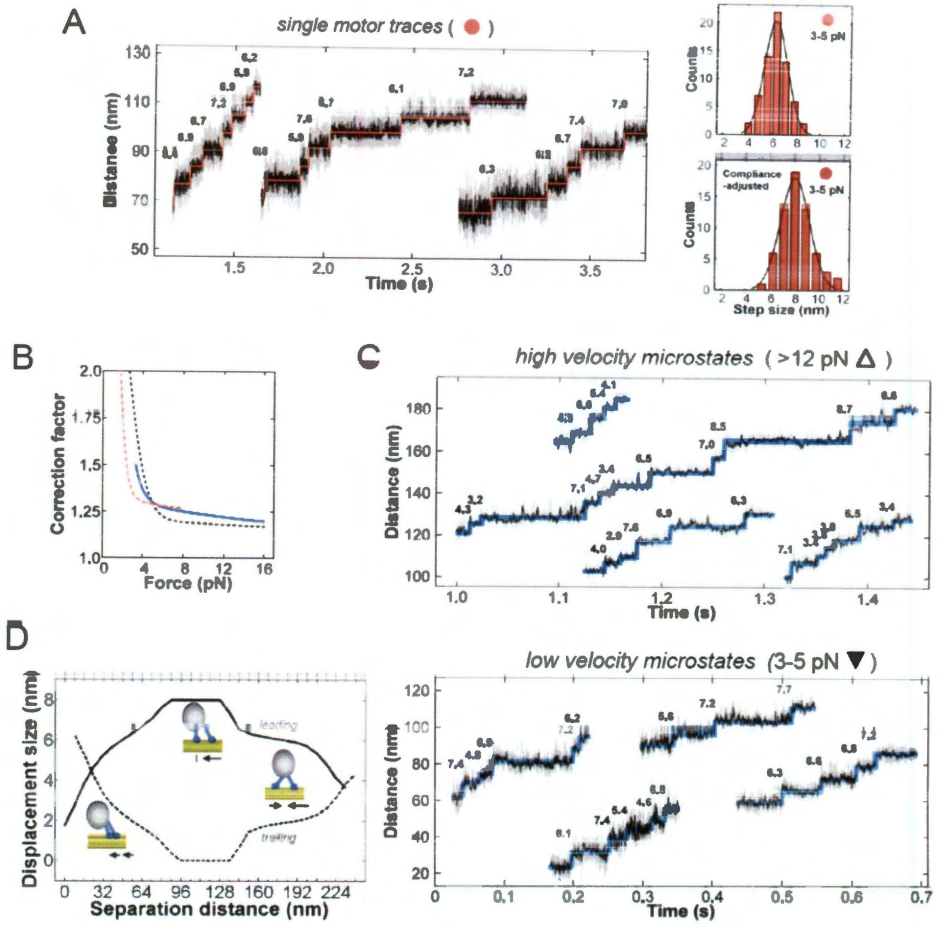

Figure 3.10 - Bead Displacement Size Analyses (*data collected by D. K. J.*)
(A) Single kinesin stepping traces and the corresponding results of a step-finding algorithm. Measured step sizes are indicated next to each trace. Raw and compliance-corrected step size distributions are shown. **(B)** Load-dependent correction factors (CF) for the single (*red dashed line*) and two-kinesin beads (*blue line*) determined as described in the supporting methods. The black dashed line denotes theoretical correction factors if the motors were assumed to share the applied load of the trap equally. **(C)** Representative two-kinesin bead traces corresponding to the data shown Fig. 3.5. The results of a step finding algorithm are indicated by the blue lines. **(D)** Calculated bead displacement sizes when the center position of the scaffold is used as a reference point. Effects stemming from bead rotations about a position other than the bead center that influence the displacement magnitudes plotted in Fig. 3.5B are less pronounced when the scaffold center position is monitored (*attenuated displacement magnitudes are found when the separation distance between the motors is large).*

Chapter 4

Productive Cooperation among Processive Motors Depends Inversely on their Mechanochemical Efficiency

Sub-cellular cargos are often transported by teams of processive molecular motors, which raises questions regarding the role of motor cooperation in intracellular transport. Although abilities to characterize the transport behaviors of multiple motor systems have improved substantially, many aspects of multiple-motor dynamics are poorly understood. This work describes a transition rate model that predicts the load-dependent transport behaviors of multiple-motor complexes from detailed measurements of a single motor's elastic and mechanochemical properties. Transition rates are parameterized via analyses of single-motor stepping behaviors, load-rate-dependent motor-filament detachment kinetics, and strain-induced stiffening of motor-cargo linkages. The model reproduces key signatures found in optical trapping studies of structurally-defined complexes composed of two kinesin motors, and predicts that multiple kinesins generally have difficulties

cooperating together. While influenced by the spatiotemporal dependence of the applied load, such behavior appears to be directly linked to the efficiency of kinesin's stepping mechanism, and other types of less efficient and 'weaker' processive motors are predicted to cooperate more productively. Thus, mechanochemical efficiencies of different motor types may distinguish how effectively they cooperate together, and hence, how motor copy number contributes to the regulation of cargo motion.

4.1. Chapter summary

The work presented in this chapter consists of modeling of the experimental data presented in the previous chapter. The work itself is exclusively my own, but I received guidance from Dr. Michael Diehl, Dr. Anatoly Kolomeisky, and D. Kenneth Jamison. The chapter itself is a manuscript that has been published in the *Biophysical Journal.*

The modeling is based on the mechanical solver described in the previous chapter, but these force-balanced geometries of a two-motor system are now treated as discrete states in a transition rate model. The states have stored elastic energies that are calculated from measurements of our kinesin construct's load-dependent stiffness, and these energies are then used to calculate transition rates between states. These transitions can be broken down into motor binding, motor stepping, and motor detachment. Motor binding is calculated from detailed balance using the configuration energies and the detachment rate. The detachment of a

single motor is itself actually modeled as a two-state process, and this model is fit to the detachment data. The motor stepping rates are computed using the model of kinesin's reaction coordinate developed by Dr. Michael Fisher; the model takes into account the effects of loads on kinesin in two dimensions. This is important since the angles of the stalks of the motors in two-motor-bound configurations varies.

The model does a good job of reproducing the experimental results. The detachment force distribution of a two-motor system in the model is qualitatively similar to the data, in that it produces one major mode around the stall force of a single kinesin. The percentage of time that the system spent in a single load-bearing motor state was quantitatively similar in silico and in vitro, and the previously unexplained peak in the observed two-motor detachment rate was recapitulated in the model. Modeling of the same system in an optical force clamp suggested that this feature was consequence of the loading conditions in the static trap. The chapter's culminating point is that motors whose velocity drops more rapidly with load actually display less negative-cooperative behavior from the standpoint of the common metrics (force-velocity, detachment force). The reason for this is that the rate of convergence of the system to load sharing configurations through stepping is higher when normalized against velocity, leading the system to load-sharing more often at any given force. Since dynein is a motor whose velocity falls more abruptly with load, we speculate that it too may display less negative-cooperative behavior and that this could be why there is experimental evidence that cells use dynein number to tune transport behavior rather than kinesin number.

4.2. Introduction

Cytoskeletal motors are molecular machines that consume ATP as fuel in order to produce the forces necessary to move vesicular and protein cargos directionally within the viscous and crowded environments of eukaryotic cells.[50] These proteins are therefore central to mechanisms that control the spatiotemporal distributions of subcellular commodities in the cytoplasm. Various microtubule motors are highly processive, and can transport cargos against piconewton-sized forces and over micron-sized distances before disassociating from their filament, suggesting they can function efficiently when acting independently as single motor molecules.[51,52] Nevertheless, processive motors often operate in groups *in vivo*,[7,17,54] which raises questions regarding the extent to which collective motor dynamics influences intracellular transport processes. Cells may rely on the combined action of motors to surmount transport challenges requiring high-force production or long distance transport,[14] and there is evidence that some transport defects associated with motor mutations can be more pronounced when cargo transport is driven by large numbers of motors.[69] Collective motor dynamics may also help to regulate cargo motion.[29,37] Many cargos move bidirectionally since they are transported by multiple, oppositely-directed kinesin and dynein motors. Cells may tune the number / ratio of kinesins and dyneins such that one motor team has a net advantage over the other in order to control the net direction these cargos are transported.[29,39]

The role multiple-motor dynamics plays in intracellular transport naturally depends on the extent to which grouping motors together enhances their transport

properties (*i.e., increased force production, velocity, or cargo-filament affinity over single motor molecules*). Until recently, characterizing these dependencies has been challenging since determining the number of motors bound to moving cargos is often difficult. However, several groups have developed experimental methods that facilitate more detailed studies of the impact of motor number and various biochemical and mechanical factors on cargo transport.[10,12,18,70] In two of these studies, our laboratory examined the collective dynamics of structurally-defined motor complexes composed of two kinesin-1 molecules.[10,12] This work showed that two interacting kinesins generally do not to transport cargos over the distances or produce the forces that are expected of a cooperative team. Instead, despite kinesin's efficiency and high processivity, kinesin complexes tended to transport their cargos while primarily using only one motor at a time (*i.e., the motors seem to cooperate negatively*).

Although the weak dependence of cargo transport on kinesin copy number can be attributed to geometric effects that reduce the ability of multiple motors to share their applied loads,[12,16] the reason such effects are so pronounced for multiple kinesins remains unclear. When transporting a cargo, motors can bind to a range of different filament lattice sites, many of which are positioned far apart from one another (*tens of motor step size units*). Yet, load-sharing only occurs if motors occupy closely-spaced microtubule lattice site positions. To cooperate productively, trailing kinesins therefore face the challenge of catching up to their continually-advancing leading partners before either motor releases from the microtubule. Naturally, a motor's microtubule-bound lifetime will influence this process.[16] However, both the

mechanical (*elastic*) and mechanochemical properties of motors are known to vary nonlinearly with force, and the evolution of a motor complex's microtubule-bound geometry should also depend on interdependent relationships between these properties. Furthermore, applied loads imposed on cargos in cells may either be relatively static or highly dynamic, as is the case when antagonistic motors compete and stretch their cargos.[5,39] In the latter circumstance, the role of loading rates must also be considered. Thus, understanding the cooperative dynamics of multiple kinesins as well as other processive motor types ultimately requires detailed and accurate parameterization of transport models to account for competing factors influencing their dynamics.

Herein, we present a model of multiple motor dynamics that predicts a cargo's load-dependent transport properties from detailed measurements of single-motor velocities, detachment rates, and elasticities. Using these data, one can account for single-motor stepping behaviors, load-rate-dependent kinetics describing motor-filament detachment, and strain-induced stiffening of motors and their resultant nonlinear, force-dependent elasticities. As a test case, we examined the transport properties of our structurally-defined two-kinesin complexes.[12] Our model reproduces key signatures found in optical trapping experiments; namely, that multiple-kinesin transport is driven primarily by a single unassisted motor molecule. While arising from generic kinetic and geometric constraints that will affect multiple kinesin dynamics in a variety of transport scenarios, the model also predicts that this behavior is influenced by spatiotemporal properties of the applied load in a static trap. In contrast, processive motors whose stepping mechanism is

less efficient than kinesin's are found to cooperate more productively regardless of whether they experience variable or constant loads and even though the geometric constraints that cause multiple kinesins to cooperate negatively still apply. Therefore, the sensitivity of cargo transport to motor copy number appears to depend inversely on the efficiency of a motor's mechanochemistry.

4.3. Discrete microstate model

4.3.1. General modeling procedure

The present model examines the progression of cargos against applied loads by computationally solving a system of master equations that describes the time-dependent transitions of multiple-motor complexes between different microtubule-bound configurations (*microstates*) (Fig. 4.1). Forces in each microstate are expected to be balanced since all of the linkages are assumed to reach their mechanical equilibrium rapidly relative to the time between the stepping,[12,25,71] binding and detachment events that drive the system from one microstate to the next. The rate at which a motor complex transitions between microstates depends on the difference in the stored mechanical energy of the final and initial configuration of the system (ΔE_{config}), which we calculate using our mechanical modeling / energy minimization procedure reported in reference 12. Below, we describe how these energies and transition rates are calculated from fits to single kinesin optical trapping data. A complete description of the modeling procedure is provided in the Appendix to Chapter 4.

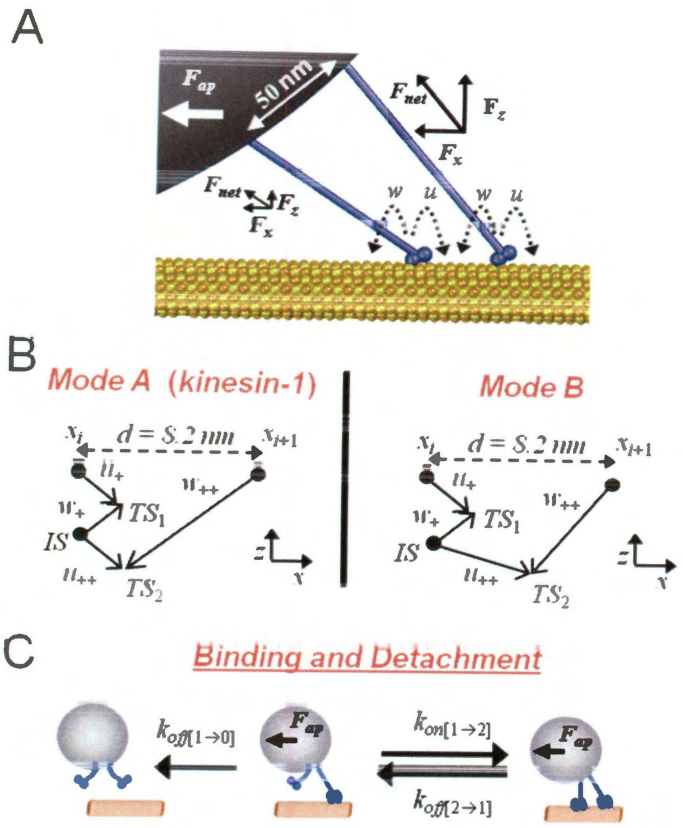

Figure 4.1 - Stepping, binding and detachment transitions enumerated in the discrete-microstate model.

(A) Illustration depicting a two-kinesin complex in a specific bound configuration; on-microtubule spacing = 32.8 nm, on-bead spacing = 50 nm, F_{ap} = 5 pN. **(B)** Reaction coordinates used to calculate two-state motor stepping rates. Sub-steps involve displacements both along and perpendicular to the microtubule axis. For stepping mode A, the positions of transition states (TS_n) for each sub-step and the intermediate state (IS) correspond directly to those reported by Fisher and Kim.[72] For stepping mode B, the position of the second transition state (TS_2) was moved toward the final microtubule lattice site position (x_{i+1}). This alteration causes the forward stepping rate to decrease more rapidly with increasing load. **(C)** Illustration depicting microstate transitions involving motor binding and detachment.

4.3.2. Defining microstate energies of multiple-motor systems using single-kinesin stiffness data

In our previous study, the force-dependent elasticity (stiffness) of a kinesin motor was determined from power spectral analyses of bead positional fluctuations of along the microtubule axis (x-axis). These data are not a direct measurement of the motor's stiffness, but rather as a projection of the motor's axial stiffness along the microtubule axis (*if stretched from its head-to-tail*), and hence, measured stiffnesses are influenced by the angle between the motor's stalk and the microtubule. We therefore fit the data to a function $\kappa_M(l_{ax})$ describing the stiffness of a single kinesin via a regression routine that uses the mechanical model to determine the vectorial component of $\kappa_M(l_{ax})$ along the microtubule axis (*i.e., the projection* $\kappa_{M,x}(l_{ax})$) over a range of applied loads. The unstretched head-to-tail length of the motor (l_o) is assumed to be 50 nm. We find that $\kappa_M(l_{ax})$ can be approximated by a sigmoid function, which may reflect the fact that the kinesins are anchored to the beads via multiple mechanical elements.[12]

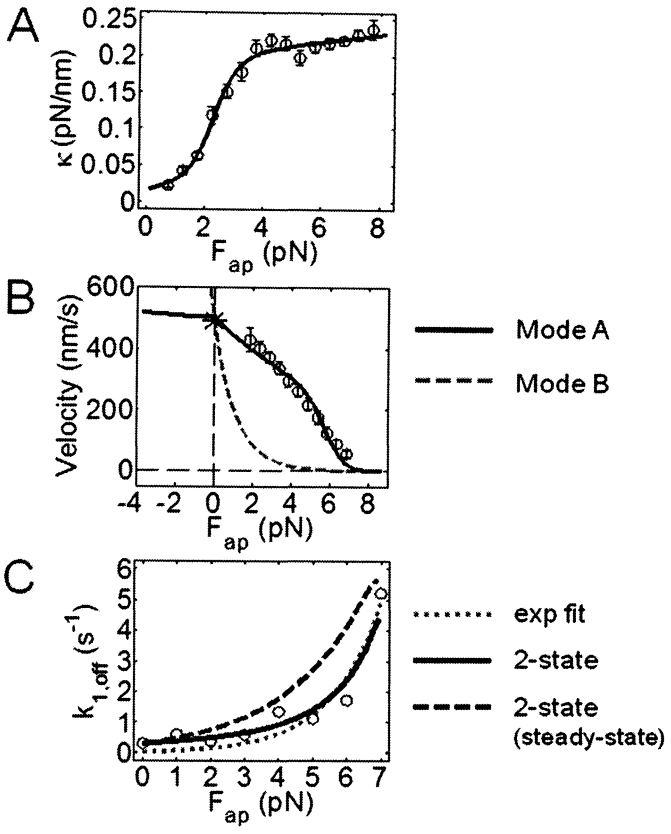

Figure 4.2 - Parameterization of motor elasticity, stepping and detachment kinetics.

(A) Experimental measurements and a best fit describing the force-dependent elasticity $\kappa_{M,x}(l_{ax})$ of the single-kinesin construct that is incorporated in the multiple motor systems.[12] **(B)** Single-motor *F-V* curves determined via a best fit of the kinesin-1 optical trapping data using stepping mode A (*solid line*) and the corresponding curve calculated for motor that advance via stepping mode B (*dashed line*). **(C)** Single-kinesin detachment rates measured in an optical trap. Best fits are shown using a two-state detachment model describing load-rate-dependent motor unbinding (*solid line*), the corresponding steady-state detachment behavior (*dashed line*), and Kramer's theory (*dotted line*).

The fitted function $\kappa_M(l_{ax})$ allows the effects from strain-induced stiffening of motor linkages (Fig. 4.2A) to be accounted for in our calculation of E_{config}.[12,73] The

configurational energy of a microstate is the sum of the potential energy of the bead in the trap and the work required to stretch each motor from its unstrained length (l_o) to the extended length (l_{ax}) found in the force-balanced microstate configuration:

$$E_{\text{config}} = \frac{1}{2}\kappa_T(x_T - x_b)^2 + \sum_M \int_{l_o}^{l_o+\Delta l_{ax}} \left\|\vec{F}_M\right\| dl$$

Equation 4.1 – Configurational energy.

where κ_T is the spring constant of the trap, ($x_T - x_b$) is the displacement of the bead from the trap center, $\vec{F}_M$ is the force pointing along the stalk of that motor from its attachment site on the bead to its microtubule-binding site, and Δl_{ax} is the magnitude of a motor's extension from its unstretched length (l_o).

4.3.3. Modeling configuration-dependent stepping rates

Even if the load experienced by a motor is the same, the angle between its stalk and the microtubule can differ greatly when cargo transport is driven by a single motor and multiple motors. Since stalk angles affect motor velocity,[58,59] motor stepping rates should be calculated using a model that accounts for the work done against vectorial loads. The model developed by Fisher and Kim assumes that kinesin's forward and backward stepping motions consist of two separate biochemical transitions (sub-steps) corresponding to displacements of the molecule in two dimensions (*x and z*).[72] Because the sub-steps involve motions of the

molecule perpendicular to the axis of the microtubule (Fig. 4.1B), loads in this direction influence stepping rates. The position of the transition state in each sub-step determines the splitting of the work done along the reaction coordinate between the forward and reverse transitions. For each transition, conservation of energy allows the work to be calculated from the difference in E_{config} from the beginning to the end of the motor stepping path via:

$$u_{+} = u_{+}^{0}\, \mathrm{e}^{-\Delta E_{\text{config}}(i \to TS_{1,i})/k_b T}$$

Equation 4.2 – Dependence of the first forward stepping rate on configurational energy.

$$u_{++} = u_{++}^{0}\, \mathrm{e}^{-\Delta E_{\text{config}}(IS_i \to TS_{2,i})/k_b T}$$

Equation 4.3 – Dependence of the second forward stepping rate on configurational energy.

$$w_{-} = w_{-}^{0}\, \mathrm{e}^{-\Delta E_{\text{config}}(IS_i \to TS_{1,i})/k_b T}$$

Equation 4.4 – Dependence of the first backward stepping rate on configurational energy.

$$w_{--} = w_{-}^{0}\, \mathrm{e}^{-\Delta E_{\text{config}}(i+1 \to TS_{2,i})/k_b T}$$

Equation 4.5 – Dependence of the second backward stepping rate on configurational energy.

In these equations, u and w refer to forward and backward sub-step transition rates as defined in Fig. 4.1B. The notation $i \rightarrow TS_{1,i}$ indicates a partial step of the motor from position i to the transition state at $TS_{1,i}$, so that $\Delta E_{\text{config}}(i \rightarrow TS_{1,i}) = E_{\text{config}}(TS_{1,i}) - E_{\text{config}}(i)$. From these rates, effective full-step transition rates and average motor velocities can be calculated:

$$u = \frac{u_+ * u_{++}}{u_+ + u_{++} + w_- + w_-}$$

Equation 4.6 – Effective forward stepping rate.

$$w = \frac{w_- * w_-}{u_+ + u_{++} + w_- + w_-}$$

Equation 4.7 – Effective backward stepping rate.

$$V_{\text{M}} = d * (u - w)$$

Equation 4.8 – Effective velocity.

where d is the total step size of the motor molecule (d = 8.2 nm for kinesin).

Assuming motors step asynchronously, their load-dependent stepping rates are calculated using the predetermined ΔE_{config} values describing transitions of motor complexes between different microtubule-bound configurations as each motor proceeds through all of its sub-step transitions, without any movement of the other motors. Thus, the only difference between this treatment and that of single

motor molecules is that some of the change in configuration energy is stored in the motor's partner(s) according to the definition of E_{config}.

4.3.4. Specifying distinct motor stepping behaviors

To specify kinesin stepping rates, we assumed that the positions of kinesin's stepping intermediate (*IS*) and transition states (TS_1 and TS_2) correspond to the values previously reported by Fisher and Kim (*stepping mode A* in Fig. 4.1B).[72] Forward and backward stepping rates were determined from fits to measured single-kinesin optical trapping data (Fig. 4.2B). Here, our mechanical modeling procedure was used to calculate force-dependent ΔE_{config} values for a single motor moving along its stepping path through each *IS* and *TS* position. Single-kinesin data can then be approximated using a generic fitting algorithm using the unloaded transition rate pre-factors in Eqns. 4.2-4.5 as fit parameters. This is likely the most appropriate adaptation of the motor stepping model for the present analyses. Our truncated kinesin-1 constructs should possess the same basic stepping mechanism as wild-type kinesins, but their zero-load, sub-step transition rates describe all other biochemical aspects of the reaction, which could be affected by other experimental factors.

The single-kinesin *F-V* fit presented in Fig. 4.2B shows reasonable agreement with the measured trend and yields unloaded motor transition rates that reflect kinesin's strong directional bias: ($u_{+}^{0} = 1.59 \times 10^{14}$; $u_{++}^{0} = 61.7$; $w_{-}^{0} = 0.654$; $w_{--}^{0} = 1.69$). To evaluate how the curvature of a motor's *F-V* relationship influences multiple-motor behaviors, we also generated an *F-V* curve for motors

possessing a slightly modified stepping reaction coordinate (Fig. 4.1B; *stepping mode B*) where the position of the second transition state TS_2 in the original coordinate was moved towards the final lattice site of the step ($i+1$) by a distance of 3.0 nm. This alteration increases the amount of work performed during the second forward sub-step, and primarily increases how sensitively the composite forward stepping rate decreases with increasing load.[74] Using the unloaded stepping rates obtained via single-kinesin fits, such behavior produces the concave upward *F-V* curve plotted in Fig. 4.2B.

4.3.5. Microstate transitions via motor detachment and binding

Average motor-microtubule detachment rates are commonly assumed to follow a load dependence described by Kramer's theory: $k_{\text{off}} = k_{\text{off}}^{0}\exp(F_{ap} \cdot \Delta s_d/k_bT)$, where Δs_d is the distance that a motor must move in order to release from the microtubule. However, this function does not reproduce our measurements of single-kinesin detachment rates (Fig. 4.2C, *dotted line*; Fig. 4.6A). This disagreement likely stems from the time dependence of the applied load in the static trapping experiments; bond affinities between biomacromolecules typically increase with increasing loading rate.[34] Furthermore, we find much weaker agreement between our theoretical and experimental data when motor detachment is parameterized using this fit (Fig. 4.7B). To address this, motor-microtubule detachment was treated as a two state process that occurs along a reaction coordinate possessing two different energetic barriers (Fig. 4.6). Barrier heights and the positions of the coordinate's intermediate and transition states were determined by fitting single-

kinesin detachment data using a procedure that solves a system of rate equations describing the time-dependent probability that a motor will occupy each of these states.

Since the above treatment allows a reaction coordinate describing motor detachment to be approximated, detachment rates can be calculated for various transport scenarios where motors may experience different loading rates. For example, if the loading rate is negligible, the model predicts motors will detach much more rapidly than the rates measured in the trapping assays (Fig. 4.2C, *dashed line*). This curve can be approximated using Kramer's theory if the quantity $k_bT/\Delta s_d = F_d$ is 2.4 pN.

Capturing the load-rate dependence of detachment transitions for multiple-motor systems ultimately requires detailed and cumbersome simulations to calculate the probability that a motor will occupy the different intermediate states along its unbinding reaction coordinate. These probabilities depend on the time-dependent progression of the loads motors experience as they bind and step along the filament, and hence, the different trajectories taken by motors within a multiple motor system. Nevertheless, the influence of load-rate can be approximated by considering generic constraints that dictate load-sharing behaviors. For example, the loading rate experienced by a motor will not only depend on how fast the bead moves and the trap's spring constant, but also on how load distributions within the complex shift in time. In general, the load assumed by a trailing motor will increase slowly since this motor has to catch up to the leading motor in the complex to take

on the applied load. Analogously, the associated shift in the transport burden from the leading to the trailing motor can decrease the loading rate experienced by the leading motor; loads can even decrease on this motor. At low applied load, detachment rates for both motors will therefore tend towards the load-rate-independent detachment curve in Fig. 4.2C instead of the fitted, (*load-rate-dependent*) function. Yet, at high loads, we expect shifts in load distributions to affect multiple motor dynamics to a lesser degree; in this regime, cargo transport necessitates load-sharing. While important to approximating observed detachment force and rate dependencies (Appendix to Chapter 4, section 4.11), these considerations allow a much simpler model of multiple-motor dynamics to be developed that incorporates load-rate-dependent effects.

Unloaded motor-microtubule binding rates were assigned their previously reported values ($k_{on[1\rightarrow 2]}(F_{ap}=0) = 4.7\ s^{-1}$). However, as in our earlier discrete state transition rate model,[11] these rates depend on the difference in the configuration energies of a motor complex before and after individual motors bind the microtubule filament. These energy differences are calculated via the same procedure used to determine ΔE_{config} for motor stepping and detachment. Of note, motor binding rates are now also influenced by forward bead displacements that arise from shifts of load-distributions between the microtubule-bound motors within a complex and are reduced by the work required to produce these displacements.

4.4. Results and discussion

4.4.1. Comparisons between theory and experiment

When parameterized by the fits to our single kinesin-1 data, the present model reproduces several key results found in our previous optical trapping studies of two kinesins.[12] First, two-kinesin complexes most commonly detach at forces near the 7 pN stalling force of a single kinesin motor (Fig. 4.3A). These distributions are qualitatively similar to our measured detachment force distributions. However, one should be cautious when making comparisons between the measured and predicted detachment behaviors of multiple motor complexes since they can detach partially during a single run prior to full detachment, and an experimentalist's choice of which events are counted can influence the resultant detachment force distributions and interpretations. We therefore present a breakdown of these detachment events in Fig. 4.3A into those caused by the release of a leading (*gold*), trailing (*blue*), or singly-bound motor (*red*) within a complex, as well as the sum of all events (*grey*). This distribution shows that both partial and full complex detachment is most prevalent at or near the stalling force of a single kinesin.

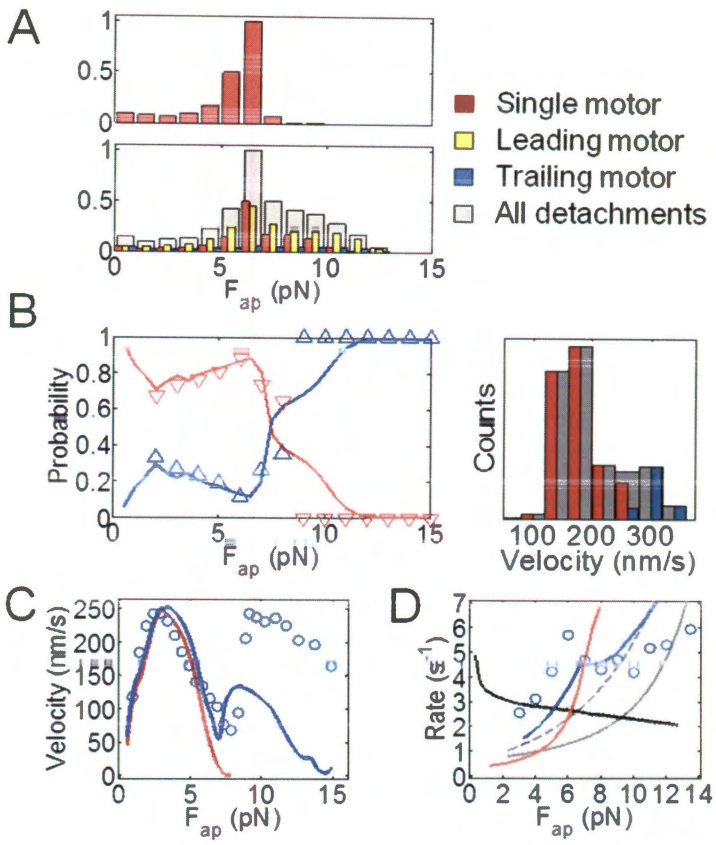

Figure 4.3 - Predicting two-kinesin behaviors in an optical trap.
(A) Histograms describing the force-dependent detachment distributions for the two-kinesin complex. Bin amplitudes are normalized by the peak bin in the cumulative histogram (gray). **(B)** The probabilities a two-kinesin complexes will adopt load-bearing microstate (*red line*) and non-load-bearing microstates (*blue line*) as a function of applied load. Optical trapping data is presented as triangles. The load-bearing probabilities are calculated as the fraction of beads at a given force that are driven by two microtubule-bound motors, each bearing at least 35% of the applied load. Non-load-bearing population fraction consists of both single- and two-motor-bound populations that do not meet this load-sharing criterion. A velocity distribution F_{ap} = 5 pN is also provided; the color coding is identical in each plot. **(C)** Average bead velocities for the single-kinesin (*red line*) and two-kinesins (*blue line*). **(D)** Calculated average motor binding ($k_{on[1 \rightarrow 2]}$) and detachment ($k_{off[2 \rightarrow 1]}$) transition rates. Experimentally-measured two-kinesin velocities and detachment rates are indicated by the blue circles in C and D.

When characterizing how effectively motors cooperate, the central issue is the amount of time cargo transport is driven by one motor within a complex compared to the time that two load-bearing motors drive transport (*or more if they are present*). Our previous velocity analyses allowed these times and the associated microstate probabilities to be measured. Predictions from the present model approximate our observed trends when it is assumed that, to exhibit load sharing behavior, both motors must bear at least 35% of the applied load (Fig. 4.3B). Here, the force dependence of microstate probabilities appears to reflect the progression of a motor complex in the optical trap. In our calculations, bead transport starts with the binding of a single motor molecule. As the simulation progresses, the second motor binds and the probability the system will adopt microstates with a single load-bearing motor decreases until the applied load reaches 2 pN; our experimental analyses cannot be performed in this force regime. However, as found experimentally, the probability that the system will adopt a single-load-bearing motor microstate increases between applied loads of 2 and 7 pN. This indicates that two-kinesin complexes do not adapt well to increasing loads in this regime; they do not cooperate by occupying load-sharing microstates where motors are bound close together on the microtubule.

Similar agreement between experiment and theory is found in analyses of average bead velocities and two-motor detachment rates at low applied loads, providing additional verification that the model captures the extent of load sharing in this region (Fig. 4.3C). Average cargo velocities follow the single-kinesin *F-V*

relationship closely up to 7 pN, after which, there is a dramatic increase in bead velocity.

As in our static trapping experiments, the transition rate describing the partial detachment of a complex, $k_{off[2\rightarrow1]}(F_{ap})$, is non-monotonic, and has a peak near the peak detachment force of the two-motor complex (Fig. 4.3D). While this feature persists regardless of our treatment of how loading rates affect motor detachment, the best agreement with the data is found when the influence of load-rate dependent effects are distinguished based on the status of the motor as described in the methods section (Appendix to Chapter 4, Figs. 4.7 and 4.8). This result further justifies our motor detachment fitting approach, but also, illustrates that two-kinesin transport against the increasing load of the static trap is much more complicated than that of a single motor molecule. In this case, inter-relationships between loading rates, load distributions, cargo velocities and motor detachment must be considered to correctly describe cargo detachment behaviors.

In the vicinity of the $k_{off[2\rightarrow1]}(F_{ap})$ peak, measured detachment rates are significantly higher than those predicted if it is assumed that motors share their load equally (*i.e.*, $k_{off[2\rightarrow1]}(F_{ap}) = 2^{*}k_{off[1\rightarrow0]}(F_{ap}/2)$) and that motor detachment is parameterized using the highest possible (*load-rate-independent*) curve in Fig. 4.3D (*the grey dashed curve*). Such rates therefore provide strong evidence against load sharing, and further support the notion that, when the static trap's load is smaller than kinesin's stalling force, cargo transport by a two-kinesin complex is primarily driven by a single motor at time.

Despite their agreement at low applied loads, there are still some significant differences between our experimental measurements and current model predictions. Measured two-kinesin velocities are appreciably higher than their calculated values above 7 pN (Fig. 4.3C). Previous analyses of bead displacement sizes indicated that the motors may coordinate / synchronize their stepping mechanics at large applied loads,[12] and this behavior is not incorporated into the present model. One would expect that such positive (*synergistic*) cooperation would depend on the separation distance between motors on the microtubule (*e.g., if this behavior stems from specific, local inter-motor interaction*). Our model predicts that motors within the two-kinesin complexes will bind to closely-spaced microtubule lattice sites at forces beyond the stall force of a single kinesin (Fig. 4.4A). Such behavior is necessary to support the type of cooperation that may be occurring in our experiments, and thus, the model's framework could be used to explore these effects.

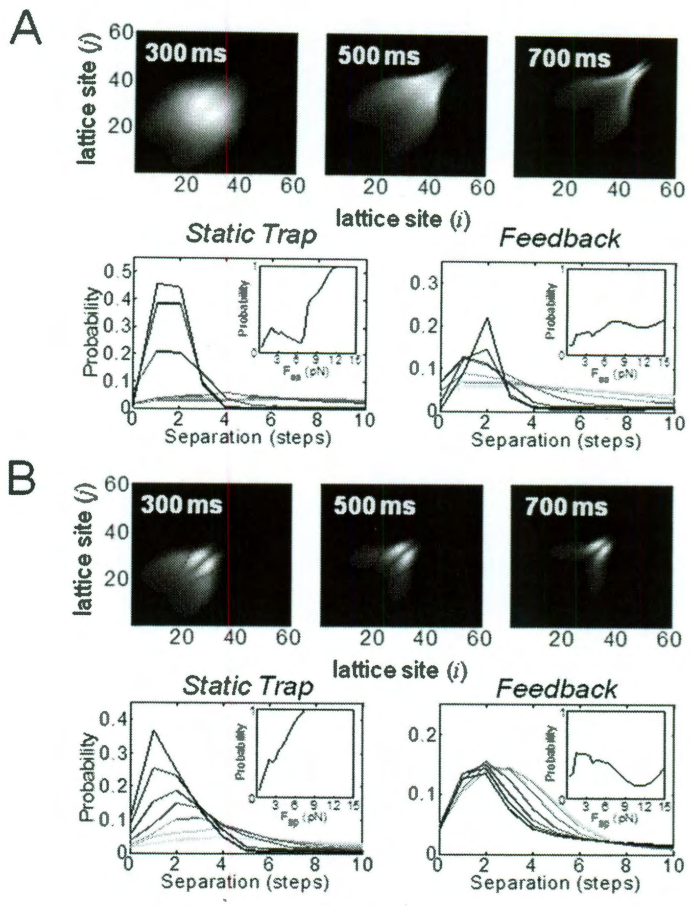

Figure 4.4 - Microstate distributions and their dependence on stepping mode. **(A)** 2-D plots showing the probability that a two-kinesin complex will adopt specific two-motor-bound configurations (*top*) at various time points when transporting cargos against the increasing load of an optical trap. Microstates are designated by the microtubule-bound positions of each motor; *i* and *j* are the lattice site positions of motor 1 and 2, respectively. Intensities along the diagonal represent microstates where motors occupy the same lattice site. (*bottom*) Two-kinesin microstate probabilities plotted as a function of motor-microtubule binding site separation distance assuming loads increase in time (*left*) or remain constant (*right*). Line colors indicate applied loads ranging from 1-13 (*light to dark*) in increments of 2 pN. The lines in the bottom panels are plotted for loads of 1-7 pN in increments of 1 pN. The inset in each plot displays the probability that a complex is predicted to adopt a load-sharing microstate (*better than 35/65 splitting the applied load*) **(B)** The equivalent plots for complexes composed of mode B motors.

We also examined how multiple-kinesin dynamics is influenced by the positions of the motors on the cargo (*bead*) and the presence of a third motor molecule (Appendix to Chapter 4, Figs. 4.9 and 4.10). In both cases, detachment force distributions and cargo velocities follow the same trends predicted for the two-kinesin complexes. This implies that the deviations between predicted and measured two-kinesin velocities at high forces cannot be explained simply by variability in the structure of our complexes or the presence of a third motor. Of interest, calculated three-kinesin velocities are only slightly higher than those produced in two-kinesin simulations between 7 and 12 pN, and, as with the two-motor systems, three-kinesin velocities exhibit a load dependence that suggests these complexes will not employ all of their motors until the applied load exceeds twice the stalling force of a single kinesin. Given this result, we do not anticipate that effects from the coordination between locally-grouped motors described above will yield significant differences between two- and three- kinesin velocities at high loads (7-14 pN) since, to contribute to cargo motion, the third kinesin would face an even more formidable challenge of 'chasing down' two synergistically-coupled motor partners.

4.4.2. Evolution of microstate densities and their load rate dependencies

The apparent inability for two kinesin motors to cooperate effectively is surprising, particularly considering the extent of the behavior and the resultant dependences of cargo velocities and detachment rates on the applied load. The unstrained binding rate of the second motor in the system ($<k_{on[1\rightarrow 2]}(F_{ap}=0)>$ 4.7 s^{-1})

greatly exceeds its detachment rate (0.31 s^{-1}), suggesting that, from a thermodynamic point of view, two-motor-bound configurations of the system should be more prevalent than single-motor-bound configurations. However, the extent to which multiple kinesin dynamics is also influenced by the spatiotemporal dependence of the applied load in the static trap must also be addressed. To explore this, we next examined the dynamics of two-kinesin complexes when they transport cargos against a constant load (*mimicking trapping assays employing force-feedback*).

Comparisons of cargo transport by two kinesins against increasing (*static trap*) and constant loads (*force-feedback*) revealed both significant similarities and differences between these two transport scenarios. In both cases, average microtubule binding rates $<k_{on[1\rightarrow 2]}(F_{ap})>$ decrease with increasing load (Fig. 4.3D; Fig. 4.10B). Thus, the energetic costs (ΔE_{config}) associated with binding transitions influence transport significantly in both circumstances. Overall, this constraint creates a strong preference unbound motors to bind microtubule sites positioned far behind the leading motor. Such behavior reflected in microstate probability distributions describing how often a two-motor complex will occupy different two-motor-bound configurations (Fig. 4.4A). For both the increasing- and constant-load cases, inter-motor separation distances are relatively large and broadly distributed below kinesin's stall force. Given the widths of and similarities between these distributions, it is not surprising that much of the negative cooperative behavior observed in the static trapping experiments is also found in the constant load

simulations, implying that kinesins will not necessarily cooperate more productively when loading rates are negligible.

Despite the similarly weak response of bead transport to kinesin number in both cases, there are still several important differences between the static trap and constant load simulations. Most strikingly, neither the rapid changes in bead velocities at kinesin's stall force nor the non-monotonic dependence of $k_{off[2\rightarrow 1]}$ in the static trap are reproduced in the constant load simulations (Fig. 4.10). Accordingly, there are significant differences in how the probabilities of two-motor-bound and load-sharing microstates change with the applied load for each simulation (Fig. 4.4A; Fig. 4.11A). The rapid increase in load-sharing microstate probabilities at kinesin's stalling force observed in the static trap is not found when applied loads are held constant. Furthermore, load-sharing microstates are more probable in constant load simulations at low applied loads, but much less probable at high applied loads; note, on top of this behavior, the probability that both motors are filament-bound decreases gradually with increasing load. Overall, these differences indicate that the two-kinesin complexes cooperate more effectively when cargo transport occurs against constant applied loads that are small. However, at high applied loads this behavior changes, and more productive cooperation via load sharing is actually predicted for the static trap.

The above comparison between static trap and constant load simulations highlights significant mechanistic differences between cargo transport by single kinesins and multiple-kinesin complexes. As indicated by our detachment rate fits

(Fig. 4.2C), motor-filament affinities are typically enhanced when single motors transport cargos against variable (*time and spatially-dependent*) applied loads since they cannot relax (*advance along their unbinding reaction coordinate*) fast enough to keep up with the changing load. However, several new pathological factors determine how multiple motor dynamics is influenced by the spatiotemporal dependence of an applied load. For example, the partial detachment of a multiple motor complex is accompanied by a backward displacement of the cargo to a new, lower force in the static trap. This process therefore raises the average number of bound motors at high forces and lowers it at low forces, and, in turn, contributes significantly to the discontinuities / non-monotonic behavior (of $\langle v \rangle$ and $k_{off[2\rightarrow 1]}$) observed in the static trap. Furthermore, the measured detachment force distribution and $k_{off[2\rightarrow 1]}$ trend cannot be reproduced when motor detachment rates are parameterized by the single-motor (*load-rate-dependent*) fit. Here, our analyses indicate that time-dependent changes in load distributions tend to lower the loading rates experienced by the motors when the applied load is small, and hence, the affinity enhancements found in single-motor assays will not influence multiple-motor dynamics. Together these effects can actually result in decreased cargo-filament affinities relative to constant-load behaviors despite the presence of a non-zero loading rate. Finally, the energetic costs associated with motor binding appear to accentuate these effects by creating a tendency for motors to attach to lattice sites positioned well behind their bound partners. Thus, the rate at which separation distances between motors evolve in time will be critical in determining how multiple motors respond to variable applied loads.

4.4.3. Motor mechanochemistry tunes collective motor function

To assess how the stepping behaviors of processive molecular motors influence their collective dynamics, the above analyses were also performed for complexes composed of less efficient motors that advance via stepping mode B (Figs. 4.1B and 4.2B). Here, the mode B motor's elastic properties and zero-load stepping rates correspond to those determined from our single-kinesin assays. However, since motors now move much slower against the applied load of the trap, motor detachment is assumed to follow the load-rate-independent curve in Fig. 4.2C.

Despite the assumption of increased motor-microtubule detachment rates, the alteration to kinesin's stepping mechanism introduced in mode B results in more effective multiple-motor cooperation than is observed with kinesins (Fig. 4.4B; Figs. 4.11B and 4.12). Microstate probabilities are much more narrowly distributed and configurations that should support load sharing are much more prevalent, even at early time points. Similar behavior is produced in constant load simulations. Motor-microtubule binding rates still decrease with increasing force in both cases. However, the curve describing average motor-filament detachment rates ($<k_{off[2\rightarrow 1]}(F_{ap})>$) does not contain a peak, and simply increases monotonically while following the equal-load-sharing trend much more closely (Fig. 4.10B). In turn, such behavior results in a stronger dependence of cargo detachment forces and average velocities on motor number (Fig. 4.12).

The enhanced load sharing ability of mode B motors indicates that a high sensitivity of forward stepping rates to increasing load, while generally reducing the efficiency of individual motors under load, actually assists in multiple-motor cooperation. This effect largely stems from the greater differential, proportionally, in motor velocities between leading (*primary-load-bearing*) and trailing (*non- or weakly-participating*) motors, meaning that the rate at which the distance between the motors closes is greater with respect to the rate at which the cargo advances against the increasing load. To explore this, we tracked the temporal evolution of average cargo velocities under constant load after microstate distributions were allowed to reach their steady-state at one force and then were subjected to an instantaneous increase of 1 pN in the applied load. After this jump, cargo velocities 'relaxed' to their steady-state levels at the increased load in an approximately exponential manner that could be fit to yield an exponential time constant (Appendix to Chapter 4). Although the absolute relaxation time constants (Fig. 4.5A, *left*) are larger (*longer*) for stepping mode B than for mode A, they are shorter when normalized by the average time that it takes the cargo to advance forward a distance of 8.2 nm (Fig. 4.5A, *right*). This means that when teams of motors with mode B stepping mechanics work against variable loads, they will be more capable of optimizing their inter-motor separation distances before the load changes and therefore defines a new optimum configuration. Moreover, the normalized relaxation time constants decrease monotonically for mode B motors, while mode A motors display a peak at 8 pN, which is close to the force where the largest discrepancy between the steady-state and static trap distributions is found. This

result strongly suggests that motors that advance via mode A (kinesin-1) are frustrated kinetically from assuming microtubule-bound configurations where they share their applied load and that such behavior hampers the function of the two-motor complex significantly.

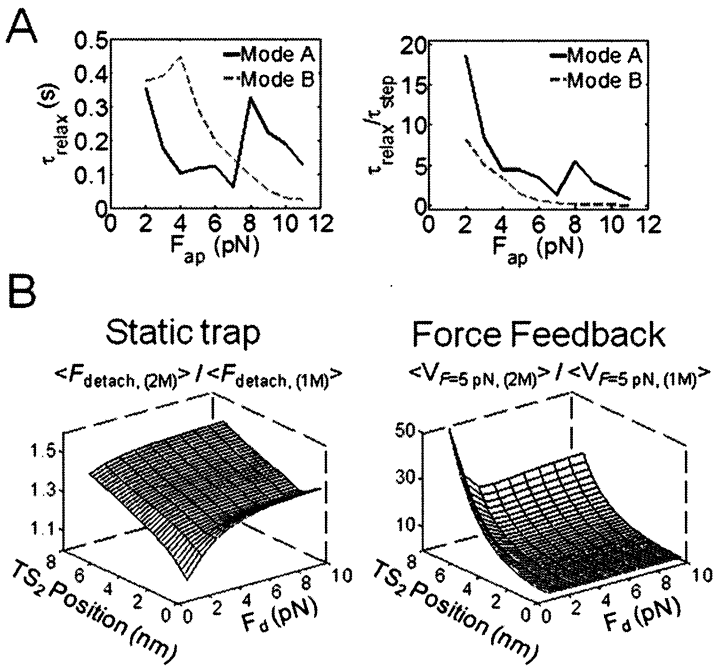

Figure 4.5 - Two-motor transport performance depends on both motor stepping efficiency and microtubule affinity.
(A) Relaxation time constant of a two-motor system in both stepping mode A and B (*left*), and the same values normalized by the stepping time constant (*right*). **(B)** Average detachment force of a two-motor system in a static trap, normalized by that of a single motor (*left*). A value of 2 indicates maximally (*additive*) cooperative behavior. Velocity of a two-motor system at constant load (F_{ap} = 5 pN), normalized by single motor velocities (*right*).

To further survey how multiple-motor cooperativity depends on the properties of a processive motor's stepping and detachment reaction coordinate, we

examined how average two-motor detachment forces and cargo velocities depend on both the position of TS_2 along a motor's stepping coordinate (*which tunes motor stepping efficiency against an applied load*), and its critical detachment force (F_d), which, as defined in the single-state Kramer's model, tunes a motor's microtubule-bound lifetime (Fig. 4.5B). Although such analyses rigorously require more exact treatments of motor detachment kinetics, the single-state model was chosen because it simplifies these calculations. Furthermore, to facilitate comparison between motor types, two-motor detachment forces and cargo velocities (*at a constant load of 5 pN*) have been normalized by the average detachment forces / velocities of their single-motor counterparts. Plots of these values both show that the weakest cooperative behavior ($F_{peak(2)}/F_{peak(1)} = 1$; $v_2/v_1 = 1.0$) occurs when the stepping and detachment reaction coordinates approximate those expected for kinesin-1; the corner of the plot near the origin. As our mode B motor simulations suggest, there is a persistent increase in detachment / velocity enhancements over single motors as they become less efficient (*as the location of TS_2 moves away from the initial motor position on the stepping coordinate*). Also, not surprisingly, motors that remain attached to the microtubule more tenaciously (*large F_d*) also cooperate more effectively. Thus, both characteristics should allow motor teams to share the applied load more equitably because in order to do so, a trailing motor must catch its leading partner before either detaches. However, what is striking is that a motor's stepping mechanism is equally and potentially even more important than its detachment behavior in determining collective motor function.

4.5. Conclusions

A theoretical framework was developed that allows the collective dynamics of multiple-motor complexes to be parameterized using fits to single-motor optical trapping data near-exclusively; all floating parameters are determined from single-kinesin fits except the unloaded motor-filament binding rate. With this treatment, differences between configuration-dependent strain energies of the complexes can be calculated and used to specify transition rates that determine how rapidly a complex's filament-bound geometry evolves in the presence of an applied load.

While the deviations from measured multiple-kinesin velocities at loads exceeding kinesin's stall force suggest motor coordination must be considered to describe multiple kinesin dynamics at high loads, most model predictions support the idea that geometric and kinetic constraints largely limit how effectively a group of kinesins can cooperate as a team. Overall, multiple-kinesin complexes have difficulties adopting microtubule-bound configurations that support load sharing, both when loads increase in time and when they remain constant. However, these difficulties are exacerbated at low applied loads (F_{ap} < 7 pN) by dynamic effects associated with the spatial and temporal dependence of the loads that multiple-kinesin complexes experience. Such effects could not be delineated through our previous experimental analyses, and were overlooked since motor-filament affinities are normally expected to increase when loading rates are appreciable. However, our present results highlight that unique load-rate dependencies can be produced when cargos are transported by teams of processive motors, and that the

time it takes for a motor complex's microtubule-bound geometry to evolve in response to a load plays a critical role in determining the forces and velocities produced by the system.

One might expect that a group of fast and efficient motors like kinesin would be able to cooperate effectively when transporting cargos since they should be able to adjust their bound geometry rapidly via motor stepping. However, we find that less efficient processive motors whose velocities drop more rapidly with increasing load are actually more capable of cooperating productively. Even though the absolute relaxation time of such motor systems is longer than those calculated for multiple kinesins given the same elastic load (*the trap's spring*), the applied load on the cargo does not increase as rapidly in this case. Consequently, while also possessing microstate distributions at steady state that lead to better load sharing behaviors, less efficient motors also have more time to adjust their bound geometry, and hence, can develop load-sharing configurations more readily.

The differences between the collective motor behaviors described above may have important implications for mechanisms that regulate cargo motion. For one, they suggest that motor stepping efficiency could distinguish how sensitively cargo transport depends on the number of processive motors grouped together on a cargo. Furthermore, motor stepping efficiencies may play a role in bidirectional transport, where oppositely-directed teams of kinesin and dynein compete antagonistically to drive cargo motion. In this case, the direction and the magnitude of the applied load will change in time as the number of motors competing against

one another also changes and since the cargo itself will be deformed (*stretched*) during this process.[5,39] Furthermore, there is evidence that dynein stalls at significantly lower forces than kinesin.[39] This inefficiency is consistent with observations that dynein's stepping patterns are much more irregular than kinesin's; backwards stepping influences dynein's average *F-V* stepping.[75] Thus, although more dyneins will be required to produce the forces of a single kinesin, a team of inefficient dyneins should still be capable of competing with a 'stronger' kinesin team given their greater ability to cooperate effectively. With this behavior, the number of dyneins, but not kinesins (*beyond binary responses*) would serve as a regulator of bidirectional transport. To date, dynein's mechanochemistry has not been characterized in detail, and hence, confirming such ideas requires further investigation. Nevertheless, the experimental and theoretical advances described here should provide a framework to investigate such behavior.

Appendix to Chapter 4

4.6. Modeling overview

One main goal of the present study is to determine the extent to which our previous optical trapping measurements of two-kinesin detachment forces, velocities and transition rates under load can be reproduced using a model that is parameterized via analyses of single kinesin optical trapping data. Here, single kinesin stiffness, force-velocity, and detachment rate data are used in combination with predictions of load distributions within a multiple motor complex and models of the kinesin detachment and stepping reaction coordinates (all of which are described below) to specify transition rates between different configurations of a two-kinesin complex as it transports a bead against the applied load of the trap (see Figs. 4.1 and 4.2). The only parameter that is not obtained from single kinesin fits is the zero-load motor binding rate $k_{on[1\rightarrow 2]}(F_{ap}=0)$, which is adopted from a previous experimental / theoretical study (π = 4.7 s^{-1}).[32] No parameters are extracted from fits to our two kinesin data; hence, the plots describing multiple motor behaviors should not be considered as fits to that data. Detailed descriptions of these methods as well as the sensitivities to different model treatments and assumptions are described below.

4.7. General modeling considerations

Our 'simulation' method utilizes a set of master equations to compute the time-dependent distribution of microstate populations. Average bead velocities are calculated from the effective stepping rates and the sizes of the bead displacements that they produce. Thus, the calculations are equivalent to data analyses where stalling events are included as zero velocities. Note, this model does not produce individual trajectories, and hence, some analyses in our prior report cannot be applied to the present modeling data (*e.g., the acceleration threshold used to determine transition rates between different load-sharing classes of two-kinesin microstates cannot be calculated computationally using the present approach*).[12]

For all calculations, motor trajectories are constrained to a single microtubule protofilament, and volume exclusion effects that would otherwise prevent motors from binding the same microtubule lattice site are neglected. These choices were made because they simplify computations significantly while still approximating the transport dynamics of the two-kinesin complexes. In general, multiple motor predictions did not change appreciably when we tested a 3-dimensional form of our model with volume exclusions (*incorporating three different parallel protofilaments*) where the motors could occupy explicitly enumerated sites on neighboring protofilaments that produce side-by-side motor-bound geometries. We believe these assumptions are appropriate since most bound geometries of the two-motor complexes are nearly two-dimensional (*planar*) when solved in three dimensions. Furthermore, the presence of parallel protofilaments

should allow motors to occupy the same longitudinal (*along the axis of the microtubule*) position, giving the appearance of violating volume exclusion in two dimensions.

For calculations of multiple motor behaviors in a static optical trap (*where motors experience time-dependent loads*), it is assumed that cargo transport begins with the binding of a single motor to a microtubule lattice site where the applied load on the bead is zero. As the bead moves forward, the number of filament-bound motors and the spacing between their microtubule binding sites changes in time depending on how motors step along, bind to, or detach from the filament. Unbound motors are able to bind sites on the microtubule that are either in front of or behind motors that are already filament-bound. Partial detachment of a complex via the unbinding of one motor and the associated retraction of the bead back towards the trap center position is allowed; the unbound motor can rebind the filament after such events. Complete bead / assembly detachment (*i.e., when a singly-bound motor releases from the filament*) ends a 'run'; rebinding after such events is not allowed.

The above constraints were also implemented for analyses of the stationary-state dynamics of two-kinesin complexes under constant applied loads with minimal alterations. This treatment emulates the experimental conditions that can be generated in an optical force clamp at long timescales. Here, microstate distributions were found by evolving the system for 2 seconds. We find that the two-motor system converges to the steady-state distribution within this timeframe given any initial distribution of two-motor bound configurations that we tested. Of note, 2

seconds substantially exceeds the relaxation time constant at any given force (<0.5 sec, see Fig. 6A).

4.8. Mechanical calculations

In order to calculate motor stepping, binding and detachment rates, the vectorial forces that the motors experience must be approximated reliably. These forces are a function of the points of attachment of the motors to both the bead and the microtubule, as well as the position of the bead within the optical trap. When the forces are not balanced, the bead adjusts its position rapidly as seen in the experimental data, where the bead moves almost instantaneously in response to the steps and detachment of the motors. It is therefore reasonable to assume that the forces within the system are balanced between transitions, and that calculating the forces on the motors requires finding these force-balanced geometries. We refer to these force-balanced geometries as "microstates".

4.8.1. Finding force-balanced microstate geometries

To find force-balanced microstate geometries, a mechanical model of the trap-bead-motor system was created. Given positions of the motors on the bead and on the microtubule, as well as the position of the trap and the position and orientation of the bead, the model is able to calculate the forces within the system. Calculations of force-balanced geometries begin with an estimate of the bead's position and orientation and initial calculations of force distributions within the system. If imbalanced, the direction and magnitude of the net imbalance is used to

estimate a new bead position. Imbalances can occur both in the '*x*' direction (*along the microtubule axis*) and in the torque on the bead (*the motors always pull the bead down to the microtubule surface - the trap is weak in this direction - so it is initially placed there and no imbalances in the 'z' direction occur*). The process of assessing force balance and repositioning of the bead is repeated reiteratively until the net imbalance decreases below a threshold of 0.1 fN in all directions, at which point it is deemed negligible. The resulting system geometry is taken as the force-balanced microstate geometry.

Once the force-balanced microstate geometry is found, the mechanical energy of that geometry is calculated. This energy, which we call "configurational energy", is equal to the sum of the stretching energies of the trap (a linear spring) and the motors (nonlinear springs, see Section 4.8.2). As stated in the text, configurational energies can be expressed by:

$$E_{\text{config}} = \frac{1}{2}\kappa_{\text{T}}(x_{\text{T}} - x_b)^2 + \sum_{\text{M}} \int_{l_{\text{o}}}^{l_{\text{ax}}} \left\| \vec{F}_{\text{ax}} \right\| dl$$

Equation 4.9 – Configurational energy.

Here, κ_{T} is the stiffness of the trap, x_{T} is the position of the trap, x_{b} is the position of the bead, l_{ax} is the head-to-tail length of the kinesin motor, l_{o} is its unstretched length, and F_{ax} is the restoring force along the axis of the motor. The summation is carried out over all microtubule-attached motors (M).

4.8.2. Stiffness of a single kinesin motor

As in other published reports,[73] we observed a nonlinear, strain-induced stiffening of our single kinesin motors in the optical trap as shown in Fig. 4.2A. These stiffness data were calculated from thermally-driven fluctuations of beads along the axis of the microtubule, and thus represent a projection of the motor's head-to-tail stiffness, $\kappa_M(l_{ax})$, along this axis (*the projection is denoted* $\kappa_{M,x}$). The motor's head-to-tail stiffness is a function of its stretched length l_{ax}, which changes with the force applied to the bead:

$$\kappa(l_{ax}) = \frac{a}{1 - b * \exp(c * (l_{ax} - l_o))} + d$$

Equation 4.10 – Length-dependent stiffness of a kinesin motor.

This empirical function was chosen to approximate the composite elasticity of the motor since the motors are linked to the beads via multiple mechanical elements (*i.e., the engineered polymers, and the streptavidin-biotin bead coating*), and a mechanistic (*analytical)* functional form of motor elasticity is therefore exceedingly difficult to define. Given $\kappa_M(l_{ax})$, $\kappa_{M,x}(F_{ap})$ is found by using the mechanical model to test the resistance of the bead to changes in its position across a range of applied loads. A standard MALAB fitting routine (nlinfit) was used to fit equation 4.2 to our stiffness data (taking a, b, c, and d as fitting parameters); $\kappa_{M,x}(F_{ap})$ was recalculated each time a new set of parameter values was tested by the routine.

4.9. Transitions between microstates

4.9.1. The need to consider load-rate-dependent effects on motor detachment

We implemented a model of motor-microtubule detachment that allows one to account for load-rate-dependent effects instead of a simple Kramer's theory for several reasons. First, Kramer's-like exponential fits under-approximate the detachment rates measured in our single kinesin experiments at low forces (Fig. 4.2C; Fig. 4.6A). Secondly, two-kinesin detachment force histograms contain a second peak at 9.5 pN that is not present on our experimental data if this function is used to parameterize the rates of motor detachment under load (*i.e., it yields a higher motor-microtubule affinity and a much lower* $k_{off[2 \rightarrow 1]}$ *than is found in our two-kinesin assays*). This result is described in more detail in section 4.11 below.

The affinity of many non-covalent bonds is known to depend not only on the force applied to them at any given time, but also on the rate at which that force was accumulated.[34] The disagreement described above therefore indicates such effects could be altering the dynamics of our two-kinesin complexes in the optical trap. In general, loading rates should influence bead detachment in both single kinesin and multiple kinesin assays. However, in the latter case, detachment and loading rates for each motor in the two-motor experiments can differ for each motor in the complex when the loads are not shared equally. As stated in the main text, loading rates will depend on how load distributions within a complex change in time; in most cases, this behavior appears to reduce the load rate experienced by a motor,

and hence, motor detachment rates will correspond more closely to their steady-state (load-rate-independent) behaviors. Thus, parameterizing motor detachment kinetics from single kinesin detachment data requires extraction of load-rate-independent trends. Below, we describe how single kinesin data is used to approximate a simple two-state reaction coordinate describing motor-microtubule detachment, and how this coordinate is used to calculate load-rate-dependent and load-rate-independent detachment behaviors when modeling multiple motor dynamics.

4.9.1.1. Load-rate-dependent model of motor detachment

The dependence of detachment rate on loading rate can be explained by a multi-state attachment/detachment model,[74] which stipulates that the two species (the motor and the microtubule in this case) stably bind in two or more states with different affinities. For the treatment employed here, motor detachment is assumed to occur along a two-state reaction coordinate (Fig. 4.6) that contains one state representing a "tightly-bound" state of the motors (T) and a second state corresponding to a "loosely-bound" state (L). There are also two energy barriers and transition states (TS_1 and TS_2) in between these states and the unbound state of the motors. Of note, if the motors are in the tightly-bound state, they must transition through the loosely-bound state to reach the unbound state. This has an important implication: *the observed detachment rate at any given time is proportional to the probability that the motor is in the loosely-bound state.*

$$k^{\text{off}} = \frac{B_L}{B_L + B_T} k_{B_L \to U}$$

Equation 4.11 – Dependence of motor detachment rate on loosely- and tightly-bound populations.

Transition rates between states within the reaction coordinate in Fig. 4.6 depend on the activation energy for the transition (*i.e., the free energy difference between T and TS_2 or L and TS_1*), and can be calculated using an Arrhenius relation:

$$k = A\, e^{-E_a/k_B T}$$

Equation 4.12 – Arrhenius equation.

We assume that the pre-exponential factor A, known as the "attempt frequency", has a value of $2.08*10^{10}$ for all transitions.[76] It should be noted that the exact value of this pre-exponential factor does not affect the results of our model significantly.

The following rate equations describe the evolution of the bound state populations of a motor in the two-state model:

$$\frac{d}{dt} B_T = -k_{B_T \to B_L} B_T + k_{B_L \to B_T} B_L$$

Equation 4.13 – Time rate of change of the tightly-bound population.

$$\frac{d}{dt}B_L = k_{B_T \to B_L}\, B_T - \left(k_{B_L \to B_T} + k_{B_L \to U}\right) B_L$$

Equation 4.14 – Time rate of change of the loosely-bound population.

In these equations, B_L and B_T are the loosely- and tightly-bound state populations, respectively. A change in load influences the rate constants by tilting the energy landscape. Thus, in order to transition between states along the reaction coordinate, work must be performed against that load. The energies for all of the different states Φ at positions x_Φ along the coordinate are therefore given by:

$$E_\phi = E_{\phi, F_{ap}=0} - F_{ap}\, x_\phi$$

Equation 4.15 – Energy of a state in the motor detachment reaction coordinate.

4.9.1.2. Model fit to single kinesin detachment rate data

To fit the single-kinesin detachment rate data presented in Fig. 4.2C, the loosely-bound fraction of motors (*which, again, corresponds to observed detachment rate through Eqn. 4.11*) as a function of the static optical trap's load is determined from the time-dependent solution to Eqns. 4.13 and 4.14. Here, the load is assumed to change in time in accordance with the single kinesin *F-V* relationship that is produced in the static optical trap where bead velocities are attenuated by the stretching of motor-bead linkages as the load builds on the motor (*i.e., these curves are used without the typical adjustments to bead velocities that are made to correct*

for the influence of motor compliance). The initial populations of B_L and B_T are assumed to correspond to a steady-state distribution of bound states that would be produced in the absence of and applied load (*this calculation is discussed in the next subsection*). The results of the time-dependent calculation change as the positions and zero-load energies of the states in the reaction coordinate are changed. A MATLAB fitting algorithm (nlinfit) was used to adjust these positions and energies to minimize the error between the calculated detachment rates and the data.

4.9.1.3. Calculating load-rate-independent motor-microtubule detachment rates

Motor detachment rates should be invariant in time when applied loads are held constant. Thus, in this case, detachment rates are determined by first solving for the fraction $B_L/(B_T+B_L)$ using a steady-state approximation:

$$\frac{d}{dt}\left[\frac{B_L}{B_T+B_L}\right] = 0 = \frac{(B_T+B_L)*\frac{d}{dt}B_L - B_L*\left(\frac{d}{dt}B_T+\frac{d}{dt}B_L\right)}{(B_T+B_L)^2}$$

$$= B_T*\frac{d}{dt}B_L - B_L*\frac{d}{dt}B_T$$

Equation 4.16 – Steady-state approximation applied to the loosely-bound fraction.

Using equations 4.13 and 4.14 to define the terms $\frac{d}{dt}B_L$ and $\frac{d}{dt}B_T$, we arrive at a quadratic equation relating B_L to B_T that can be solved for B_T.

$$B_T = \frac{k_{(B_L \to B_T)} - k_{(B_T \to B_L)} + k_{(B_L \to U)} + \sqrt{k_{(B_L \to B_T)}^{\,2} + [k_{(B_T \to B_L)} - k_{(B_L \to U)}]^2 + 2 \cdot k_{(B_L \to B_T)} [k_{(B_T \to B_L)} + k_{(B_L \to U)}]}}{2\, k_{(B_T \to B_L)}} B_L$$

Equation 4.17 – Steady-state level of the tightly bound population.

Rearrangement allows the fraction of loosely-bound motor at constant load in Eqn. 4.11 to be calculated.

$$\frac{B_L}{B_L + B_T} = \frac{1}{1 + \dfrac{k_{(B_L \to B_T)} - k_{(B_T \to B_L)} + k_{(B_L \to U)} + \sqrt{k_{(B_L \to B_T)}^{\,2} + [k_{(B_T \to B_L)} - k_{(B_L \to U)}]^2 + 2 \cdot k_{(B_L \to B_T)} [k_{(B_T \to B_L)} + k_{(B_L \to U)}]}}{2\, k_{(B_T \to B_L)}}}$$

Equation 4.18 – Steady-state of the loosely-bound fraction.

This relationship is implicitly a function of applied load because the rate constants (k) are functions of the applied load through Eqns. 4.12 and 4.15.

4.9.2. Calculating motor-microtubule binding and stepping rates

Motor-microtubule binding rates k^{on} were calculated using detachment rates and the detailed balance equation.

$$\frac{k^{\text{on}}}{k^{\text{off}}} = \frac{k_{\text{o}}^{\text{on}}}{k_{\text{o}}^{\text{off}}} * \exp\left(-\frac{\Delta E_{\text{config}}}{k_{\text{B}}\text{T}}\right)$$

Equation 4.19 – Detailed-balance relationship for calculating motor-microtubule binding rates.

Here, k^{off} is the detachment rate when the load is held constant on the motor. The subscript "o" indicates the zero-strain value of the binding or detachment rate. The change in configurational energy is calculated between the single-motor-bound microstate and the two-motor-bound microstate of the transition.

Motor stepping rates were calculated using the model of Fisher and Kim described in Chapter 4.

4.10. Numerical calculation methods

4.10.1. Defining and solving master equations

We use the rates of transition between microstates described in section 4.9 to define a system of ordinary differential equations, the "master equations", describing the evolution of the motor system probabilistically as it transitions through all enumerated microstates of the model. The generalized set of master equations for a two-motor system can be written as follows:

$$\frac{d\psi^0}{dt} = \sum_i k_i^{\text{off}} \psi_i^a + \sum_j k_j^{\text{off}} \psi_j^b$$

$$\frac{d\psi_i^a}{dt} = u_{(i-1)\to i}\, \psi_{(i-1)}^a + w_{(i+1)\to i}\, \psi_{(i+1)}^a - \left(k_i^{\text{off}} + \sum_j k_{i\to(i,j)}^{\text{on}} + u_{i\to(i+1)} + w_{i\to(i-1)} \right) \psi_i^a + \sum_j k_{(i,j)\to i}^{\text{off}}\, \psi_{(i,j)}^{a,b}$$

$$\frac{d\psi_j^b}{dt} = u_{(j-1)\to j}\, \psi_{(j-1)}^b + w_{(j+1)\to j}\, \psi_{(j+1)}^b - \left(k_j^{\text{off}} + \sum_i k_{j\to(i,j)}^{\text{on}} + u_{j\to(j+1)} + w_{j\to(j-1)} \right) \psi_i^b + \sum_i k_{(i,j)\to j}^{\text{off}}\, \psi_{(i,j)}^{a,b}$$

$$\frac{d\psi^{a,b}_{(i,j)}}{dt} = \left(k^{\text{on}}_{i\to(i,j)}\,\psi^{a}_{i} + k^{\text{on}}_{j\to(i,j)}\,\psi^{b}_{j}\right) + u_{(i-1,j)\to(i,j)}\psi^{a,b}_{(i-1,j)} + u_{(i,j-1)\to(i,j)}\,\psi^{a,b}_{(i,j-1)} + w_{(i+1,j)\to(i,j)}\,\psi^{a,b}_{(i+1,j)}$$
$$+ w_{(i,j+1)\to(i,j)}\,\psi^{a,b}_{(i,j+1)}$$
$$- \left[k^{\text{off}}_{(i,j)\to i} + k^{\text{off}}_{(i,j)\to j} + u_{(i,j)\to(i+1,j)} + u_{(i,j)\to(i,j+1)} + w_{(i,j)\to(i-1,j)} + w_{(i,j)\to(i,j-1)}\right]\psi^{a,b}_{(i,j)}$$

Equation 4.20 – Model master equations.

In these equations, ψ denotes the probability of an individual microstate. Its superscript indicates whether the cargo is completely detached (ψ^0), bound via only one motor (ψ^a or ψ^b), or via both motors in the complex ($\psi^{a,b}$). The subscripts *i* and *j* denote the microtubule lattice-site position of the motors. Microstate transition rates for motor binding (k^{on}), detachment (k^{off}), and stepping (u and w) also use *i* and *j* indices to indicate the initial and final microstates of the system for that transition (see section 4.9).

Note, a different notation was used to specify individual microstate transitions in the master equations to distinguish them from average rates describing how rapidly motors transition between different classes of microstates (*e.g.*, $k_{off[2\to1]}(F_{ap})$ *in the text describes the average of all transitions where a single motor in a complex detached at a specified load,* F_{ap}). In addition, Eqn. 4.20 clearly separates detachment transitions from motor stepping transitions, meaning these reaction coordinates are uncoupled in our model. This approximation is appropriate for kinesins since fitted pre-factors in Eqns. 4.2 and 4.3, as well as those of Fisher and Kim, both dictate that kinesin will primarily occupy the intermediate state position along its stepping reaction coordinate; steps are fast and the occupancy of

other sub-step positions is small. Furthermore, the ground state and the intermediate state positions are very close to one another, so the difference between their strain energies and detachment rates is negligible.

To evaluate dynamic properties of motor protein complexes, we utilize the following method. The master equations can be written formally in matrix form, with ψ being a vector containing all microstate populations and A being the transition rate matrix,

$$\frac{\mathrm{d}}{\mathrm{dt}}\Psi = \mathrm{A}\,\Psi$$

Equation 4.21 – Matrix form of the master equations.

From this matrix equation and the definition of the time derivative, a forward Euler approximation can be obtained for evolving a distribution of microstates in small time steps (from t to time $t+\Delta t$):

$$\Psi_{t+\Delta t} \approx \Psi_t + \Delta t\,\mathrm{A}\,\Psi_t$$

Equation 4.22 – Euler's approximation applied to the master equations.

This approximation can be used reiteratively to obtain numerical estimates of time-dependent distributions of microstate populations (Fig. 4.4).

4.10.2. Calculating average microstate probabilities, bead velocities, and detachment forces

4.10.2.1. Using microstate probabilities to calculate average (observed) behaviors

To calculate experimental observables, time-dependent distributions of microstate populations are first integrated over time to give a weighting that describes the relative probabilities of microstates over the entire course of the numerical calculation. These probabilities can be used to calculate measured properties such as the bead velocity and kinetic rates via (Fig. 4.3):

$$\langle O \rangle = \frac{\sum_{i,j} O_{i,j} \int_0^{t_{end}} \psi_{(i,j)}(t)\, dt}{\sum_{i,j} \int_0^{t_{end}} \psi_{(i,j)}(t)\, dt}$$

Equation 4.23 – Microstate population-weighting of observables.

The letter O denotes a generalized observable, $<O>$ is its expectation (*average*) value, and $O_{i,j}$ is the value of the observable for the microstate (i,j). The state sum can be extended over all microstates (*single- and two-motor-bound*) or over a specific subset (e.g., two-motor-bound only), depending on what is being measured.

4.10.2.2. Bead velocity

Bead velocity is a function of the stepping rates of the motors driving its motion and the displacement that those stepping events produce in the bead's center position.

$$V_{i,j} = u_{(i,j)\to(i+1,j)}\,\Delta x^{\mathrm{B,eq}}_{(i,j)\to(i+1,j)} + u_{(i,j)\to(i,j+1)}\,\Delta x^{\mathrm{B,eq}}_{(i,j)\to(i,j+1)}$$

$$+ w_{(i,j)\to(i-1,j)}\,\Delta x^{\mathrm{B,eq}}_{(i,j)\to(i-1,j)} + w_{(i,j)\to(i,j-1)}\Delta x^{\mathrm{B,eq}}_{(i,j)\to(i,j-1)}$$

Equation 4.24 – Bead velocity as a function of stepping rates and displacements.

The quantity $\Delta x^{\mathrm{B,eq}}_{\mathrm{trans}}$ refers to the change in the bead's steady-state position across the transition in the subscript. This method is valid for both variable and constant load numerical calculations. Average bead velocities are calculated using the $V_{i,j}$ in Eqn. 4.24 as the observable (O) in Eqn. 4.23.

4.10.2.3. Detachment force distribution

Our theoretical approach allows us to describe detachment processes in a two-motor system. A detachment force histogram (Fig. 4.3A *bottom, grey bars*) presents all individual motor detachment events predicted to occur over the course of a numerical calculation. In a two-motor system, this includes the detachment of either the leading (*gold bars*) or the trailing (*blue bars*) motor in two-motor-bound microstates, as well as detachment from single-motor-bound microstates (*red bars*).

In the transition rate model, these "events" reflect changes in microstate densities that arise from transitions out of two-motor-bound microstates to a single-motor-bound microstate, or from a single-motor-bound microstate to the unbound microstate. An example of this calculation can be described as follows: for a generic two-motor-bound detachment transition, the total population $\psi^{\mathrm{tot}}_{(i,j)\to i}$ that passes from the two-motor-bound microstate $\psi^{a,b}_{(i,j)}$ into the single-motor-bound microstate ψ^{a}_{i} during the simulation is:

$$\psi^{\mathrm{tot}}_{(i,j)\to i} = \sum_{\mathrm{t=0}}^{\mathrm{t_{end}}} \Delta \mathrm{t}\, k^{\mathrm{off}}_{(i,j)\to i}\, \psi^{a,b}_{(i,j)}(\mathrm{t})$$

Equation 4.25 – Time-integrated detachment from a two-motor-bound microstate.

Here, the detachment force is taken as the force on the cargo (F_{ap}) when the system was in the two-motor-bound microstate. All other single- and two-motor detachment transitions are treated analogously. The heights of the bars of the detachment force histogram are equal to the sum of every ψ^{tot} whose detachment force falls within the bounds of the bin, normalized to the height of the tallest bar in the histogram.

4.10.3. Evaluating multiple-motor relaxation times

At any given applied load, the observed behavior of the two-kinesin system will depend on the distribution of microstates that it occupies. However, that

distribution will also evolve in time towards a steady-state distribution at "long" times if the applied load is held constant. If loads on the cargo change more quickly than this convergence timescale, then the behavior of the system will be a function of both the applied load and the loading rate, analogous to the case of the single-motor detachment rates discussed in section 4.9.1. We refer to these convergence timescales as "relaxation" times (reported in Fig. 4.5), which are defined as the exponential rate of convergence of the cargo velocity to its long-time value in the constant load experiment when the initial microstate populations are set to their steady-state values for a loading force 1 pN below that of the current experiment. For example, to calculate τ_{relax} for a two-motor system under a 5 pN load, one would initialize the microstate distribution to that of the long-time limit distribution under a 4 pN load, then simulate the evolution of the distribution, keeping track of the average velocity at each time point. The dependence of the average velocity on time is then fit to the exponential function:

$$V_{\text{av}}(t) = A - B\, e^{-t/\tau_{\text{relax}}}$$

Equation 4.26 – Time-dependent convergence of the average system velocity to steady-state.

The values of τ_{relax} are given in Fig. 4.5A (*left*), as well as the same values normalized by the "stepping" timescale τ_{step} (*right*), which is the average time it takes for the bead to travel 8.2 nm under the same constant load at steady-state (*i.e. this time is simply 8.2 nm divided by the steady-state average cargo velocity*).

4.11. Sensitivities to model assumptions and parameters

As stated in the main text, the rate that a multiple motor complex's filament-bound configuration evolves in time will depend on inter-relationships between its mechanical and mechanochemical properties, all of which are nonlinear functions of the applied load. Below, we evaluate the sensitivities of two-kinesin transport behaviors to the treatments of these functions, particularly with respect to motor detachment kinetics. Overall, these analyses illustrate the importance of enumerating a full range of microstates in a model, and highlight the central need to accurately approximate the difference in strain energies associated with transitions between these microstates. Treatments of load-rate-dependent effects are also important, but with respect to composite behaviors, the combined effects of the strain-dependence to motor binding and the absence of load sharing due to kinesin's efficient mechanochemistry (*mode A F-V dependence*) tends to dominate the average behaviors of the motors, producing generically-weak responses to motor copy number. Treatment of the loading rates (*the decreased load rate experienced by the motors at low applied loads*) is necessary to refine model predictions and, especially, to best reproduce the observed dependence of the microstate detachment transitions from two-motor-bound configurations to single-motor-bound configurations $<k_{off[2\rightarrow 1]}>$.

4.11.1. Importance of considering the strain-dependence of motor binding rates

Analyses of detachment forces indicate the treatment of the strain dependence of motor binding as specified in Eqn. 4.19 is very important to reproducing the generic shape of our measured detachment force distribution (Fig. 4.7B). Without this treatment, a second the peak in the detachment force distribution at 9.5 appears that is not in our data. Although detachment rates are essentially unaffected by this change, the overall force production is much more additive.

The above result suggests the mechanical work required to move an unbound motor in a two-motor system to a particular microtubule lattice site (*which is equal to the difference in configurational energy between the two geometries*) will, according to Arrhenius theory, reduce the rate of that transition exponentially. Strain (*elastic energy*) therefore reduces the total rate of binding into all microstates and generally dictates that the second motor would bind to lattice sites at which it does not experience load, meaning that in order to share load with the first motor it would have to narrow the separation distance between them through stepping. This effect likely contributes to the distinction of the mode A and mode B results described in the text, given that the difference in these stepping behaviors influences how rapidly motor can catch one another when bound to the microtubule.

4.11.2. Sensitivity of multiple-motor dynamics to the motor detachment behaviors

We tested several permutations of our motor detachment treatment to assess whether exponential fits (Kramer's model) are sufficient to reproduce the two-motor detachment force and transition rate trends present in the trapping data. As discussed below, these analyses indicate a need to enhance the detachment rates of motors within a complex (*from two-motor-bound microstates*) over those of single motor molecules experiencing the same force to reproduce the single peak observed in the two-kinesin detachment force distribution. Therefore, the absence of load sharing cannot account for the shape of this distribution or the load dependence of $k_{off[2\rightarrow 1]}$ alone. This result indicates that appropriate treatments of load-rate-dependent effects are important in describing multiple-kinesin behaviors. Furthermore, best agreement between detachment force and $k_{off[2\rightarrow 1]}$ trends are observed when the full model treatment is implemented. These results are summarized below.

4.11.2.1. Deviations assuming a Kramer's-like single exponential detachment behavior

Multiple exponential fits to the single kinesin data were generated (*e.g., over the full data range and while omitting the high-force data point*) to more fully test the appropriateness of this treatment of single-motor detachment data (Fig. 4.6A). As with the removal of the strain-dependence to motor binding, parameterizing motor detachment rates using any of these fits produces two peaks in the detachment

force distribution (Fig. 4.7A). Furthermore, the two-motor detachment rate $k_{off[2\rightarrow 1]}$ is generally much lower than the data and nearly smooth, whereas the data is highly non-monotonic. These results clearly suggest that the average detachment rate of one or both of the motors in the two-motor system must be higher than those observed in our single motor assays.

4.11.2.2. Sensitivities to the treatment of load-rate-dependent effects

A treatment where the two-state model is used to parameterize motor detachment exclusively (*i.e., this assumes load rates experience by motors are not attenuated by collective effects*) produces qualitatively similar behaviors as the single-exponential fit (Fig. 4.8A), although the high force peak in the detachment force distributions is somewhat less pronounced. In addition, the non-monotonic character of $k_{off[2\rightarrow 1]}(F_{ap})$ is reproduced to a larger degree than with the Kramer's treatment (Fig. 4.8D). This occurs due to the higher curvature of the single-motor detachment fit near the stalling force of the motor. Nevertheless, despite this behavior, calculated $k_{off[2\rightarrow 1]}(F_{ap})$ rates greatly under-approximate measured detachment rates as low applied loads in the two motor case.

An analogous treatment where motor detachment is assumed to follow the load-rate-independent detachment trend produces a single peak in the detachment force distribution, but appears to over-approximate the $k_{off[2\rightarrow 1]}$ rates at high forces (Fig. 4.7B). Our complete model possesses a mixture of these behaviors, and best reproduces the high detachment rates (*low affinity and extensive negative motor*

cooperation) below kinesin's stalling force, and the increased affinities observed due to the predominance of load sharing above kinesin's stalling force.

4.11.3. Sensitivity to the model of motor stepping

The model of Fisher and Kim provides a relatively simple framework to define motor stepping efficiencies while allowing treatment of vectorial forces within in multiple-motor systems. In comparison, empirical fits to single-kinesin data cannot implicitly account for the direction of the load vector on the motor; stalk angles of motor within a complex can be different that those of single motor molecules experiencing the same loading force in the x-direction. Nevertheless, in the model of Fisher and Kim, motor stepping rates vary moderately with stalk angle (*the amount of work in the 'z' direction is usually small because the displacement is small*), so this treatment mostly refines the results rather than changing them qualitatively.

It is also important to note that the explicit treatment of back stepping is not necessarily critical to capturing multiple kinesin dynamics since this transition rate is small compared to kinesin's forward stepping rate until applied loads become very large. Thus, similar behaviors will emerge if the backward stepping rates are removed from the master equations describing the two-kinesin system. However, this will not be the case for other classes of motors whose velocities change with load via a larger modulation of their backward stepping rate. Multiple motor systems of such motors can be analyzed much more easily through modifications to the parameters in the Fisher-Kim model.

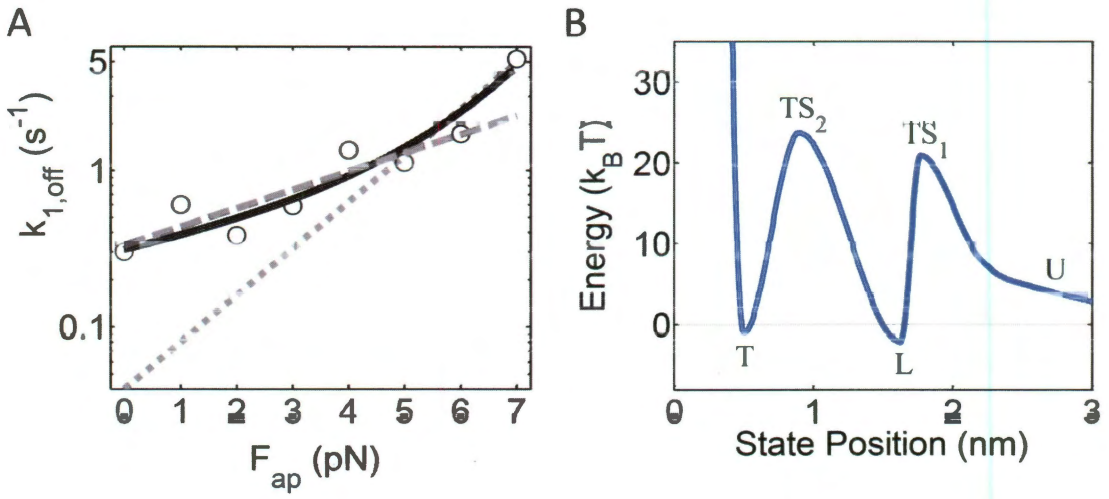

Figure 4.6 – Detachment rate and reaction coordinate.
(A) Log plot of single kinesin detachment rates and fits. The single exponential fit to the full data set (*dotted line*) and to the first seven points (*dashed line*) show less agreement with the data than the load-rate-dependent model (*black line*) and tend to under-approximate motor detachment rates. **(B)** Motor-microtubule detachment reaction coordinate and its effects on the two-kinesin detachment force distribution. Energies and positions of the tightly bound (T), loosely bound (L), and unbound (U) states as well as those of the transition states in between are depicted in the plot above. All values are derived from the simulation and fitting procedure for the two-state model described in Section 4.9.1.

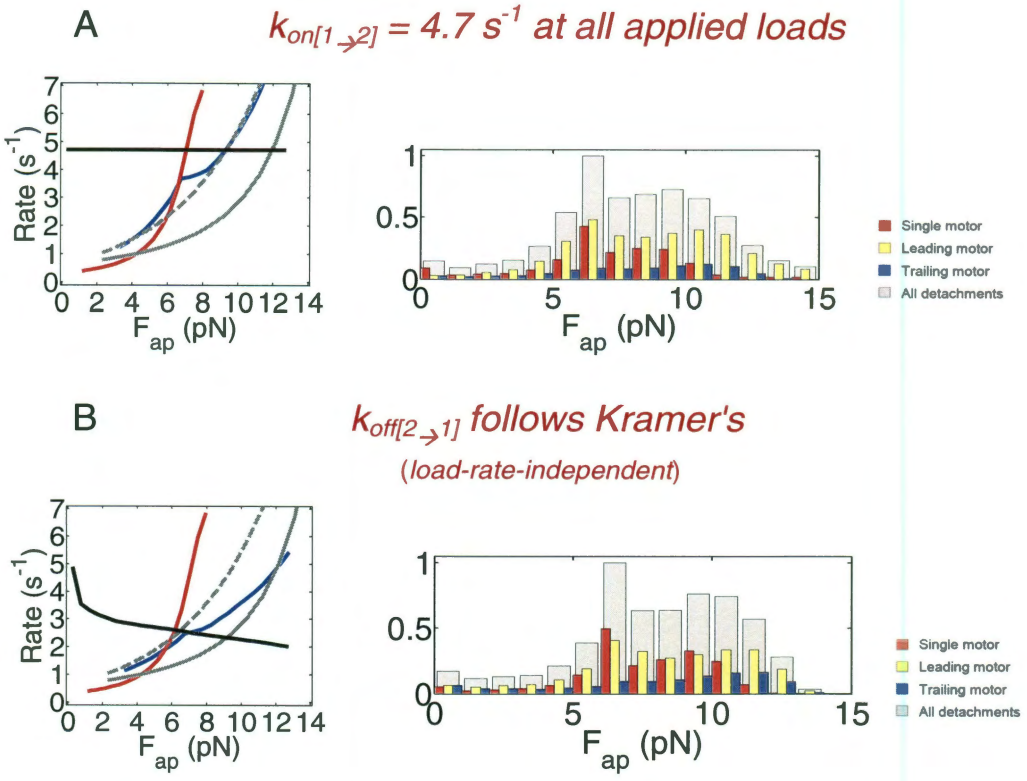

Figure 4.7 – Effects of strain-dependent binding and load-rate-dependent model of detachment.

Transition rates (*left*) and detachment force histograms (*right*) when **(A)** binding is strain-independent and **(B)** when a single-exponential model of detachment is used. In both cases, detachment force distributions show more additive function than the model presented in Chapter 4. Two-motor detachment rates in B are much lower and show less non-monotonic character than in our complete model.

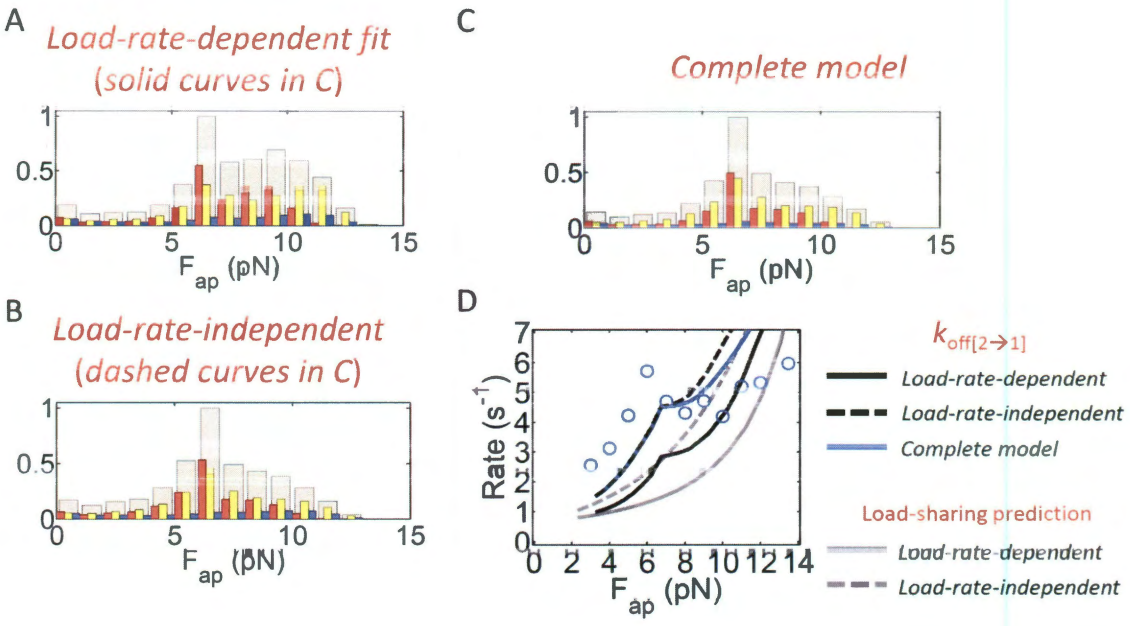

Figure 4.8 – Effects of different detachment dependencies.
Two-kinesin detachment force distributions, produced assuming motor detachment follows **(A)** the two-state model's load-rate-dependent fit in Fig. 4.2C, **(B)** the corresponding load-rate-independent prediction, and (C) the complete model. **(D)** Plots of the detachment rate $k_{\mathrm{off}[2\rightarrow 1]}(F_{ap})$ for each model treatment.

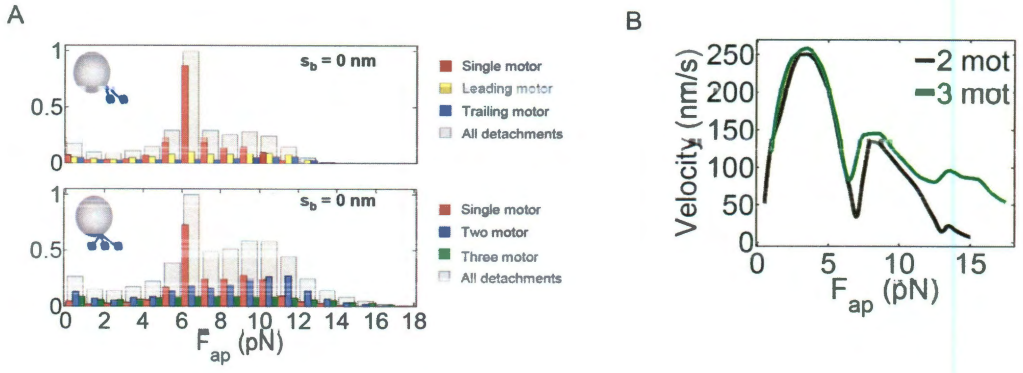

Figure 4.9 - Effects of separation distance at the bead and a third kinesin.
(A) Detachment force distributions with a breakdown of events for kinesins anchored to the same point on the bead surface. Kinesins follow the same switching detachment dependence employed to approximate the data in Chapter 4 (Fig. 4.3A). The two-kinesin distribution (*top*) shows that the system is slightly less cooperative than the one with a 50 nm separation distance at the bead. The three-kinesin distribution (*bottom*) shows that adding a third kinesin enhances the activity of the complex, but only enough to give two peaks, the tallest still being near kinesin's stall force. The breakdown consists of all detachment events beginning in three-motor-bound microstates (*green*), two-motor-bound microstates (*blue*), and single-motor-bound microstates (*red*). **(B)** Bead velocities as a function of applied load for the systems analyzed in A show that cargos are driven by n load-sharing kinesins when they experience loads less than $\sim n^* F_s$, where F_s is the stall force of a single kinesin.

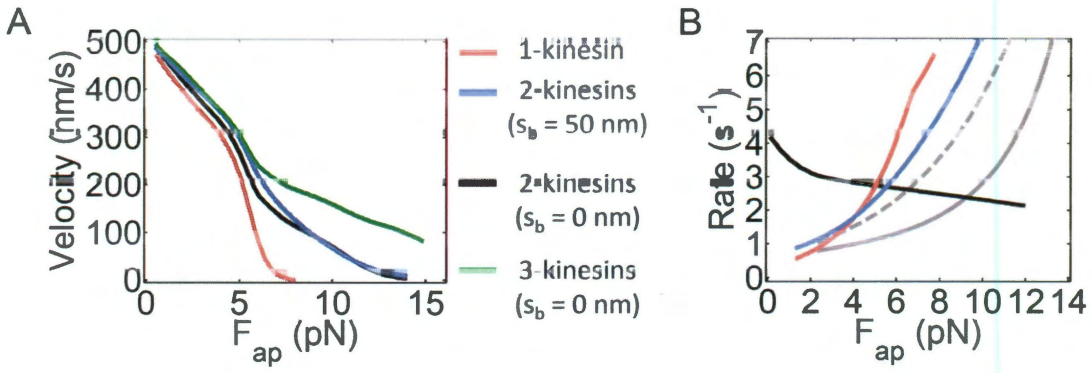

Figure 4.10 - Kinesin-driven bead velocities and transition rates under constant applied loads.

(A) Average bead velocities as a function of applied load for a single kinesin (*red*), two kinesins (s_b = 50 nm, *blue*; s_b = 0 nm, *black*), and three kinesins (*green*) demonstrate that load sharing does not occur below the stall force of a single kinesin even when loads are held constant and the motors are given time to reach their steady-state separation distance(s). **(B)** Motor binding rates (*black*) are very similar to those measured in the static trap (Fig. 4.3D). The detachment rate $\langle k_{off[2 \rightarrow 1]}(F_T) \rangle$ (*blue*) shows a monotonic increase with load, in contrast to the dependence found in the static trap. Equal-load-sharing predictions for motors with steady-state detachment dependence (*dashed grey*) and non-steady-state, single-motor fitted detachment dependence (*solid grey*) are presented for comparison. The single-motor detachment rate $\langle k_{off[1 \rightarrow 0]}(F_T) \rangle$ (*red*) comes from the load-rate independent behavior in Fig. 4.2C.

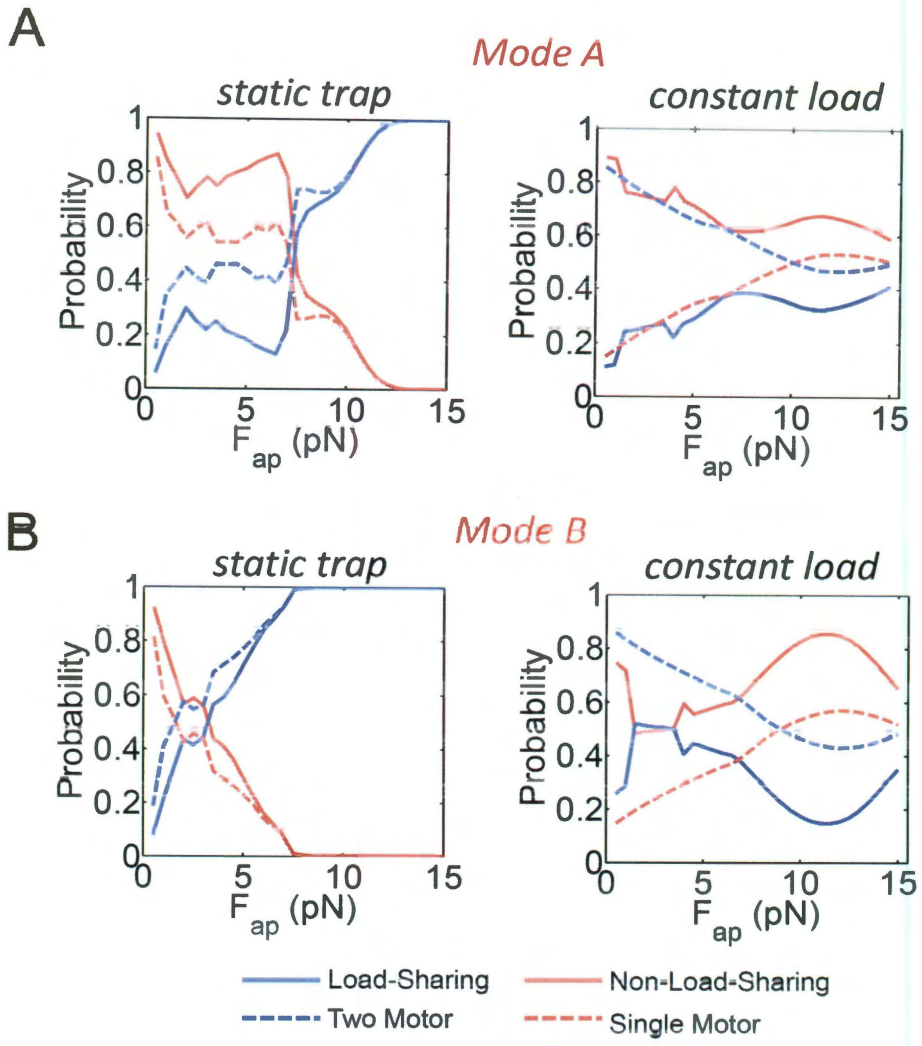

Figure 4.11 - Probability of two-motor-bound and load sharing fractions as a function of applied load.

In each plot, single and two-motor-bound microstate populations are plotted (*dashed lines*), as well as the load-sharing and non-load-sharing microstate populations (where "load sharing" means that both motors carry at least 35% of the total load, *solid lines*). Red is used to denote single-motor or non-load-sharing populations while blue is used for two-motor or load-sharing populations. (**A** and **B**) Results for stepping modes A and B, respectively, are shown for both increasing (*left*) and constant loads (*right*).

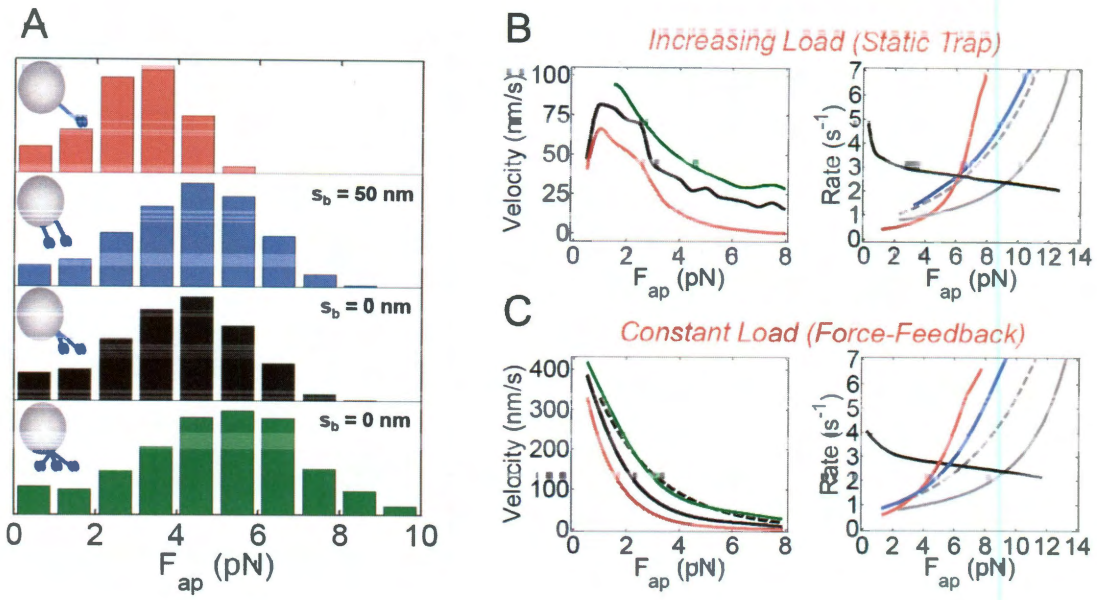

Figure 4.12 - Multiple-motor transport against increasing and constant loads (stepping mode B).

(A) Calculated detachment force distribution histograms for a single motor and multiple motor complexes in a static optical trap. The total motor number and on-bead motor separation distance (s_b) is shown in each panel. **(B** and **C)** Average motor binding / detachment transition rates and *F-V* curves calculated assuming cargos are transported against increasing **(B)** or constant **(C)** applied loads. Transition rates describing motor binding ($k_{on[1 \rightarrow 2]}$, *black line*) and detachment ($k_{off[1 \rightarrow 0]}$, *red line*, and $k_{off[2 \rightarrow 1]}$, *blue line*). The grey lines in the transition rate plots correspond to the expected detachment rates under equal load sharing for the load-rate-dependent fit (*solid*) and the load-rate-independent calculation (*dashed*). Line colors in the *F-V* plots correspond to those used to designate motor number and s_b in A.

Chapter 5

Conclusions and Future Work

The field of motor biophysics has made great strides recently in deciphering the purpose of coupling multiple processive molecular motors together into a transport system. Multiple-motor systems are driven by complex dynamics and are defined by both the motors from which they are composed and the geometric and mechanical properties of their coupling.

Like any multivalent receptor, a coupled motor system binds a filament with an energy that is not equal to simply the sum of the binding energies of the constituent motors; the mechanical coupling introduces an interaction energy that must be accounted for and that has been shown experimentally to affect the processivity of a multiple-motor system.[10] This mechanical energy is proportional to the stiffness of the overall system and affects the binding rate of the motors primarily. Importantly, this binding rate attenuation is, by nature, independent of any gain or loss of affinity induced by the stepping dynamics and thus is the first and most important aspect of a multiple-motor system to account for. The second

chapter of this thesis demonstrates that, in an unloaded experimental two-motor system, the decrease in the binding rate of the motors from the previously measured zero-strain value is all that is needed to adequately explain the decrease in processivity from that which was previously predicted.

It was long believed that *N* motors transporting a cargo should produce *N* times the force of a single motor. Specifically, it was thought that if one measured the stall force distribution of a cargo with an unknown number of motors on its surface, that the magnitude of the largest mode in the distribution would reveal the number of motors present. This is not true in any meaningful sense, as the barriers to load sharing between the motors are substantial. Unbound motors nearly always bind into positions on the filament where they do not share load, and thus must step forward relative to their partner(s) before any motor detaches in order to share load. The significance of this was shown experimentally using a synthetic two-kinesin system of known geometry and stiffness.[12] The design of this novel system centered on the precision and addressability of a self-assembling DNA template that facilitated a mild, non-covalent coupling of the motors. Creating a synthetic system of two kinesins in high yield solved the problem of ambiguous motor number and on-bead spacing in optical trapping assays, and allowed for the first true assessment of two-motor performance, independent of assumptions about the results of the measurement itself. Contrary to previous findings and predictions, the two-kinesin system usually produced around the same amount of force as a single kinesin, though some high-force events were recorded. Within events driven by two-kinesins, distinct transitions between one- and two-kinesin-like velocities were

identifiable, marking shifts in the system between non-load-sharing and load-sharing microstates. At forces below the stall of a single kinesin, the system spent the vast majority of its time in a single-kinesin-like, non-load-sharing state, demonstrating the negative-cooperative behavior of kinesin in this regime. As a result of this negative-cooperative behavior, the system had a marked tendancy to detach in the low-load regime. This may explain the lack of an enhancement in transport performance with increasing kinesin number.[18]

Negative cooperativity in systems of multiple kinesins can be explained theoretically from measurements of a single kinesin's stiffness, velocity, and microtubule detachment rate as a function of applied load. Accurate mechanical modeling is required to capture all of the binding, stepping, and detachment rates correctly, but parameterizing in this way reproduces the negative cooperativity seen in the experimental assay along with distinctive features found during data analysis, and also provides a means of explaining these things.[13] Even at low applied loads, binding of a second kinesin occurs far behind its leading partner (e.g., ~15 steps at 5 pN) because of the plethora of sites available and because binding much closer introduces significant strain energy into the system, and binding rates fall exponentially with respect to this energy. The overall rate of binding is concomitantly reduced by a factor of ½ or more. After binding, the trailing motor usually has several steps to take (~10 at 5 pN) before it begins to assume some of the load, which it most often does not get the opportunity to do because the leading kinesin's velocity does not fall very quickly with increasing load. Given this, it is natural to wonder whether other motor types with higher sensitivities to load

would perform differently. We treated this problem theoretically by modifying our kinesin stepping reaction coordinate to increase the extent to which load reduced the motor's forward stepping rate. This hypothetical, "weak" motor, whose force-velocity relationship bore a resemblance to dynein's, performed noticeably better (less negative-cooperative) in a two-motor system than kinesin when normalized against the strength of the individual motors. Since the only thing that changed was the motor's stepping mechanics, it was concluded that something about the two-motor system's convergence to load-sharing microstates through stepping had improved. This trend of decreased negative-cooperativity persisted over a large range of motor strengths, both from the standpoint of average detachment force in the static trap and cargo velocity in the force clamp. Mechanistically, it was shown that a system of weak motors converges to load-sharing microstates at a rate that is greater with respect to its overall velocity than does a system of strong motors like kinesin.

One logical next step would be to test this prediction in vitro using a system of weak motors similar to the system of kinesins in the third chapter of this thesis. Ideally, the motor tested would be cytoplasmic dynein. Dynein has been targeted to small organelles using both recombinant protein techniques and natural dynein-binding proteins,[19,20] but this motor is notoriously difficult to work with in vitro. An alternative would be to use a kinesin mutant with a similar force-velocity relationship.[74] While perhaps not quite as compelling, one could argue that the kinesin mutant and dynein would be similar enough that the information gleaned from the study would be relevant to dynein behavior *in vivo*. The model presented in

chapter four, at least, would make concrete predictions that could be tested and proven or disproven, potentially bolstering its credibility in making claims about transport by motors of all strengths and stepping mechanisms.

The model from chapter four also predicts that while loading conditions affect the exact degree of negative-cooperative behavior observed, kinesin is robustly negative-cooperative under a wide range of loading conditions. The simplest loading condition, conceptually, is the constant loading condition as in an optical force clamp. Since the work presented in the last chapter of this thesis was completed, the efforts of our group have focused on this experiment. We were most interested in the speed with which a system of two kinesins adapts to an instantaneous change in applied load (then held constant), and to what degree that adjustment period affected overall transport performance. We have found that the adjustment period usually lasts around one tenth of a second, in general agreement with the predictions from the model, and that this has a measurable, if modest effect on run length. Our comprehensive data set, composed of data from very different loading conditions, supports the notion of robust negative-cooperative behavior in systems of kinesin-1.

Despite the conclusion that systems of kinesin-1 are generally negative-cooperative, the studies in chapter 3 did find evidence of positive cooperativity at high loads, even though high-force events were uncommon. The nature of this cooperativity is unknown, though in light of the corresponding measurements done on single kinesin, the mechanism must be truly unique to the circumstance of having

two (or more) motors on the same cargo. We speculate that this cooperativity may be, among other things, dependent on the physical proximity of the motors on the microtubule, given that the enhancement is seen at high force, where inter-motor spacings are low. Of course, these are also the load-sharing configurations, so it is not clear a priori whether such cooperation would be due to a mechanical coupling through the bead, or whether some aspect of the interaction of the motors with the microtubule is altered. Regardless, these high velocities, which were measured in both static trapping and force clamp assays, could be used to theoretically characterize the cooperativity and, at the very least, rule out explanations that are not sufficient.

To relate the findings of these studies to the behavior of motor proteins in living cells, our group is building on the technology developed by Kapitein et al. to transform various cell types into experimental systems where the number of kinesins and dyneins on specific cargo types can be modulated in real time.[20] With independent control over both motors in a bidirectional system, one would be able to observe the full range of options available to a cell to regulate cargo motions via motor number. Even without knowing absolute motor number, it would be very interesting to characterize the response across a well-probed range of motor concentrations. Particularly, how non-linear is the response? If the 'response' is semi-linear over a substantial range of expression levels (or the equivalent) when measured either through final cargo distribution or microscopic behavior, it would provide strong circumstantial evidence for the utility of motor number as a higher-order transport control point. The other obvious question to answer is whether or

not there is a difference in the character of the response seen in different motor types. It should be quite possible to determine whether, *in vivo*, dynein is less negative-cooperative than kinesin. Quantitating the motor levels on the cargos, even in a relative sense, would only increase the value of the study. Naturally, back focal plane detection and the optical trap could be brought to bear to study the short-timescale behaviors of these cargos in the presence and absence of load to glean additional mechanistic information.

The mechanisms of multiple-motor transport discussed in this thesis provide a framework from which to approach future studies of transport, both in vitro and *in vivo*. Our interpretations of the meanings of basic things such as cargo step sizes, run lengths, and velocities have changed dramatically from what they were prior to these studies. We have made substantial contributions to the field of motor biophysics and believe that this work represents a near-comprehensive treatment of the topic, at least from the perspective of the biophysics of coupled kinesins in vitro, and our laboratory is uniquely positioned to answer questions of transport biophysics *in vivo* and the regulation thereof.

References

1 Liebler, S. and D. A. Huse. 1993. Porters versus rowers: a unified stochastic model of motor proteins. *J. Cell Biol.* **121**:1357-1368.

2 Debold, E. P., Patlak, J. B., and Warshaw, D. M. 2005. Slip sliding away: load-dependence of velocity generated by skeletal muscle myosin molecules in the laser trap. *Biophys. J.* **89**:L34-L36.

3 Rosenfeld, S. S., P. M. Fordyce, G. M. Jefferson, P. H. King and S. M. Block. 2003. Stepping and stretching: how kinesin uses internal strain to walk processively. *J. Biol. Chem.* **278**:18550-18556.

4 Ross, J. L., K. Wallace, H. Shuman, Y. E. Goldman and E. L. Holzbaur. 2006. Processive bidirectional motion of dynein-dynactin complexes in vitro. *Nat. Cell Biol.* **8**:562-570.

5 Gennerich, A., and D. Schild. 2006. Finite-particle tracking reveals submicroscopic-size changes of mitochondria during transport in mitral cell dendrites. *Phys. Biol.* **3**:45–53.

6 Hirokawa, N. 1998. Kinesin and dynein superfamly proteins and the mechanism of organelle transport. *Science* **279**:519-526.

7 Kulic, I. M., A. E. X. Brown, H. Kim, C. Kural, B. Blehm, P. R. Selvin, P. C. Nelson, and V. I. Gelfand. 2008. The role of microtubule movement in bidirectional organelle transport. *Proc. Natl. Acad. Sci. USA* **105**:10011-10016.

8 Vershinin, M., Carter, B. C., Razafsky, D. S., King, S. J., and Gross, S. P. 2007. Multiple-motor based transport and its regulation by tau. *Proc. Natl. Acad. Sci. USA* **107**:87-92.

9 Lakadamyali, M., Rust, M. J., Babcock, H. P., and Zhuang, X. 2003. Visualizing infection of individual influenza viruses. *Proc. Natl. Acad. Sci. USA* **100**:9280-9285.

10 Rogers, A. R., J. W. Driver, P. E. Constantinou, D. K. Jamison, and M. R. Diehl. 2009. Negative interference dominates collective transport of kinesin motors in the absence of load. *Phys. Chem. Chem. Phys.* **11**:4882-4889.

11 Driver, J. W., A. R. Rogers, D. K. Jamison, R. K. Das, A. B. Kolomeisky, and M. R. Diehl. 2010. Coupling between motor proteins determines dynamic behaviors of motor protein assemblies. *Phys. Chem. Chem. Phys.* **12**:10398-10405.

12 Jamison, D. K., J. W. Driver, A. R. Rogers, P. E. Constantinou, and M. R. Diehl. 2010. Two kinesins transport cargo primarily via the action of one motor: implications for intracellular transport. *Biophys. J.* **99**:2967-2977.

13 Driver, J. W., D. K. Jamison, K. Uppulury, A. R. Rogers, A. B. Kolomeisky and M. R. Diehl. 2011. Productive cooperation among processive motors depends inversely on their mechanochemical efficiency. *Biophys. J.* **101**:386-395.

14 Klumpp, S., and R. Lipowsky. 2005. Cooperative cargo transport by several molecular motors. *Proc. Natl. Acad. Sci. USA* **102**:17284-17289.

15 Beeg, J., Klumpp, S., Dimova, R., Gracia, R. S., Unger, E., and Lipowsky, R. 2008. Transport of beads by several kinesin motors. *Biophys. J.* **94**:532-541.

16 Korn, C. B., Klumpp, S., Lipowsky, R., Schwarz, U. S. 2009. Stochastic simulations of cargo transport by processive molecular motors. *J. Chem. Phys.* **131**:245107.

17 Ally, S., A. G. Larson, K. Barlan, S. E. Rice, and V. I. Gelfand. 2009. Opposite-polarity motors activate one another to trigger cargo transport in live cells. *J. Cell Biol.* **187**:1071-1082.

18 Shubeita, G., S. Tran, J. Xu, M. Vershinin, S. Cermelli, S. Cotton, M. Welte, and S. P. Gross. 2008. Consequences of motor copy number on the intracellular transport of kinesin-1-driven lipid droplets. *Cell* **135**:1098-1107.

19 Hoogenraad, C. C., P. Wulf, N. Schifermeier, T. Stepanova, N. Galjart, J. V. Small, F. Grosveld, C. I.de Zeeuw and A. Akhmanova. 2003. Bicaudal D induces selective dynein-mediated microtubule minus end-directed transport. *Eur. Mol. Bio. Org.* **22**:6004-6015.

20 Kapitein, L. C., Schlager, M. A., van der Zwan, W. A., Wulf, P. S., Keijzer, N., and Hoogenraad, C. C. 2010. Probing intracellular motor protein activity using an inducible cargo trafficking assay. *Biophys. J.* **99**:2143-2152.

21 Gross, S. P., Tuma, M. C., Deacon, S. W., Serpinskaya, A. S., Reilein, A. R., and Gelfand, V. I. 2002. Interactions and regulation of molecular motors in Xenopus melanophores. *J. Cell Biol.* **156**:855-865.

22 Deacon, S. W., Nascimento, A., Serpinskaya, A. S., Gelfand, V. I. 2005. Regulation of bidirectional melanosome transport by organelle bound MAP kinase. *Curr. Biol.* **15**:459-463.

23 Bieling, P., Telley, I. A., Piehler, J., Surrey, T. 2008. Processive kinesins require loose mechanical coupling for efficient collective motility. *Eur. Mol. Bio. Org.* **9**:1121-1127.

24 Roostalu, J., Hentrich, C., Bieling, P., Telley, I. A., Schiebel, E., and Surrey, T. 2011. Directional switching of the kinesin cin8 through motor coupling. *Science* **332**:94-99.

25 Leduc, C., Ruhnow, F., Howard, J., and Diez, S. 2007. Detection of fractional steps in cargo movement by the collective operation of kinesin-1 motors. *Proc. Natl. Acad. Sci. USA* **104**:10847-10852.

26 Leduc, C., Pavin, N., Julicher, F., and Diez, S. 2010. Collective behavior of antagonistically-acting kinesin-1 motors. *Phys. Rev. Lett.* **105**:128103.

27 Shroeder, H. W., Mitchell, C., Shuman, H., Holzbaur, E. L. F., and Goldman, Y. E. 2010. Motor number controls cargo swiching at actin-microtubule intersections in vitro. *Curr. Biol.* **20**:687-696.

28 Mallik, R., Petrov, D., Lex, S. A., King, S. J., and Gross, S. P. 2005. Building complexity: an in vitro study of cytoplasmic dynein with in vivo implications. *Curr. Biol.* **15**:2075-2085.

29 Hendricks, A. G., Perlson, E., Ross, J. L., Schroeder, H. W., Tokito, M., and Holzbaur, E. L. F. 2010. Motor coordination via a tug-of-war mechanism drives bidirectional vesicle transport. *Curr. Biol.* **20**:697-702.

30 Sims, P. A., and Xie, X. S. 2009. Probing dynein and kinesin stepping with mechanical manipulation in a living cell. *Chem. Phys. Chem.* **10**:1511-1516.

31 Mammen, M., Choi, S.-K., Whitesides, G. M. 1998. Polyvalent interactions in biological systems: implications for design and use of multivalent ligands and inhibitors. *Angew. Chem. Int. Ed.* **37**:2754-2794.

32 Leduc, C., O. Campás, K.B. Zeldovich, A. Roux, P. Jolimaitre, L. Bourel-Bonnet, B. Goud, J.-F. Joanny, P. Bassereau, and J. Prost. 2004. Cooperative extraction of membrane nanotubes by molecular motors. *Proc. Natl. Acad. Sci. USA* **101**:17096-17101.

33 Diehl, M. R., Zhang, K., Lee, H. J., Tirrell, D. A. 2006. Engineering cooperativity in biomotor-protein assemblies. *Science* **311**:1468-1471.

34 Evans, E. 2001. Probing the relation between force-lifetime-and chemistry in single molecular bonds. *Ann. Rev. Biophys. Biomol. Struct.* **30**:105-128.

35 Mallik, R., B. C. Carter, S. A. Lex, S. J. King, and S. P. Gross. 2004. Cytoplasmic dynein functions as a gear in response to load. *Nature* **427**:649-652.

36 Vale, R. 2003. The molecular motor toolbox for intracellular transport. *Cell* **112**:467-480.

[37] Levi, V., A. S. Serpinskaya, E. Gratton, and V. Gelfand. 2006. Organelle transport along microtubules in Xenopus melanophores: evidence for cooperation between multiple motors. *Biophys. J.* **90**:318-327.

[38] Kunwar, A., Vershinin, M., Xu, J., and Gross, S. P. 2008. Stepping, strain gating, and an unexpected force-velocity curve for multiple-motor-based transport. *Curr. Biol.* **18**:1-11.

[39] Soppina, V., A. K. Rai, A. J. Ramaiya, P. Barak, and R. Mallik. 2010. Tug-of-war between dissimilar teams of microtubule motors regulates transport and fission of endosomes. *Proc. Natl. Acad. Sci. USA* **106**:19381-19386.

[40] Ross, J. L., Shuman, H., Holzbaur, E. L., Goldman, Y. E. 2008. Kinesin and dynein-dynactin at intersecting microtubules: motor density affects dynein function. *Biophys. J.* **94**:3115-3125.

[41] Laib, J. A., Marin, J. A., Bloodgood, R. A., Guilford, W. H. 2009. The reciprocal mechanics and coordination of molecular motors in living cells. *Proc. Natl. Acad. Sci. USA* **106**:3190-3195.

[42] Muller, M. J. I., Klumpp, S., and Lipowsky, R. 2008. Tug-of-war as a cooperative mechanism for bidirectional cargo transport by molecular motors. *Proc. Natl. Acad. Sci. USA* **105**:4609-4614.

[43] Kunwar, A., and Mogilner, A. 2010. Robust transport by multiple motors with nonlinear force-velocity relations and stochastic load sharing. *Phys. Biol.* **7**:016012.

[44] Constantinou, P. E., Diehl, M. R. 2010. The mechanochemistry of integrated motor protein complexes. *J. Biomech.* **43**:31-37.

[45] Kerssemakers, J., Howard, J., Hess, H., and Diez, S. 2006. The distance that kinesin-1 holds its cargo from the microtubule surface measured by fluorescence interference contrast microscopy. *Proc. Natl. Acad. Sci. USA* **103**:15812-15817.

[46] Fisher, M. E., and Kolomeisky, A. B. 2001. Simple mechanochemistry describes the dynamics of kinesin molecules. *Proc. Natl. Acad. Sci. USA* **98**:7748-7753.

[47] Kolomeisky, A. B., and Fisher, M. E. 2007. Molecular motors: a theorist's perspective. *Ann. Rev. Phys. Chem.* **58**:675-695.

[48] Schmeidl, T., and Seifert, U. 2008. Optimal finite-time processes in stochastic thermodynamics. *Europhys. Lett.* **83**:108301.

[49] Dixit, R. , J. Ross, Y. E. Goldman and E. L. F. Holzbaur. Differential regulation of dynein and kinesin motor proteins by tau. *Science* **319**:1086-1089.

[50] J. Howard. 2001. Mechanics of motor proteins and the cytoskeleton. *Sinauer Associates,* Sunderland, MA.

[51] Carter, N. J., and R. A. Cross. 2005. Mechanics of the kinesin step. *Nature* **435**:308-312.

[52] Hancock, W. O., and J. Howard. 1998. Processivity of the motor protein kinesin requires two heads. *J. Cell Biol.* **140**:1395-1405.

[53] Schnitzer, M. J., Visscher, K., and Block, S. M. 2000. Force production by single kinesin motors. *Nat. Cell Biol.* **2**:718-723.

[54] Holzbaur, E. L., and Y. E. Goldman. 2010. Coordination of molecular motors: from in vitro assays to intracellular dynamics. *Curr. Opin. Cell Biol.* **22**:4-13.

[55] Schweller, R. M., Constantinou, P. E., Frankel, N. W., Narayan, P., and Diehl, M. R. 2008. Design of DNA-conjugated polypeptide-based capture probes for the anchoring of proteins to DNA matrices. *Bioconjug. Chem.* **19**:2304-2307.

[56] Coppin, C. M., Pierce, D. W., Long, H., and Vale, R. D. 1997. The load dependence of kinesin's mechanical cycle. *Proc. Natl. Acad. Sci. USA* **94**:1913-1917.

[57] Kojima, H., E. Muto, H. Higuchi, and T. Yanagida. 1997. Mechanics of single kinesin molecules measured by optical trapping nanometry. *Biophys. J.* **73**:2012-2022.

[58] Fehr, A. N., C. L. Asbury, and S. M. Block. 2008. Kinesin steps do not alternate in size. *Biophys. J.* **94**:L20-L22.

[59] Gittes, F., E. Meyhöfer, S. Baek, and J. Howard. 1996. Directional loading of the kinesin motor molecule as it buckles a microtubule. *Biophys. J.* **70**:418-429.

[60] Yildiz, A., M. Tomishige, R. D. Vale, and P. R. Selvin. 2004. Kinesin walks hand-over-hand. *Science* **303**:676-678.

[61] Lan, G., and S. X. Sun. 2005. Dynamics of myosin driven skeletal muscle contraction I: steady state force generation. *Biophys. J.* **88**:4107-4117.

[62] Kawaguchi, K., S. Uemura, and S. Ishiwata. 2003. Equilibrium and transition between single- and double-headed binding of kinesin as revealed by single-molecule mechanics. *Biophys. J.* **84**:1103-1113.

[63] Bruno, L., M. M. Echarte, and V. Levi. 2008. Exchange of microtubule molecular motors during melanosome transport in Xenopus laevis

melanophores is triggered by collisions with intracellular obstacles. *Cell. Biochem. Biophys.* **52**:191-201.

64 Laney, D. E., R. A. Garcia, S. M. Parson, and H. G. Hansma. 1997. Changes in the elastic properties of cholinergic synaptic vesicles as measured by atomic force microscopy. *Biophys. J.* **72**:806-813.

65 King, S. J., and T. A. Schroer. 2000. Dynactin increases the processivity of the cytoplasmic dynein motor. *Nat. Cell Biol.* **2**:20-24.

66 Svoboda, K., and S. M. Block. 1994. Force and velocity measured for single kinesin molecules. *Cell* **77**:773-784.

67 Kerssemakers, J. W. J., E. L. Munteanu, L. Liedewij, T. L. Noetzel, M. E. Janson and M. Dogterom. 2006. Assembly dynamics of microtubules at molecular resolution. *Nature* **442**:709-712.

68 Carter, B. C., M. Vershinin, and S. P. Gross. 2008. A comparison of step-detection methods: how well can you do? *Biophys. J.* **94**:306-319.

69 Ori-McKenney, K. M., J. Xu, S. P. Gross, and R. B. Vallee. 2010. A cytoplasmic dynein tail mutation impairs motor processivity. *Nat. Cell Bio.* **12**:1228-1234.

70 Ali, M. Y., H. Lu, C. S. Bookwalter, D. M. Warshaw, K. M. Trybus. 2008. Myosin V and kinesin act as tethers to enhance each others' processivity. *Proc. Natl. Acad. Sci. USA* **105**:4691-4696.

71 Astumian, D. R. 2006. The unreasonable effectiveness of equilibrium theory for interpreting nonequilibrium experiments. *Am. J. Phys.* **74**:683-688.

72 Fisher, M. E., and Y. C. Kim. 2005. Kinesin crouches to sprint but resists pushing. *Proc. Natl. Acad. Sci. USA* **102**:16209-16214.

73 Jeney, S., E.H.K Stelzer, H. Grubmüller, and E.-L. Florin. 2004. Mechanical properties of single motor molecules studied by three-dimensional thermal force probing in optical tweezers. *ChemPhysChem* **5**:1150-1158.

74 Khalil, A. S., D. C. Appleyard, A. K. Labno, A. Georges, M. Karplus, A. M. Belcher, W. Hwang, and M. J. Lang. 2008. Kinesin's cover-neck bundle folds forward to generate force. *Proc. Natl. Acad. Sci. USA* **105**:19246-19251.

75 Gennerich, A., Carter, A. P., Reck-Peterson, S. L., and Vale, R. D. 2007. Force-induced bidirectional stepping of cytoplasmic dynein. *Cell* **131**:952-965.

76 P.L. Houston, Chemical Kinetics and Reaction Dynamics, McGraw Hill, New York, 2001.